

Synne Standal Solheim

Characterisation and Studies of Microplastics in Marine Environments

Gradient from Bermuda to the Arctic and
Laboratory Based Weathering

Master's thesis in Chemical Engineering and Biotechnology
Supervisor: Øyvind Mikkelsen

June 2019

Synne Standal Solheim

Characterisation and Studies of Microplastics in Marine Environments

Gradient from Bermuda to the Arctic and
Laboratory Based Weathering

Master's thesis in Chemical Engineering and Biotechnology
Supervisor: Øyvind Mikkelsen
June 2019

Norwegian University of Science and Technology
Faculty of Natural Sciences
Department of Chemistry

"I want to say one word to you.


Just one word."

"Yes, sir."

"Are you listening?"

"Yes, I am."

"Plastics."

— The Graduate, (1967) 

Preface

This thesis was written in the spring 2019 as the concluding assessment for the 5-year integrated master's degree program 'Chemical Engineering and Biotechnology' at the Norwegian University of Science and Technology (NTNU). It is the evaluation basis for the course 'TKJ4900 – Master's thesis in Chemistry', worth 30 ECTS credits. The project was a collaboration with Norner AS, who provided all samples and materials. Experiments were carried out at both NTNU and Norner, while sample analysis were performed at NTNU, Norner and at the Norwegian Geotechnical Institute (NGI).

11th of June, 2019.



Synne Standal Solheim

Acknowledgements

First and foremost, I would first like to thank my thesis supervisors Professor Øyvind Mikkelsen (NTNU) and Professor Hans Peter Arp (NTNU/NGI) for their guidance and assistance through the research and writing. Their enthusiasm to this project has been unparalleled and contagious.

I greatly appreciate the collaboration I have had with Norner, thank you for granting me such an exciting project and the effort that was put in to make it work. It has been nothing but a pleasant experience. I especially want to show great gratitude to the assistance I received from Dr. Ravindra Reddy Chowreddy and Thor Kamfjord as they have given me great guidance through the project, as well as having clear objectives from the beginning.

I need to thank Professor Rudolf Schmid (NTNU) for training, patience and advice through the pyr-GC/MS analysis. I would also like to show gratitude to Senior Researcher Asbjørn Iveland (Norner) for assistance and counselling during the hours of FT-IR analysis.

Further, I would like to thank Senior Engineer Syverin Lierhagen (NTNU) for performing the ICP-MS analysis and Senior Engineer Liv Thobru (Norner) for performing the HT-GPC analysis.

My years at the Norwegian University of Science and Technology would not be possible without the encouragement from my family and in particular the remarkable support from the family's matriarch - my incredible grandmother.

Lastly, these years would not have been this phenomenal and remarkable had it not been for 'Hydrogenjentene'. Thank you.

Abstract

The aim of this thesis was to contribute to the growing field of microplastic research. To do so the aims were threefold: to characterise real-life sea-surface micoplastics that were sampled on the Arctic Expedition, create an accelerated weathering study and investigate possible adsorption of metals to microplastic particles.

387 particles from 11 locations in the North Atlantic Ocean was analysed using ATR FT-IR and was verified by analysing 50 of the particles by pyr-GC/MS. An average of 0.0252 particles per m^3 was found. The majority of the samples were fibre (44%) and 2D/films (37%) over 3D. White (35%), blue (19%) and clear (16%) were the most common colours of the particles. 362 of the 387 particles were identified as synthetic polymers, PE (57%) and PP (29%) showed to be the most abundant types of plastics found.

An accelerated weathering study was executed on LLDPE in both particle and film form, with and without 100ppm of the anti-oxidant Vitamin E additive as well as LDPE commercial bread bag from Meny. Two particle sizes were used (200-425 μm and 425-600 μm), and the total time in the UV chamber was 1600 hours. The weathered samples were analysed by GPC and ATR FT-IR. It was found that the anti-oxidant properties of the vitamin E additive decreased the rate of chain breakage compared to LLDPE without, both for films and particles. A smaller particle size increases the rate of chain breakage. The commercial LDPE bread bag from Meny appears to contain some type of additive as it has a slower chain-breakage than the other LLDPE films.

Using LLDPE powder particles weathered for 1200 hours a study of the adsorption of six metals (Cd, Cr, Cu, Hg, Pb, Zn) in simulated seawater was done. ICP-MS was used to analyse the solutions and PCA was conducted on the results. It showed that the particles had some adsorption of Hg ($K_{pw} = 0.36$) and that the particles released Zn to the water ($K_{pw} = -0.20$). For the 4 other metals no interaction was found and there were no indication of particle size effecting adsorption.

Samandrag

Sikte med denne oppgåva var å bidra med kunnskap om mikroplast, eit nytt veksande felt. For å oppnå dette var eit tredelt føremål forma: (1) å karakterisere verkelege mikroplast partiklar frå sjøoverflata som vart sampla på 'the Arctic Expedition', (2) skapa ein akselert forvitningsstudie for polyetylene og (3) undersøka mogelig adsorpsjon av metall til mikroplast partiklar.

387 partiklar frå 11 ulike stadar i Nord-Atlanteren vart analysert ved bruk av metoden ATR FT-IR og vart verifisert ved å analysera 50 av partiklane ved pyr-GC/MS. Eit gjennomsnitt på 0,0252 partiklar per m^3 vart funnen. Fleirtalet av prøvene var av typane fiber (44%) og 2D/filmar (37%). Kvit (35 %), blå (19 %) og gjennomsiktig (16 %) var dei vanlegaste fargane. 362 av dei 387 partiklane vart identifiserte som syntetiske polymerar. Størstepart av platen som blei påvist var av typane PE (57%) og PP (29%).

Ein akselerert forvitningsstudie vart utført ved LLDPE i både partikkel- og filmform, med og utan 100 ppm av anti-oksidant vitamin E tilsetning, i tillegg til ein kommersiell brødpose (LDPE) frå Meny. To partikkelstorleikar vart brukte (200-425 μm og 425-600 μm), og den totale tida i UV-kammeret vart 1600 timar. Dei forvitra prøvene vart analyserte ved GPC og ATR FT-IR. Det vart funne at anti-oksidant eigenskapane til vitamin E reduserte graden av kjede-brot i polymeren samanlikna med LLDPE utan. Dette gjeld både for filmar og partiklar. Det vart også funne at ein mindre partikkelstorleik aukar farten på kjede-brot. Den kommersielle LDPE-brødposen frå Meny ser ut til å innehalda noko additiv, då kjeda til polymeren brot langsamare enn for LLDPE-filmane.

Ved bruk av LLDPE-pulverpartiklar som vart forvitra i 1200 timar vart det gjort ei gransking av adsorpsjonen til seks metall (Cd, Cr, Cu, Hg, Pb, Zn) i simulert sjøvatn. ICP-MS vart brukt til å analysera løysingane og prinsippal komponent analyse (PCA) vart utført på resultatane. Resultatane viste at partiklane hadde noko adsorpsjon av Hg ($K_{pw} = 0.36$) og at partiklane frigjorde Zn til vatnet ($K_{pw} = -0,20$). For dei resterande 4 metalla vart ingen interaksjon funne, og det var ingen indikasjon på at storleiken til partiklane påverka adsorpsjon.

Acronyms and Abbreviations

ATR Attenuated Total Reflection

CI Carbonyl Index

EVA Ethylene-Vinyl Acetate

FT-IR Fourier Transform Infrared Spectroscopy

GC Gas Chromatography

GPC Gel Permeation Chromatography

HDPE High-Temperature Gel Permeation Chromatography

HT-GPC High-Density Polyethylene

ICP-MS Inductively Coupled Plasma Mass Spectrometry

LDPE Low-Density Polyethylene

LLDPE Linear Low-Density Polyethylene

M_n Number-Average Molecular Weight

MP Microplastics

MS Mass Spectrometry

M_w Weight-Average Molecular Weight

m/z Mass to Charge Ratio

NGI Norwegian Geotechnical Institute

NTNU Norwegian University of Science and Technology

PCA Principle Component Analysis

PE Polyethylene

PET Polyethylene Terephthalate

PDI Polydispersity Index

PP Polypropylene

PS Polystyrene

PVC Polyvinyl Chloride

Pyr-GC/MS Pyrolysis Gas-Chromatography Mass Spectrometry

SEC Size Exclusion Chromatography

UV Ultraviolet Radiation

Contents

Preface	i
Acknowledgements	iii
Abstract	v
Acronyms and Abbreviations	ix
1 Introduction	1
1.1 The Arctic Expedition by S/Y Fairwinds	3
1.2 Aim and Objective of the Thesis	3
2 Theory	4
2.1 Synthetic Polymers	4
2.2 Plastic Today	6
2.3 Microplastics	7
2.4 Plastic Pollution	8
2.4.1 Plastics in the Ocean and Marine Environments	11
2.4.2 Presence in the Arctic	13
2.5 Degradation of Plastics	14
2.5.1 Photo-Oxidation of the Polymer.	16
2.5.2 Artificial Weathering	18
2.6 Toxicity of Plastic Pollution	19
2.6.1 Adsorption of Metals in Plastics	21
2.6.2 Principal Component Analysis	22
2.7 Characterisation and Analysis of Microplastics	23
2.7.1 FT-IR	25
2.7.2 Pyr-GC/MS	28
2.7.3 GPC	30
2.7.4 ICP-MS	31

3	Experimental	33
3.1	Characterisation of Samples From the Arctic Expedition	33
3.1.1	On board the S/Y Fairwinds	33
3.1.2	Analysis by ATR FT-IR	35
3.1.3	Analysis by Pyr-GC/MS	36
3.2	Weathering Study	38
3.2.1	Production of Samples for Weathering	38
3.2.2	Weathering in UV-Chamber	39
3.2.3	ATR FT-IR Analysis of Weathered Samples	41
3.2.4	GPC Analysis of Weathered Samples	41
3.3	Adsorption of Metals in Microplastics	42
3.3.1	Exposure to Metals	42
3.3.2	ICP-MS Analysis of Exposed Samples	44
4	Results	45
4.1	The Arctic Expedition	45
4.1.1	ATR FT-IR Analysis	49
4.1.2	Pyr-GC/MS Analysis	52
4.1.3	Summary of Results From the Arctic Expedition	56
4.2	Weathering of LLDPE	58
4.2.1	Weathering of Samples	59
4.2.2	ATR FT-IR Analysis	60
4.2.3	Carbonyl Index	64
4.2.4	GPC Analysis	67
4.3	Microplastic Adsorption of Metals	72
4.3.1	ICP-MS Analysis	73
4.3.2	Principle Component Analysis	76
5	Discussion	80
5.1	Samples from The Arctic Expedition	80
5.1.1	ATR FT-IR Analysis	82

5.1.2	Pyr-GC/MS Analysis	83
5.1.3	Comparison of Methods	84
5.2	Artificial Weathering of LLDPE	86
5.3	Metal Pollution in Microplastics	91
6	Conclusion	95
7	Suggestions for Future Research	96
A	Calculations	I
A.1	Calculation of Volume Trawled	I
A.2	Accelerated Aging	II
B	Results	VI
B.1	ATR FT-IR Results from Fairwinds	VII
B.2	Pyr-GC/MS Results from Fairwinds	XVI
B.3	Thickness Profile of films	XVIII
B.4	Calibration Review of Carbonyl Index Model	XXI
B.5	Results from ICP-MS	XXIV
B.6	Pre-processing of PCA	XXXI
B.7	MATLAB code for PCA	XXXII

1 Introduction

Plastic use has increased exponentially since synthetic organic polymers were developed in the mid-20th century. Over 300 million tons of plastic are currently produced yearly to manufacture objects in plastic [2]. Synthetic plastic products are designed to be durable and do not decompose easily in the environment compared to natural polymers, leading to accumulation. Synthetic polymers are today identified as one of the most significant pollutants, especially in the aquatic environment. It is estimated that between 4.8 to 12.7 million tons of plastics are released into the oceans every year [3]. Plastics have been found in the stomachs of many marine organisms from plankton species to whales [4].

The term 'microplastics' is commonly used to describe plastic particles < 5 mm [5]. Compared to macroplastics, the small size complicates their determination in environmental samples and demands for more sophisticated analytical approaches [6]. Microplastics are not uniform, as there are many different types of synthetic polymers commercially available and as a consequence there are a large variety of different polymer types present in the aquatic environment [7]. The analysis of microplastics is a new challenge for the scientific community. Microplastics have also shown to be heterogeneously distributed in nature, and this complicates getting representative sampling of sediments and water [8].

Microplastics are split in two for classification [9]. Primary microplastics are manufactured as microbeads, capsules, fibers or pellets. Examples include microbeads used in cosmetics and personal care products, industrial scrubbers used for abrasive blast cleaning, microfibers used in textiles, and virgin resin pellets used in plastic manufacturing processes [10]. Secondary microplastics are the result of larger pieces of plastic breaking down into smaller pieces. This occurs when plastic debris is exposed to elements and the plastic begins to weather and fragment. The global release of primary microplastics is estimated to be in the range of 0.8 to 2.5 million tons annually [11].

The timeframe for complete degradation of plastics is claimed to be many hundreds of years [12]. Available data for fragmentation indicates that many types of macroplastics are

fragmented to a certain degree within a timeframe of years or decades. Current estimates suggest that fragmentation of larger macroplastics in the environment is likely to contribute significantly more than the emission of primary microplastics. The quantities and rate of microplastics formation and fragmentation from macroplastics is however unknown. The most important processes for the degradation of a synthetic polymer can be divided into: physical degradation (abrasive forces, heating/cooling, freezing/thawing, wetting/drying), photodegradation (usually by UV light), chemical degradation (oxidation or hydrolysis) and biodegradation by organisms (bacteria, fungi, algae) [13]. The mechanical degradation does not stop if the particles are within the size range of microplastics. Thus, the formation of even smaller particles, so-called nanoplastics, is very likely [14]. These nanoplastics and microplastics particles could have different properties compared to the original macroplastics.

As plastic pollution has gained a large interest there is a growing concern about both the ubiquity of nano- and microplastics and the uncertainties surrounding their impacts, hazards and risks to our environment and to human health [15]. The interactions between the nano- and microplastics and pollutants are of concern as there has been an increased focus on the ingestion of microplastics by marine biota, and what effect it can have on humans through the food chain uptake. Adsorption and adsorption capacity of priority inorganic substances such as metals to the particle is now being researched [16]. However, exposure in nature is not to one specific and defined particle type, but to a complex mixture of particles of different polymers, sizes, shapes, surface characteristics and chemical composition. Most of these effect studies, have so far been performed using concentrations higher than what is reported in the natural environment, or using virgin spherical particles which are not representative of types of particles found in nature [9]. Today most plastic products are formulated with various colourants and functional or performance enhancing additives [17]. Because of this, as well as the possible changes in the polymer structure as the particle becomes weathered current studies are far from real-world situations. Currently today, it is not known to what extent these conditions will apply to the real-world environment which limits the reliability of these attempt to risk assessment nano- and microplastic [18].

1.1 The Arctic Expedition by S/Y Fairwinds

Norner supported S/Y Fairwinds on the “Arctic Expedition 2018”, that sailed from the Bahamas to Bermuda - Nova Scotia – Newfoundland - Labrador – Greenland - Iceland and back to Norway. S/Y Fairwinds therefore explore parts of the Arctic waters which is significantly less investigated, but also known to be contaminated by some plastic pollution and microplastics. The Arctic Expedition trawled for macro- and microplastics over a distance more than 5000 nautical miles. Samples were collected on 11 locations, to be investigated to further build knowledge of macro- and micro-plastic in the oceans.

1.2 Aim and Objective of the Thesis

There are still much knowledge lacking on the subject of microplastics. The overall aim of this thesis is to contribute to the increase of the knowledge in the field, as a result the following threefold study aim and objectives were composed:

Aim (1) *Characterise, identify and describe real-life samples of microplastics.*

Objectives - *Describe the 11 samples collected on the Arctic Expedition.*
 - *Characterise the samples with FT-IR.*
 - *Verify and compare the sample results by analysis by pyr-GC/MS.*

Aim (2) *Investigate degradation mechanisms of microplastics.*

Objectives - *Create an accelerated weathering study.*
 - *Measure weathering with FT-IR.*
 - *Evaluate chain-breaking with GPC.*
 - *Investigate the impact of additives on degradation.*

Aim (3) *Investigate interaction with microplastics and inorganic pollutants*

Objectives - *Expose degraded particles to metals.*
 - *Analyse samples using ICP-MS.*
 - *Determinate factor of adsorption of metals to particles.*

2 Theory

2.1 Synthetic Polymers

The word polymer stem from the Greek ‘poly’ which means many, and ‘mers’ which translates to particles [19]. A polymer can be described as a molecule that is composed of many repeating identical parts, called monomers. Polymers are high molecular weight substances. The molecular weights of polymers range between 5000 to $2 \cdot 10^7$ Da [20]. Polymers can be grouped in two; natural and synthetic polymers. This depends on where the macromolecules are sourced from. Examples of natural polymers can be starch, wool, cotton, cellulose and DNA, which can be found in nature. Synthetic polymers are those manufactured to serve specific needs and can be made with unique properties tailored for different uses. Man-made polymers are often commonly referred to as plastics, which per definition are synthetic organic polymers. Examples of common plastics are polyethylene, polypropylene, nylon and Teflon. Most synthetic polymers today are derived from fossil hydrocarbons like petroleum [21]. An overview of some of the most common synthetic polymers be seen in the table 2.1 below.

Table 2.1: Overview of common synthetic polymers listed after their density [22].

Name	Acronym	Density (g/cm ³)	Example of use
Polypropylene	PP	0.90	Bottle caps
Low Density Polyethylene	LDPE	0.91	Plastic bags
High Density Polyethylene	HDPE	0.94	Food containers
Ethylene Vinyl Acetate	EVA	0.95	Plastic wraps
Nylon 12	-	1.01	Packing material
Polystyrene	PS	1.03	Fishing floats
Nylon 6	-	1.08	Textile
Polycarbonate	PC	1.30	Bottles
Poly(Ethylene Terephthalate)	PET	1.35	Electronic components
Poly(Vinyl Chloride)	PVC	1.32	Plastic Film

The first produced polymer was the semi-synthetic polymer celluloid, which was obtained by nitration of cellulose. The first synthetic plastic, Bakelite, was formed from a condensation reaction of phenol with formaldehyde in 1907 [19]. However, large-scale production only dates back to the 1950s. The rapid growth in plastic production has been extraordinary, surpassing almost every other man-made material and to date a world without plastics seems unimaginable. Today the production of plastics is about 381 million tons per year [23]. Plastics have found a myriad of uses in very diverse field such as household appliances, construction, medicine, packaging, electronics and automotive components.

The reason for the success plastics have had in replacing traditional materials such as metals, wood and glass is the ability to modify its properties. It is versatile, high performance, cost effective and is processed with ease. Most synthetic polymers, like PE, PP, PVC, PS and PET are thermoplastics [24]. Meaning that the polymers can be repeatedly heated to a softening point and cooled to solidify. Intermolecular forces hold the polymer chains together, as opposed to thermosets in which polymer chains are covalently bonded and decompose upon heating. The material to make most plastic materials are in the form which is called 'virgin' grade. That is materials which is straight from the manufacturer and have not been processed. The polymer content in a plastic can vary from less than 20% to close to 100%, which is adapted to the application [19].

Depending on the desired use of a plastic, the polymers can be adjusted to leverage advantageous properties like impact resistance, brittleness, elasticity and ductility. This is often achieved by mixing in additives with the polymer [20]. Pigments can be mixed to give a plastic colour, for aesthetic or technical purposes. Glass or carbon fibres can be added for increased strength. Flame-retardants can be added for flame resistance, or stabilisers to ensure better resistance against heat or light [25]. Antioxidants are used to minimise the deterioration when the plastic is exposed to heat, light or chemicals by hindering oxygen to bind to the hydrocarbons in the plastic. An example of a such additive is the antioxidant alpha-tocopherol, more commonly known by the name Vitamin E [26]. Vitamin E is environmentally safe and has good thermal stability which also helps

as a processing stabiliser. There are a multitude of choices for modification by additives, and in order of volume used they can be classified as; reinforcing fibres, fillers, coupling agents, plasticizers, colourants, stabilisers (halogen, antioxidants, UV absorbers and biological preservatives), processing aids, flame retardants, peroxides and antistats [25]. As the levels of additives can be varied and mixed, this give numerous possibilities for plastics.

2.2 Plastic Today

"It is a world free from moth and rust and full of colour, a world largely built up of synthetic materials made from the most universally distributed substances, a world in which nations are more and more independent of localised naturalised resources, a world in which man, like a magician, makes what he wants for almost every need out of what is beneath and around him - how much brighter and cleaner a world [it would be] than that which preceded this plastic age" The future world imagined by Yarsley and Couzens in 1941 ([27], p. 152). Over a decade before the plastic age really begun.

Nearly all aspects of our daily life involve plastics, it is in transport, computers, clothing, footwear and as packaging materials used to transport a wide range of food, drink and other goods [2]. Plastic conserves flavour and freshness when utilised to store food and beverages. Leak-proof and child-resistant plastic containers are especially advantageous for holding dangerous household products such as bleach, ammonia, and other caustic cleaners [28]. Its has a remarkable capability to guard against contamination makes it useful in sterile environments such as hospitals or medical purposes. The benefits of plastics are so far unrivalled by any other material. It is evident that plastics bring many societal benefits and offer future technological and medical advances [29].

Rapid growth in global plastic production was not realised until the 1950s. The annual production of plastics increased nearly 200-fold to 381 million tonnes in 2015 [23]. Assuming an average weight of 75kg, this is equivalent to the weight of 5 billion people - roughly the mass of 2/3 of the world population. At this time the world had in total produced 7.8 billion tonnes of plastic, more than one tonne per person alive [30]. In 2017 it

was estimated that 8300 million metric tons of virgin plastics had been produced.

In Europe, plastic production can be split into three categories [31]; around 40% is created for single-use disposable applications such as food packaging, agricultural films and disposable consumer items. 20% is for long-lasting infrastructure such as pipes, cable coatings and structural materials. The remaining 40% are for more durable consumer applications with an intermediate lifespan, such as electronic goods, furniture, and vehicles.

2.3 Microplastics

Microplastics are defined as small pieces of plastic, often as a sub-fraction of plastic debris [9]. It is not a specific kind of plastic but defined as any type of plastic fragment under a certain size. In most cases that is anything that is less than 5 mm in length [8]. This is the most common definition, but a consensus definition of microplastics has not been reached. This is mostly due to the fact that there is no scientific reason for the cut-off at 5 mm, as no crucial difference in environmental behaviour compared to larger particles has been proven. However, microplastics release into the environment may have far reaching consequences, and there are growing concerns for human health suspected through the accumulation of microplastics in the food chain and/or sorption of toxicants to microplastic while travelling through the environment [32]. Therefore, there is a need to separate the larger plastic debris from the smaller. A lower size boundary for microplastics at 0.1 mm (100 μm) is also commonly used, and any fragments of a lower size is referred to as ‘nanoplastics’ [18].

Microplastics are typically classified into two groups; primary microplastics and secondary microplastics [6]. Shortly one can say primary microplastics occurs at various stages of the lifecycle of plastic products, while secondary microplastics mostly originate from mismanagement of waste during the disposal of plastic products. In the figure 2.1 different ways of generating microplastics are illustrated.

Primary microplastics are pieces of plastic that are manufactured in microscopic sizes for specific applications, and/or are directly released into the environment [34]. It can be a voluntary addition to products like microbeads in toiletries and cosmetics. It can also come

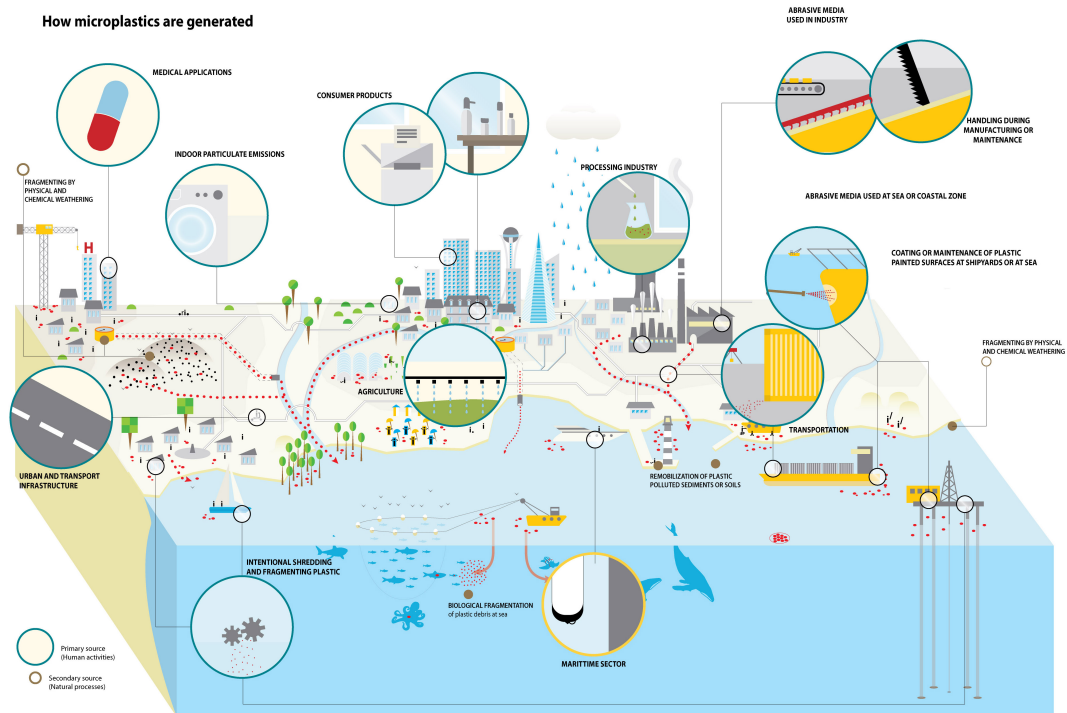


Figure 2.1: Ways of generating microplastics [33].

from the abrasion of large plastic objects during manufacturing, use or maintenance. Examples of this is the erosion of tyres, or the abrasion of synthetic textiles during washing. It can also come from plastic pellets losses, which can occur during the production, transport or recycling stages of plastic [30].

Secondary microplastics are originating from the degradation of larger items of plastic into smaller plastic fragments after it has been exposed to the environment. This occurs through photodegradation and other weathering processes of mismanaged waste, such as accidental losses of fishing nets or disregarded plastic bags [35].

2.4 Plastic Pollution

Plastic debris has been found in all major oceans [36]. It is reported in a multitude of biota. Microplastics have been detected in a variety of terrestrial ecosystems, such as agricultural fields [37]. Contamination of freshwater systems and terrestrial habitats is also increasingly reported, as is environmental contamination with synthetic fibres to indoor

and outdoor air [38]. Plastic waste is now so ubiquitous in the world's environment that it has been suggested as a geological indicator of the proposed Anthropocene era [30].

Plastic pollution, on macro- and micro-level, have attracted considerable public attention in recent years. None of the commonly used plastics are biodegradable and as a result, plastics waste accumulate rather than decompose. By one estimate, in the year 2015 approximately 6300 metric tonnes of plastic waste had been generated where of only around 9% of which have been recycled [30]. Of the remaining 91% only 12% was incinerated, and 79% was accumulated in landfills or the natural environment. If the current production levels and poor waste management trends continue, 12,000 metric tonnes of plastic waste will be in landfills or in the natural environment by 2050 [30].

Today plastics' largest market is packaging. The large growth was accelerated by a global shift from reusable to single-use containers [3]. As a result, the share of plastics in municipal solid waste (by mass) increased from less than 1% in 1960 to more than 10% by 2005 in middle- and high-income countries [30]. Today's society have adapted to production and consumption of large amounts of plastic at very low prices, however the waste treatment come at a much higher cost. Since plastic materials are widely used and for many different purposes in our society, any change in the plastic use system will affect a wide range of societal groups [28]. An illustration of how plastic moves from the production, to society and to the environment can be seen in figure 2.2.

The only way to permanently eliminate plastic waste is by destructive thermal treatment, such as combustion or pyrolysis [39]. Recovering plastic from the waste stream for recycling or to create energy has the potential to minimise these problems, but energy recovery from plastics is often inefficient. It requires air emissions controls and produces hazardous ash. Much of the plastics collected for recycling in the western world is today shipped to countries of lower economic standing, which there often are lower environmental standards, making the balance between environmental protection, clean material cycles, and resource use unstable [40]. Therefore contamination of the natural environment with plastic waste is a growing problem.

The growing concern from the public through the high media attention has now put plastic

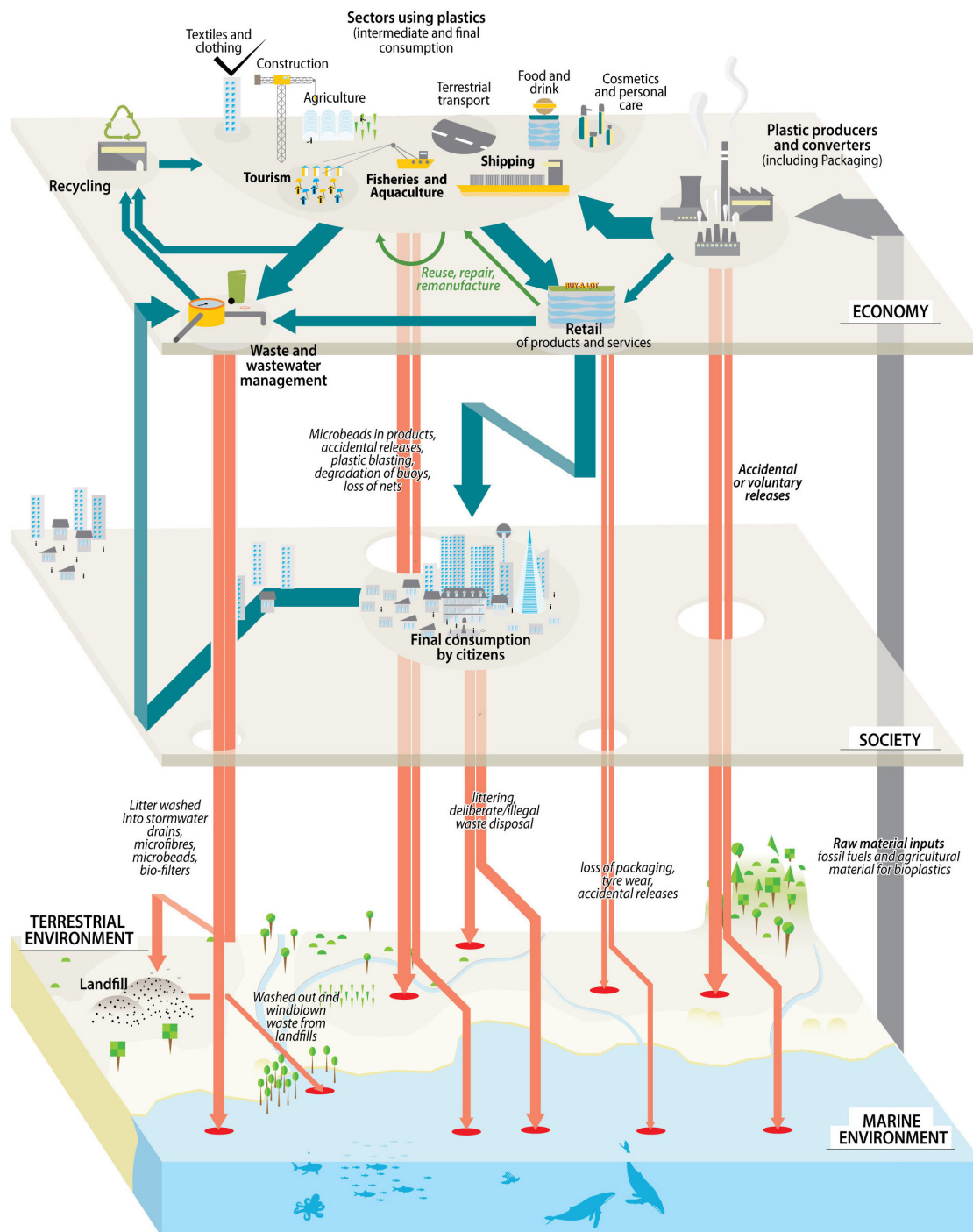


Figure 2.2: How plastic moves from the economy to the environment [41].

pollution on the policy agenda. Participants in a survey across 16 European countries reported to be concerned by littering, and especially marine litter [42]. This year the European Parliament approved a new law banning single-use plastic cutlery, plates, straws

and other plastic items by 2021 [43]. They have also set new targets for the recycling of plastic bottles, and taxes on plastic carrier bags are becoming more common world wide. However there is still a long way to go to solve the problems of plastic pollution.

2.4.1 Plastics in the Ocean and Marine Environments

Marine litter is a result of improper disposal of waste items that are either directly or indirectly transferred to the seas and oceans. Ocean plastic can persist in sea surface waters, eventually accumulating in remote areas of the world's ocean [44]. Estimates suggests that up to 10% of all plastics produced end up in the oceans, where they may persist and accumulate. This means that plastics make up most of the marine litter worldwide [3]. Numbers indicate that its proportion consistently varies between 60% and 80% of the total marine debris [36]. It is so bad that today the area between California and Hawaii has been titled 'the Great Pacific Garbage Patch' (also known as the Eastern Garbage Patch), as a series of currents create a circular effect, accumulating debris and garbage inside the North Pacific Gyre [45]. Here there are mountains of plastic waste, which are reported to be containing at least 79 thousand tonnes of floating ocean plastics [46].

It is also clear that debris reaching the marine environment accumulates in different areas including coastal beaches, mangroves, wetlands and deltas, the water column and the sea floor [36]. In the water column, plastic waste can be found floating at the surface as well as being submerged down in the deepest waters [47]. Plastic waste is also present on the seabed and in the sediment from the shallow coast to the floor of abyssal plains [48]. In addition, marine organisms can through ingestion accumulate some of the debris within the marine environment. Using models and collected data from expeditions there are several estimates on the order of plastic pollution in the ocean. One found that there is a minimum of 5.25 trillion particles weighing 268,940 tons [49]. And that a tremendous loss of microplastics is observed from the sea surface compared to expected rates of fragmentation. The accumulated number of microplastic particles is estimated to range from from 15 to 51 trillion particles, weighing between 93 and 236 thousand metric tons

[50]. This is approximately 1% of global plastic waste that entered the ocean in 2010. In figure 2.3 the estimations from van Sebille is used, showing the estimation of plastic pollution in the oceans as well as where in the sea it is located.

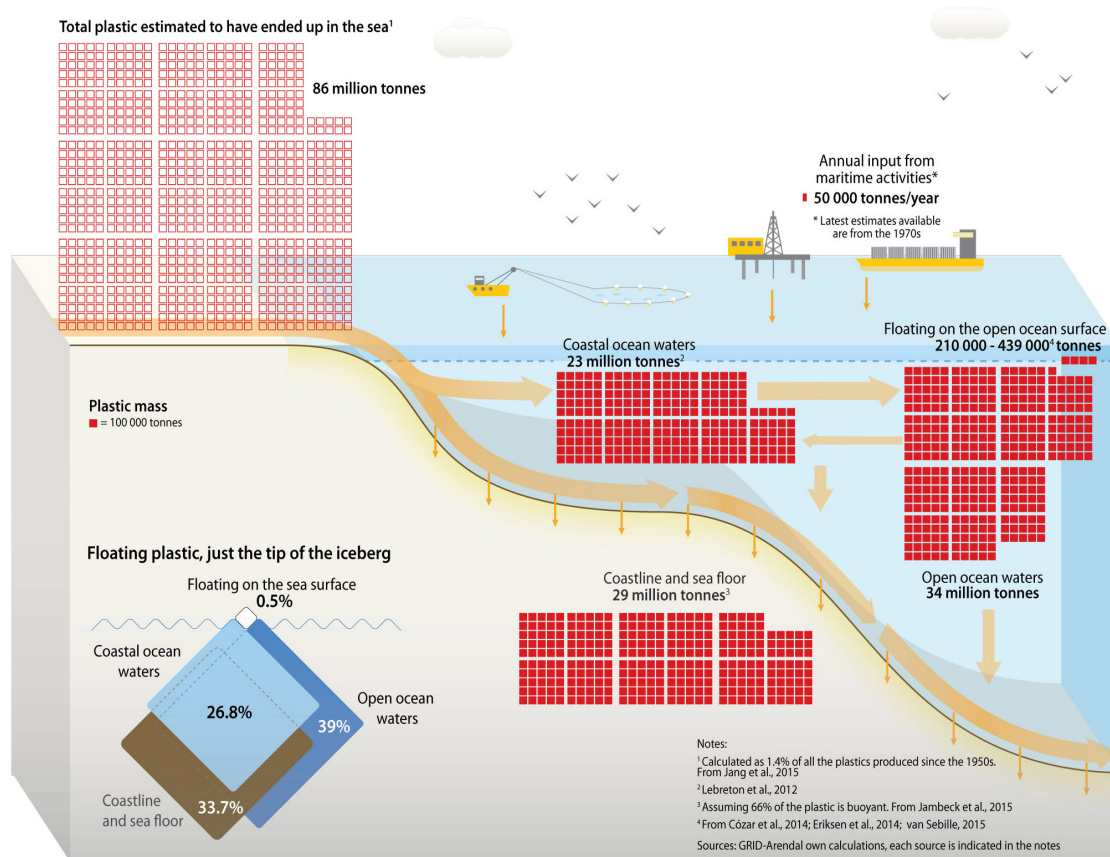


Figure 2.3: How much plastic is estimated to be in the oceans and where it may be [51].

Microplastic contaminates shorelines worldwide. An increasing number of studies have estimated or quantified the environmental occurrence of microplastic in many marine areas such as surface waters, shorelines, coastal sediments, beach sands, fjords, arctic waters and deep-sea environments [52]. There have also been a significant number of studies identifying microplastic particles present in a multitude of different wild-caught marine organisms, from plankton to whales. The amount of microplastics in and on the ocean surface is not well known. Estimates vary greatly and rarely include plastic fragments that are smaller than 0.3mm. This is mostly due to the fact that most sampling is done by trawling for plastics on the surface have been done using plankton type nets that have mesh size larger than or equal to 0.3mm (300 μm) [53]. There are also limited

methodologies for analysing plastic fibres in samples, as well as a lack of understanding in how these particles fragments and sink.

Microplastic is a term used for a variety of particles and can have a large diversity in characteristics like shape, size, density and polymer type as shown in table [2.1](#). This will affect their fate in the ocean. As different plastics have different densities, they will occur at different places in the world's oceans and seas [54](#). Plastics that are made with polymers that have a low density are typically expected to float and would spend a significant period of time at the surface. Seawater has an average density of 1.0236 g/cm^3 [55](#). Plastic types with densities much higher than this would be expected to sink immediately through the water column towards the seafloor. However, in reality the processes are slightly more complicated. Buoyant plastic items can be transported to the seafloor if natural processes alter their relative density [22](#). Occurrences such as biofouling by bacteria, algae and large marine organisms can lead to sinking [56](#). For some small low density microplastic particles, heteroaggregation with other dense particulate matter and repackaging in faecal materials after ingestion by organisms can promote sedimentation. Sinking of small dense microplastics can also be slowed by frictional forces [49](#). Any additives added to the plastic can also add to this complexity.

As a result, marine sediments have been proposed as long-term sinks for microplastic, and studies have shown results with high concentrations of microplastic reported [48](#). On highly contaminated beaches the sediment weight could have shown to be up to 3% microplastics. While sampling from shorelines and beaches are easily collected, costal sediments and especially sampling from deep sea sediments are complicated, and expensive [34](#). There are therefore few studies done, and much uncertainty around the estimated numbers on pollution.

2.4.2 Presence in the Arctic

The subtropical ocean gyres are recognized as great marine accumulation zones of floating plastic debris [45](#). Levels of plastic pollution are typically thought to decrease away from areas of high human impact and commercial activity, thereby assumed to be

decreasing towards the polar latitudes [57].

The population north of the 60° latitude is low but an oceanic circulation model by van Sebille predicts a plastic accumulation zone within the Arctic Polar Circle, specifically in the Greenland and Barents Sea [58]. This is due to the fact that the Arctic Ocean is a part of the global Thermohaline Circulation.

Warmer water from lower latitudes flows north where it cools and forms deep water, and this could lead to the accumulation of plastic waste from higher populated latitudes [59]. It is found that plastic debris is scarce or absent in most of the Arctic waters. However, high concentrations in the Greenland and Barents seas were found [60]. On inspection of the plastic particles found it is assumed to be aged debris that originated from distant sources.

Analysis of ice collected around the Arctic Circle pointed to a considerable abundance of microplastics in the sea ice, in contrast to the low concentrations found in surface waters [61]. The concentrations found in the Arctic Sea ice is even of magnitudes greater than what is reported in highly contaminated surface waters, as the Pacific Gyre [45]. It is hypothesised that when the sea ice forms it scavenges and concentrates particulates from the water column, where irregularly shaped particles and particles less dense than water can be effectively trapped. This contradicts the expectation that the Arctic would show low levels of pollution as it is a fragile area of relatively low direct human impact.

2.5 Degradation of Plastics

The timeframe for complete degradation of plastics is claimed to be many hundreds of years [23]. In the polymer industry the term “degradation” is most often used to describe processes that lead to a decline of polymer properties. However, in environmental science, when talking about degradation one is more interested in the chemical reactions that cause the breakdown of polymers, and the properties and potential hazards associated with chemicals liberated by degradation of the polymers [62].

The most important processes for the degradation of a synthetic polymer can be divided into [35]; physical degradation (abrasive forces, heating/cooling, freezing/thawing,

wetting/drying), photodegradation (usually by UV light), chemical degradation (oxidation or hydrolysis) and biodegradation by organisms (bacteria, fungi, algae) [55]. Mechanical degradation is also an important factor with regard to plastics in the aquatic environment. For marine debris the mechanical degradation occurs as a result of the motion of the waves, wind and sand [63]. The waves can lead to grinding, or to fragmentation due to the with mechanical impact on the particles due to impact with sediments, rocks or other hard surfaces.

The polymer characteristics such as mobility, tacticity, crystallinity, molecular weight, the type of functional groups and substituents present in its structure, and plasticizers or additives added to the polymer all play an important role in its degradation rate [64].

Most plastics degrade first at the polymer surface, which is exposed and available for chemical or enzymatic attack [65]. This is called 'deterioration' which is a superficial degradation that modifies the mechanical, physical, and chemical properties of a given polymer [66]. The second step is the de-polymerisation which is characterised by the cleavage of polymeric molecules into oligomers, dimers, or monomers. Therefore, degradation of microplastic proceeds faster than meso- and macroplastic, as microplastic has a higher surface to volume ratio [67]. Current estimates suggest that fragmentation of macroplastics in the environment is likely to contribute significantly more than the emission of primary microplastics.

The first visual effects of polymer degradation are changes in colour and crazing of the surface. As the surface cracks, the inside of the plastic material becomes more degradation [69]. When plastic materials are in the environment they are exposed to conditions that could promote weathering by one or more of the above processes. However, not all kinds of degradation pathways are effective on all polymer types [35].

When plastic is floating on the surface of the sea it is exposed to moderate temperatures, solar radiation, and oxidising conditions. Since temperatures are moderate, the most important factors initiating degradation are oxygen and sunlight [70]. The different degradation paths plastic particles in the ocean can take are illustrated in the figure 2.4.

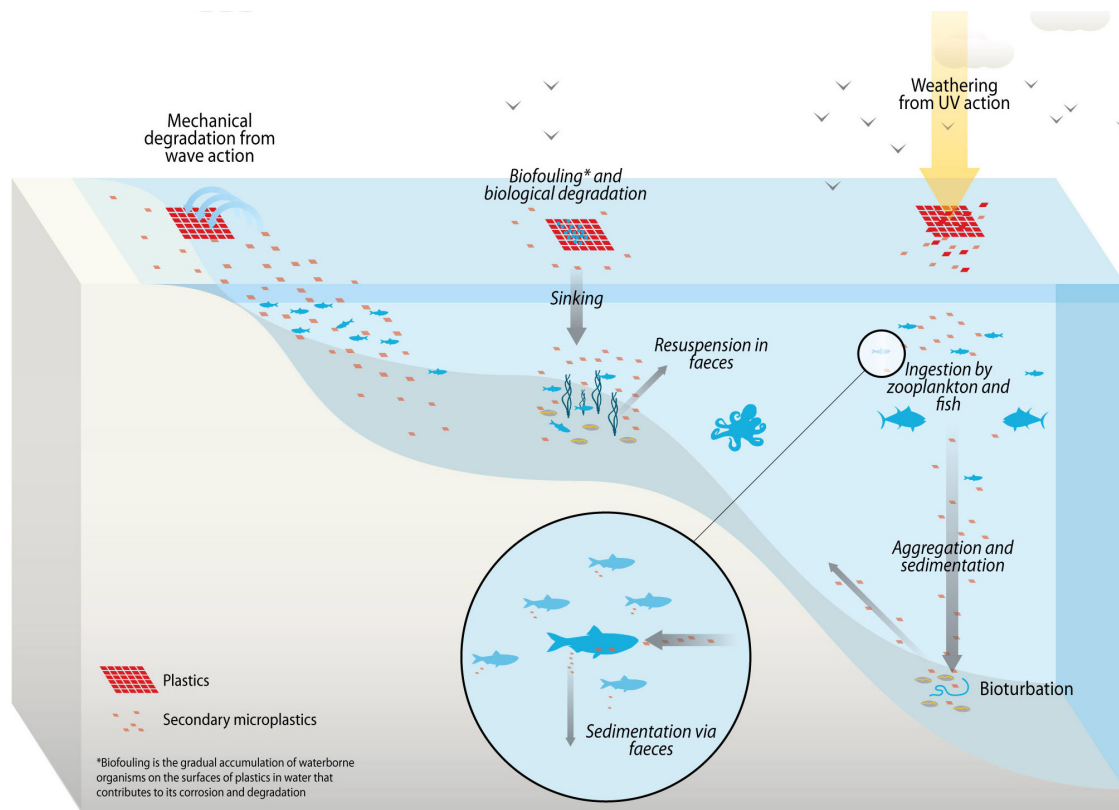


Figure 2.4: Natural processes acting on the distribution and fate of plastics in the ocean [68].

As mentioned, fragmentation of plastics leads to smaller particles which increases the surface area, and therefore increases the polymer's susceptibility to further degradation [67]. The degradation mechanisms are highly linked, as for example photodegradation can make the particle brittle, which would make it more likely to be affected by mechanical degradation [71]. If the resulting mechanical stress breaks up the polymer chains on the surface, further erosion or embrittlement can occur, and enough force can result in the particle getting fragmented into two or more particles. A common result of weathering is breaking of the polymer chains. Polymers have long chains entangle with each other to give structural integrity. If degradation results in cleaving the chains, the molecular weight of the polymer decreases [72].

2.5.1 Photo-Oxidation of the Polymer.

Ultraviolet irradiation, which has the wavelength from 10 – 400 nm, in combination with oxygen is commonly known as the most effective degradation of synthetic polymers [73]. It

causes chain scission in the polymer material which results in the loss of important physical properties such as impact strength, tensile strength, elongation at break and can be observed as cracking, chalking and colour changes. The term of photodegradation can be distinguished from photo-oxidation of the polymer. In the latter, oxygen is involved in the process while in the former only energy from light is responsible for the photodegradation [74].

The principle of photodegradation states that the amount of energy absorbed by the polymer must exceed the bond energy to cause degradation. In general UV-A irradiation does not have enough energy to break the chemical bonds, therefore cause degradation, of the most common synthetic polymers. UV-B radiation have however shown particularly efficient in photodegradation of synthetic polymers [74]. UV-C radiation has sufficient energy to break the bonds, but as the radiation is absorbed by the atmosphere it never reaches the earth's surface [75]. Therefore, only the UV-A and UV-B have any effect on the degradation process.

Temperature increase also helps the degradation process, as it speeds up the oxidation rate. At sea there is little heat build-up, so oxidation rates are therefore expected to be slower than on land [76]. There is a general rule that the reaction rate doubles for a polymer with a 10°C increase in temperature. Degradation is as a consequence also expected to be quicker in tropical region, compared to polar regions.

The UV irradiation causes hydrogen radicals to form in synthetic polymers [14]. The polymer radicals have limited mobility and are restricted to hydrogen abstraction or recombination with nearby radicals. Hydrogen is mostly abstracted on the tertiary carbon bond, causing the chain scission and cross-linking of the polymer backbone. The polymer can then react further with oxygen, which leads to the formation of carbonyls (C=O) and vinyl (CH₂=CH) groups [77]. This then leads to conformation and crystallinity of the polymer.

2.5.2 Artificial Weathering

The problem with the traditional method of service life prediction is that it takes too long to obtain the needed assessment. For many decades, accelerated tests have been used successfully to assess the lifetime of products. By definition durability of a material or product implies its performance over a longer time scale [78]. The expected life span of polymer products varies considerably but is generally measurable in years and can be 20 or even 50 years.

Artificial weathering is a very helpful test procedure to assess the performance of a product against environmental conditions and UV exposure [79]. It allows for a product to be treated under an artificial weathering environment and helps to show any physical changes that can be expected over its lifetime. Artificial weathering can include simulation of the effect of UV-light, oxygen, moisture, humidity, temperature and other climatic cycling on materials durability [80]. At least one environmental stress has to be taken outside its natural range in order to achieve acceleration. This can be higher light intensity, shorter dark periods or higher temperature.

The UV component of sunlight only accounts for 5% of its energy, but is responsible for most of polymer degradation [81]. The UV-A and UV-B wavelengths that affect degradation are from 295 - 385 nm. Many weathering chambers equipped with xenon arc lamp filters are normalised to daylight at 340 nm. Thus, laboratory weathering equipment in the United States commonly measure UV irradiance during exposure in a 1 nm band at 340 nm. A rule of approximation is then done assuming the irradiance at 340 nm is one percentage of the total irradiance at the wavelengths 295 - 385 nm [82].

As a rule of thumb in the polymer engineering it is said that the polymer degradation doubles with a temperature increase of 10 °C [82]. However, studies shows that increasing temperature 10°C might accelerate one material by 25% and another by 100% [83]. Some materials are greatly accelerated by UV with shorter wavelengths than naturally occurring and some are not [84]. A good accelerated test will keep conditions as close to natural as possible and properly account for most or all of its acceleration so that the number of

hours it will take to apply a year's worth of photos can be calculated, corrections can be made for the effects of temperature and the moisture effects can be properly simulated.

In principle, the rates of pure photochemical reactions do not depend on temperature [85]. However, polymer degradation is much more complicated. The degradation is due to the reaction of the carbon atoms in the polymer with oxygen, followed by further decomposition and reaction of the initial products through many stages [86]. Absorption of light energy serves at the initial step, where each branching series in the polymer has its own temperature dependence. Over a small temperature range, temperature effects can therefore be estimated from the Arrhenius Equation [82], which can be seen below.

$$k(T)=A \cdot e^{\left(\frac{-E_a}{RT}\right)} \quad (2.1)$$

Where k is the reaction energy, A is the scaling factor related to entropy, E_a is the activation energy, R is the gas constant, and T is the temperature in kelvins.

The Arrhenius equation is one of the best-known models for assessing the lifetime of polymers and is commonly used to predict the combined effects of temperature and time [87]. It is particularly useful for the accelerated testing of polymers as it allows short-term tests conducted at elevated temperatures to be used to assess long-term exposures at lower temperatures.

2.6 Toxicity of Plastic Pollution

Microplastic pollution is perceived as an environmental threat much because the ingestion of larger plastic debris has been observed to cause gastrointestinal blockage in mammals, fish, and birds [56]. If the large marine mammals do not ingest them directly, from marine environment they can indirectly through the ingestion of other organisms that can adsorb or have consumed microplastics. It has been demonstrated that microplastic particles can induce both physical and chemical toxicity [18]. This can occur when the particles attach

to the outer or inner surfaces of an organism in water. This can have consequences such as physical injuries, inducing inflammation and stress, or can result in a blockage of absorptive surfaces (like blockage in the intestines) and subsequently reduced energy intake or respiration issues. Physical toxicity can also manifest itself after tissue translocation of particles, that is, a transfer from the outside of the body into tissues [9]. In addition to the mechanical impacts of plastics on marine organisms, such as suffocation or starvation due to entanglement or ingestion of plastic pieces, a relationship between chemical burden and plastic ingestion has been reported [4].

Considering the effect of sizes only, it has been concluded that exposure to microplastics has a significant negative effect on food consumption, growth, reproduction and survival across all population groups [5]. Especially sensitive are Zooplankton, non-mollusc macroinvertebrates and juvenile fish [88].

Studies have indicated that microplastics can absorb or adsorb organic pollutions from the surrounding sea water. Marine plastic debris is recovered globally with measurable amounts of organic pollutants [32]. Outside possible sorption from surrounding sea water, several additives are contained in plastic particles. Colorants, UV-stabilizers and matting agents, brominated flame retardants, phthalate plasticizers, bisphenol A and anti-microbial agents are additives of particular concern [89]. It is estimated that these chemical compounds can escape rapid degradation and may thus become persistent and subject to long-range transport. The rate, as well as the extent of sorption can vary depending on the nature of the pollutant, the chemical composition, the plastic type, and other variables. However, plastic particles recovered from the ocean have been found to contain pollutant concentrations orders of magnitude higher than the water from which they were collected [15]. When ingested by organisms, plastic particles could be a biomagnification route of organic chemicals sorbed to or contained in the plastics [90]. However, the significance of plastic particles as transport vectors of organic pollutants to marine organisms and to remote regions such as the Arctic remains uncertain and has not been quantified.

Major flaws in most effect studies have been pointed out as that they are either performed using concentrations that are much higher than what is currently being reported in the

environment or using types of microplastics for which limited exposure data exists [9]. Most studies are performed on spherical virgin polystyrene plastics particles, these are not representative of the plastics that can be found in the real-world environment. Many studies have been conducted using homogenous virgin PE or PS particles that do not represent the heterogeneity in real-world particles from nature [91]. Polypropylene, polyester and polyamide particles have so far been underrepresented in exposure studies. Most research studies have assessed the effects of microplastics on individuals instead of the effects on cells, organs or populations. Amid the biological effects identified in organisms exposed to microplastics in laboratory studies, the environmental relevance of such laboratory studies is not yet clear. This is due to the fact that the majority of such studies have used particle sizes that are smaller, or concentrations that are greater, than what is reported realistic for the environment [6]. Nonetheless, it should be recognised that there are uncertainties about what concentrations are realistic in the environment as well, since the ability to isolate and quantify particles from environmental media is methodologically restrained, especially for smaller particles [92].

2.6.1 Adsorption of Metals in Plastics

It is established that microplastic ingestion can cause different problems. The presence of organic chemicals on plastic debris has been established, but the presence of metals has only become a concern [4]. The concern is due to the ability of microplastics to adsorb and accumulate metals on their surfaces from the surrounding environment. Metals like Al, Cd, Co, Cr, Cu, Fe, Hg, Mn, Pb and Zn are known to have a variety of harmful effects on living organisms [93]. The accumulation of metals on marine plastic debris may be explained by both the chemical ingredients of the plastic like catalysts, fillers, and plasticizers in addition to the degradation and fouling of aquatic plastic debris that may generate active sites for the sorption and/or bioaccumulation of metals [32]. Therefore, plastic pellets may serve as a passive sample for metal contamination in the marine environment similar to that of organic chemicals. Recent studies also show that microplastics are able to adsorb and accumulate metals, most of which come from

industrial waste, fuel combustion and antifouling paints [16].

Studies done by trace metals to virgin and aged plastic pellets show that the ability to adsorb metals were attributed to the modification of the surface through the attachment of organic matter during the experiments, with regard to weathered pellets, their long-term pre-modification through photooxidation and attrition of charged material [94]. This suggests that plastic debris may accumulate greater concentrations of metals the longer it remains at sea. Other studies show a significant interaction between these the metals copper (Cu) and zinc (Zn) to virgin polystyrene (PS) beads and aged polyvinyl chloride (PVC) [16].

Studies comparing the metal adsorption of five plastic types: polyethylene terephthalate (PET), high-density polyethylene (HDPE), polyvinyl chloride (PVC), low-density polyethylene (LDPE), and polypropylene (PP) show that accumulation patterns were not consistent over time, and in general all types of plastic accumulated similar concentrations of metals [95].

To describe and compare the rate of metal adsorption onto microplastic pellets modelling adsorption kinetics data is useful [96]. One possible way of doing this is to calculate the partition coefficients (K_{pw}) [16]. The application of partitioning coefficient is based on the concentration ratio of adsorbed metals on the respective plastic to aqueous metals. The K_{pw} is calculated using the following equation:

$$K_{pw} = \frac{[MeP]}{[MeW]} \quad (2.2)$$

where $[MeP]$ is the concentration of the respective metal on the surface of the plastic indicating the adsorption in $\mu\text{g/g}$ and $[MeW]$ is the concentration of the metal in the surrounding seawater in $\mu\text{g/L}$.

2.6.2 Principal Component Analysis

Finding a solution for pollution is a permanent task of researchers, which involves not only finding new and advanced analytical methods to identify quality and quantity of

contaminants, but also applying complex statistical methods that allow an overall assessment of the interaction of these contaminants in the food chain and the health risk associated with their consumption by humans [97]. Principal Component Analysis (PCA) is a dimensionality-reduction method that is often used to reduce the dimensionality of large data sets, by transforming a large set of variables into a smaller one that still contains most of the information in the large set. It has been reported used in many studies assessing metal pollution [98]. This powerful method allows identifying the different groups of metals that correlate and thus can be considered as having a similar behavior and common origin [99].

PCA can be seen as a technique that constructs the theoretical variable that reduces the total residual sum of squares after fitting a straight line to the data for each species using latent variables covering most of the variance. The latent variables can be described using scores and loadings [100]. The scores are the coordinates using the principal components as a new coordinate system, and the loadings are the direction of the latent variable. A plot of the scores can be used to detect clusters, potential outliers and other groupings within the data set [101]. A positive score means that the concentration of variables increases along the PC axis, while a negative score means that the concentration of variables decreases along the axis and a score close to zero means that the concentration is poorly related to the PC axis [97]. By inspecting the loadings plot, correlated variables can be detected. If the angle between two variables in the loadings plot is close to zero they are positively correlated, if it is close to 180 it is negatively correlated, while a 90 degree angle indicates no correlation.

2.7 Characterisation and Analysis of Microplastics

To understand the potential impacts microplastics have on the planet, the first important step is to understand the particles in themselves. There has been a huge focus on quantifying the abundance in nature, especially in the marine environment [102]. One of the issues is that microplastics are a very heterogenous group that vary greatly in size, shape, colour, specific density, chemical composition, and other characteristics. There are many

different types of synthetic polymers commercially available and as a consequence there are a large variety of different polymer types present in the aquatic environment [103].

The analysis of microplastics is a new challenge for analytical scientists. So far there is no specific methodical criteria to estimate the composition, abundance or distribution of MPs, and a wide variety of approaches are reported for identification and quantification [104]. The small size of microplastics complicates their determination in environmental samples compared to macroplastics.

For large plastic particles visual identification relying on physical characteristics are relatively common, but with decreasing particle size the probability of misidentification grows. Chemical identification is therefore necessary to ensure the accuracy of collected pollution data [105]. Raman and Fourier-Transform Infrared (FTIR) spectroscopies are the most commonly reported techniques employed to identify MPs [7]. Quantification of MPs from personal-care products have been reported through density separation and a subsequent quantitation with high-temperature gel-permeation chromatography (), which is also commonly referred to as Size Exclusion Chromatography (SEC) [106]. Thermal analysis methods, such as differential scanning calorimetry (DSC) can give chemical identification and mass quantification of particles, and is often used together with optical microscopy [107]. Another thermal analysis technique which is more commonly utilised on MPs is pyrolysis-Gas Chromatography coupled with Mass Spectrometry (pyr-GC/MS).

Chromatographic techniques are generally limited to pyrolysis gas chromatography (Pyr-GC) for identification of MPs due the fact that most polymers have a high molecular weight. However, other chromatographic techniques such as GC/MS used for identification of organic pollutants found in MPs. For the analysis of inorganic pollutants, such as metals, inductively coupled plasma-optical emission spectroscopy (ICP-OES) and inductively coupled plasma-mass spectrometry (ICP-MS) are common [108] [109]. High MW is also an issue for analysing MPs by traditional mass spectrometry (MS) techniques, but the development of matrix-assisted laser desorption/ionization time-of-flight (MALDI-TOF) shows promise for analysing polymers under 10,000 Da [110] [111]. Another promising technique is Nuclear magnetic resonance (NMR) [8]. As a technique it yields

structural and quantitative information, such as the polymer functional groups, percentages of copolymers and orientation of functional groups. However, the technique has until now only been used qualitative but not quantitative on this type of samples [112].

The analysis methods used in this thesis are FTIR, Pyr-GC/MS, GPC (SEC) and ICP-MS.

2.7.1 FT-IR

Infrared (IR) spectroscopy is ideally suited to qualitative analysis of polymer as well as to quantification of components in polymer mixtures [113]. Fourier-transform infrared (FT-IR) spectroscopy is known to be a dependable method for accurate identification [102]. Infrared radiation excites molecular vibrations, and the excitable vibrations depend on the interaction between specific wavelengths and the molecular structure of a substance. As energy of the IR radiation excites a specific vibration on a specific wavelength a certain amount of this is absorbed, and as this is recorded the measurement enables the characteristic IR spectra of a sample [105]. The positions of absorption bands in the spectrum give information about the presence or absence of specific functional groups in a molecule and as a whole the spectrum constitutes a ‘fingerprint’ that can be used to determine the identity of the sample [7].

Rather than shining a beam of only one wavelength at a sample, a beam with many frequencies of light is shined at once. The returning light is then recorded. Different wavelengths are modulated at different rates, so that at each moment the beam has a different spectrum [114]. The acquisition of a spectrum is obtained by a mathematical algorithm called Fourier transform, which converts the raw data containing information on the light absorption into a spectrum of light absorption for each wavelength. This processing to decompose the output signals into wavelengths, is the reason for the name Fourier transform infrared spectroscopy (FT-IR).

Spectra are recorded by amount of IR light that is absorbed or transmitted by the material versus the wavenumber. The wavenumber the reciprocal of the wavelength of the wave and is commonly given in reciprocal centimeters (cm^{-1}). Most bond vibrations occur in the

middle of the infrared range, at around $4000\text{--}400\text{ cm}^{-1}$ [115]. Two factors determine the absorbance at a wavelength. The first is the dipole moment. Vibrations will only occur if there is a change in the dipole moment caused by the IR irradiance at a certain wavelength [116]. And the second is the number of bonds and/or molecules that has a vibrational mode at the wavelength. As an example, the electric dipole moment in H-O is larger than that in C-H, which will result in greater absorbance bands. However, on symmetric bonds like C-C and O-O there are is no electric dipole and therefore no absorbance bands observed.

In general, a non-linear molecule with n atoms will have $3n - 6$ normal modes of vibration, but a linear molecule has $3n - 5$ such modes, as rotation around its axis cannot be observed [117]. All vibrations can be described by names depending on the effect the irradiation has on the positions of atoms in a molecule, a list can be seen below [115]:

- Stretching: a change in the length of a bond, such as C-H or C-C.
- Bending: a change in the angle between two bonds, such as the H-C-H angle in a -CH_2 group.
- Rocking: a change in angle between a group of atoms, such as a -CH_2 group and the rest of the molecule.
- Wagging: a change in angle between the plane of a group of atoms, such as a -CH_2 group and a plane through the rest of the molecule.
- Twisting: a change in the angle between the planes of two groups of atoms, such as a change in the angle between 2 -CH_2 groups.
- Out-of-plane: a change in the angle between any one of the C-H bonds and the plane.

Furthermore, phenomenons like overtones, combination vibrations and resonance give rise to additional IR bands [118].

Absorbance bands can be classified in two types; group and fingerprint frequencies. Group frequencies are characteristic of small groups of atoms or functional groups such as the common CH_2 , OH, and C=O [116]. These bands are usually absorbed above 1500 cm^{-1} . Fingerprint frequencies are characteristic of the molecule as a whole. These types of

absorbances are typically seen below 1500 cm^{-1} . As a result, this region of the spectrum is less reliable for identification, and the absence of a band is often more indicative than the presence of a band in this region.

Plastic polymers have very specific IR spectra, and different distinct band patterns makes FT-IR an optimal technique for identification of microplastics [104]. The comparison with a reference spectra is necessary for correct plastic identification. There are several different FTIR sampling techniques, but the most common and also most suitable for MP analysis is attenuated total reflectance (ATR). Here the sample is pressed against a diamond, zinc selenide or germanium crystal and the absorption of the evanescent wave is measured. The IR light is directed on the sample, and the changes in the IR beam due to internal reflection in the sample is recorded. This is a reflection technique, and will therefore only penetrate the top $2\text{ }\mu\text{m}$ of solid samples [102]. This technique requires little to no sample preparation and very reliably produces high quality spectra.

For microplastics, the application of FT-IR microscopy is important [7]. Here the use of both reflectance and transmittance is feasible. The reflectance mode has the disadvantage that irregularly-shaped particles, such as microplastics, have challenges because of the refractive error [105]. The transmittance mode needs IR transparent filters and is limited by a certain thickness of the samples. The use of micro-ATR objectives in combination with microscopy is promising as the spectra can be collected at the surface without manual handling.

FT-IR can also give information on the physico-chemical weathering of a sample by detecting the intensity of oxidation. The formation of double bonds from chain scission can be detected by vinyl C-H bending and C=C stretching [7]. Numerous oxidation products can also be detected by the appearance of O-H, C=O and C-O stretching bands. The specific location of absorption bands is dependent on the specific mechanism behind the degradation of a polymer, and the local chemical environment which affects the dipole moment of the vibration [118].

2.7.2 Pyr-GC/MS

Gas chromatography coupled with mass spectrometry (GC/MS) is widely recognized as one of the most powerful analytical methodologies, where mass resolving, and mass determination are synergistically enhanced through the high-resolution ability of GC [119]. There is however a limitation of the method, and it lies in the volatility of the sample. 30% of all molecules on the planet have a volatility to be analysed with GC, and by the use of good solvents about 85% can be treated with liquid chromatography (LC) [120]. However, most polymers have troubles being properly solved and for this reason, common synthetic polymers are out of the GC and LC application. GC/MS combined with pyrolysis (pyr-GC/MS) ranges all organic substances as long as they can be fragmented by thermal energy or chemically assisted thermolysis. Therefore, pyr-GC/MS is one of the emerging techniques for polymer characterisation [120].

Under controlled conditions at higher temperatures (300 – 1400°C) in the presence of an inert gas as helium, reproducible decomposition products which are characteristic for the original sample are formed [106]. The pyrolysis unit is connected to the injection port of the GC so the pyrolyzed products are swept in by the carrier gas to be chromatographically separated. The pyrolysis systems are generally classified into two groups depending on the heating mechanism; the continuous-mode pyrolyzer (also called furnace pyrolyzer) and the puls-mode pyrolyzer (flash pyrolyzer) [119].

Gas chromatography is based on the separation of compounds between a mobile and stationary phase. The mobile phase is an inert carrier gas, and the stationary phase is a microscopic layer on the inside of the column [121]. The separation of compounds is based on the different strengths of interaction of the compounds with the stationary phase. The boiling point of a compound is often related to its polarity, and therefore the interaction to the column. The lower the boiling point of a component is, the higher the vapour pressure of the compound and the shorter retention time usually is because the compound will spend more time in the gas phase. The pyrolyzed compounds elute through the column at different times depending on their chemical and physical properties that leads to different interactions with the column. After the column the compounds are detected by mass

spectrometry. MS is used to determine the nominal mass and is able to give detailed structural information about the analyte [122]. The instrument measures the m/z abundances of the ions or fragments that are formed by ionization.

One of the main advantages of Pyr-GC/MS for analyzing microplastics is that it does not require any sample isolation and it allows for the analysis of whole MP particles [113]. Polymers and any residual matrix can be placed directly into the pyrolysis unit and still yield qualitative and semi-quantitative data. Pyr-GC/MS also allows detection of polymer-associated substances, which can be detected during the pyrolysis of the polymer itself, for example at 700° C or by thermal desorption at lower temperatures [17].

Pyrolysis of polyethylene generates a large homologue series of n-alkadienes, n-alkenes and n-alkanes [17]. They are eluted in triplets, where the n-alkene has the highest abundance. HDPE has minimal branching, and therefore pyrolysis of it will result in a smaller number of pyrolysis products in the triplet homologue series than for example LDPE. This can be used to distinguish between the types of polymer. Virgin polyethylene is often shown to have different pyrolysis products than aged PE, as aging can lead to chain scissoring [122].

A range of polymer additives and manufacturing residues have been reported to be detected by Pyr-GC/MS, by thermal desorption and at pyrolysis temperatures [106]. However, additive identification has proven to be challenging as there are several thousands of different additives, many of which have similar structures and will therefore produce similar mass spectra and/or pyrolysis products [123]. It is also common to add more than one additive to a polymer, adding to the complexity. Additives of higher molecular weight does not desorb at lower temperatures (300°C) and therefore it is necessary to fragment at higher temperatures, requiring elucidation of their pyrolysis pattern.

Pyr-GC/MS allows for a relatively good assignment of polymer types in microplastics, however there are some disadvantages. For one, it has the disadvantage that particles will have to be manually placed into the pyrolysis tube [105]. Only particles of a certain minimum size can be manually this results in that a lower size limitation of particles that can be analysed. Also, Pyr-GC/MS only allows for one particle per run and it is therefore very time consuming to process large quantities of samples.

2.7.3 GPC

In the polymer industry Size Exclusion Chromatography (SEC) is the most common separation method. SEC is commonly used for characterisation of the mass distribution of the different products or polymer chain lengths. SEC separates macro-molecules on porous particles with a defined pore size [124]. For polymers and non-aqueous mobile phases, the term gel permeation chromatography (GPC) is also used. In principle SEC separates purely according to size, or hydrodynamic volume, and there is an assumption of no interactions taking place between the solutes and the stationary phase [124].

Analytes that are too large to penetrate the pores of the particles are transported with the mobile phase between these particles and elute fastest (V_0). The smaller analyte that completely penetrates into all the pores elute slower and has the retention volume V_i . Solute of intermediate size elute in between. Therefore the elution volume V_e , for a compound is given by the equation below:

$$V_e = V_0 + K \cdot V_i \quad (2.3)$$

where the K is the coefficient for distribution, and will have values between 0 and 1.

When the analytes elute to the end of the column they can be detected [125]. There are several detectors available, like a viscometry detector, light scattering detector, infrared detector or a differential refractometer. Most modern SEC materials are made from silica-based particles or from polystyrenes. The surface function of the materials are related to whether the applications are in aqueous or non-aqueous solvents [126].

Due to low solubility of many industrial polymers in common solvents at room temperature, increasing the temperature might be required [127]. High-Temperature Gel Permeation Chromatography (HT-GPC) is a specialised form of GPC that allows analysis of the molecular weight distributions of polymers such as polyethylene and polypropylene, which require elevated temperatures for their dissolution in the mobile phase [126].

Polyethylenes and polypropylenes need mobile phases such as trichlorobenzene at 140°C, while polystyrenes and polybutadienes can be separated in toluene at 40-70°C [128].

Values obtained through HT-GPC for polymers is the weight average molecular weight (M_w) which is the arithmetic mean of the molar mass distribution and determines the polymer's colligative properties and tensile strength [129]. The weight average molecular number weight (M_n) which is the sum of the products of the molar mass of each fraction multiplied by its weight fraction, this accounts for the distribution of molar mass in the polymer [130]. And the molecular weight distribution (M_w/M_n) also called the polydispersity index (PDI) [126]. The dispersity indicates the distribution of individual molecular masses in a batch of polymers.

Using the information obtained through GPC the average number of random chain scissions per unit mass of a polymer (n_t) can be calculated according to the following Equation [131]:

$$n_t = \left(\frac{1}{M_{nt}}\right) - \left(\frac{1}{M_{n0}}\right) \quad (2.4)$$

where n_t is the bond breakage number, meaning the number of chain scission. M_{n0} and M_{nt} are the number-average molecular weights at the beginning and at reaction time t , respectively.

2.7.4 ICP-MS

Inductively coupled plasma mass spectrometry (ICP-MS) is a qualitative analytical technique for determining trace multi-elemental and isotopic concentrations in liquid, solid, or gaseous samples. It can detect metals and several non-metals at concentrations as low as part per quadrillion [132]. It allows for determination of elements with atomic mass ranges 7-250 (element lithium to uranium), and in some cases even higher [133]. It is today a leading analytical technique for assessment of mass concentrations. One of the largest volume uses for the technique is in the medical and forensic field, specifically, toxicology. ICP-MS have very low detection limits, multi elemental capacity, and wide linear range which has increased the usage of the instrument in recent years.

It combines an ion-generating argon plasma source that ionises the sample before using a

mass spectrometer to separate and quantify the ions. The ionized sample atoms travel through the conductive rods of the quadrupole MS and the ions are separated on the bases of their mass-to-charge ratio (m/z) [134]. An ion detector then converts these ions into an electrical signal, which is multiplied and read by computer software. This arrangement makes ICP-MS extremely sensitive. The sensitivity can reach down to ppb levels for a 0.1 g sample [135]. The advantages of ICP-MS are mainly its capability to detect multiple elements simultaneously as well as its speed and sensitivity.

Using ICP-MS can limit human error. However, there are some disadvantages. Machine drift can be a huge factor in limiting the accuracy and precision of the instrument, and consequently, the variation of the instrument as a function of mass. Some elements and isotopes can be hard to separate, for example ^{40}Ca will overlap with ^{40}Ar and ^{40}K [136]. The reference samples must be chosen for each sample as the material must also be similar to the matrix of the samples analysed, and this can be a challenge [134]. Especially for environmental samples which usually have different composition within the same batch of samples. Sample preparation is necessary for using ICP-MS, as the sample must be liquid. Acid digestion of solid might not always dissolve all the available analytes in the sample, and there is always the possibility that an acid can cause contamination to the sample [135].

3 Experimental

3.1 Characterisation of Samples From the Arctic Expedition

The Arctic Expedition 2018 resulted in 11 samples from 11 different locations. All samples were then analysed using Attenuated Total Reflectance Fourier-Transform Infra-Red Spectroscopy (ATR FT-IR), and a selection of samples were analysed with Pyrolysis-GC/MS.

3.1.1 On board the S/Y Fairwinds

May 2018 S/Y Fairwinds commenced the ‘Arctic Expedition 2018’. The ship sailed over 5000 nautical miles starting from the Bahamas to Bermuda – Nova Scotia – Newfoundland – Labrador – Greenland – Iceland and back to Norway. On the Arctic Expedition S/Y Fairwinds trawled for macro- and microplastics in the ocean through the support and cooperation of Norner AS. The trawl was built on site in Bahamas, and the dimensions can be seen in the figure [3.1](#) below. The netting used for the trawl was a 350 μm net from Filtra AS.

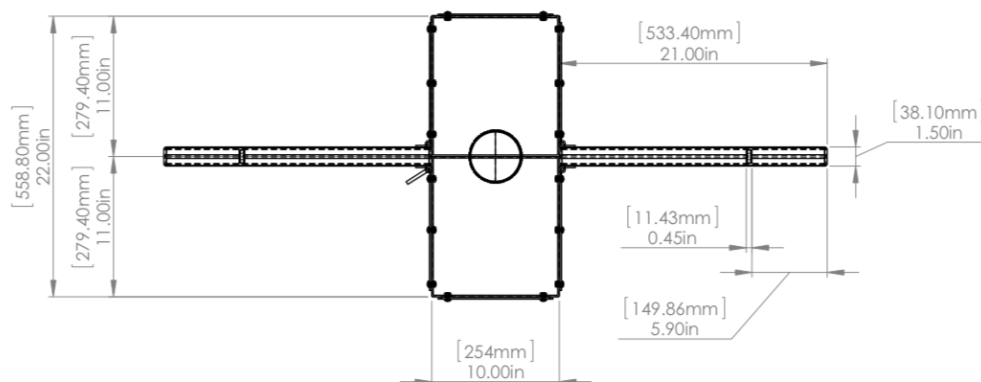


Figure 3.1: Dimensions of the trawl built for the Arctic Expedition by the crew of S/Y Fairwinds.

3. EXPERIMENTAL



(a) The trawl in use on S/Y Fairwinds.



(b) Samples getting sorted.

Figure 3.2: Photos from the Artic Expedition 2018

On board for the expedition was Simen Wingerei who was responsible for the trawling of macro and microplastics, following methods developed by the 5Gyres Institute – a non-profit organisation in special consultative status with the United Nations Economic and Social Council. Trawling took place when the weather conditions allowed for it. The trawl was placed in the water and covered about half-ways as can be seen in the figure [3.2a](#). After a trawl the content of the net was emptied into a bucket and sorted through first visually and then by the help of a microscope on board. This can be seen in the photo [3.2b](#). The route the S/Y Fairwinds sailed and locations of the trawls can be seen in the figure [3.3](#).

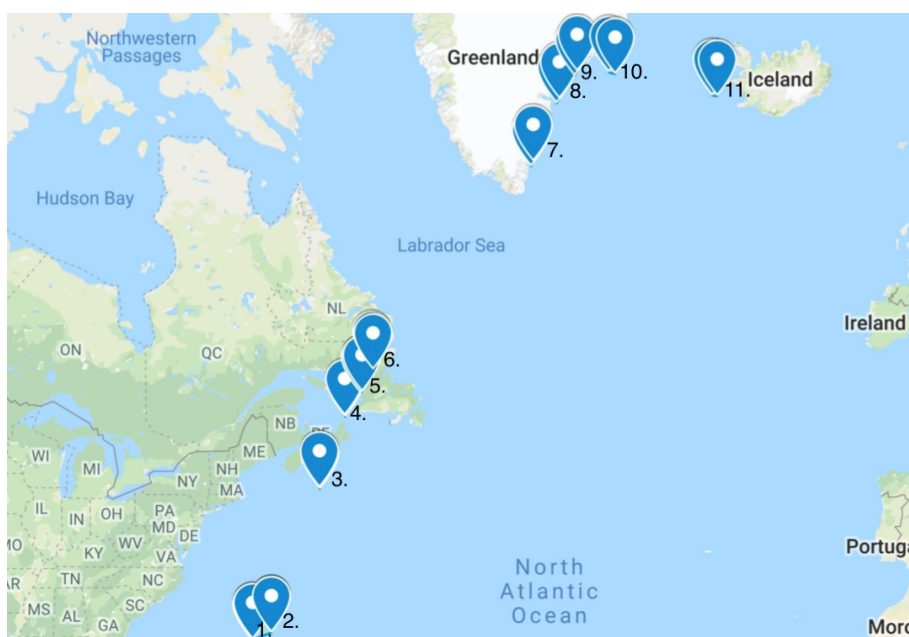


Figure 3.3: Map that shows the trawling done by S/Y Fairwinds on the Artic Expedition.

The content of each trawl were then transferred to a zip-lock back, which was placed into another zip-lock bag and labelled. The expedition resulted in 11 bags of samples from 11 different trawls. A summary of the trawling dates, distances and coordinates can be seen in the table below.

Table 3.1: The details of the trawls done on the Artic Expedition by S/Y Fairwinds.

	Coordinates Start	Coordinates Stop	Date	Time start	Time stop
1	30°45.098'N 69°19.101'W	31°24.226'N 67°25.160'W	04/05	14.30	17.30
2	30°49.033'N 69°14.069'W	31°24.226'N 67°25.160'W	26/05	11.30	14.30
3	42°23.371'N 62°46.269'W	42°28.809'N 62°47.103'W	09/06	18.30	21.30
4	47°18.567'N 60°21.146'W	47°24.360'N 60°22.400'W	01/07	16.20	19.20
5	48°49.754'N 58°52.805'W	48°56.161'N 58°41.811'W	02/07	16.30	19.30
6	50°26.094'N 57°48.156'W	50°17.116'N 57°38.659'W	07/07	17.00	20.00
7	61°12.815'N 42°28.42'W	61°26.318'N 42°15.500'W	23/07	12.30	15.30
8	64°0.041'N 40°1.006'W	64°10.867'N 39°46.736'W	27/07	13.00	16.00
9	65°7.589'N 38°20.377'W	65°18.658'N 38°3.951'W	28/07	09.30	12.45
10	65°16.466'N 35°0.202'W	65°12.158'N 34°25.056'W	01/08	12.15	15.20
11	64°19.407'N 25°6.814'W	64°18.518'N 24°37.040'W	03/08	18.00	21.00

3.1.2 Analysis by ATR FT-IR

The Fairwinds Expedition resulted in 11 bags of samples from 11 different locations. Each bag was emptied then every sample was weighed, described according to colour and shape, and measured using a caliper. All samples were then analysed using Attenuated Total Reflectance Fourier-Transform Infra-Red Spectroscopy (ATR FT-IR).

Sample 1 and 5 to 11 were analysed at the Norwegian Geotechnical Institute (Norges geotekniske institutt, NGI) in Oslo using a PerkinElmer Frontier FT-IR Spectrometer with a diamond crystal. This was done in the range of 4000 - 650 cm^{-1} . The obtained spectra were compared with libraries of polymer spectra available at NGI through Perkin-Elmer, namely 'Polymer'. Particle identification was carried out through the software, which

3. EXPERIMENTAL

compares it to those in the library. This includes a wide variety of plastic polymers, organic substances, salts and minerals. In general samples with a quality index over 0,7 was accepted, but they were also identified using a comparison with reference spectra. In cases where there was several matches above 0,7 the most fitting was chosen manually by comparing the spectra.

The remaining samples, which were the content of bag two to six were analysed at Norner in Stathelle using Perkin Elmer FT-IR Spectrometer Spectrum Two with the ATR unit Specac Quest (also with a diamond crystal). This was done in the range of 4000 - 550 cm^{-1} . For some smaller particles identification was not possible as it did not cover the crystal and here microscopy was used (Perkin Elmer FT-IT Spectrometer Spectrum Two with Spotlight 200i Microscopy). Here the smaller particles were attached to the plate before analysis using a double-sided tape and tweezers. The obtained spectra were compared with those in the library of polymer spectra available at Norner. Norner also has the library 'Polymer' through Perkin-Elmer as NGI, in addition to an extensive range of other polymer libraries. Norner have also have their own polymer libraries. Therefore, many of the spectra obtained at NGI with a quality index below 0,7 were re-run in the Norner library.

For all FT-IR background was recorded before start and re-recorded regularly during the analysis. The crystal was wiped off between each run, as well as cleaned with methanol or acetone and air-dried.

3.1.3 Analysis by Pyr-GC/MS

50 of the total of 387 particles in the 11 samples were re-analysed for verification using Pyrolysis Gas Chromatography Mass Spectrometry (Pyr-GC/MS) at NTNU, Trondheim. This was done as a comparison to the FT-IR analysis. The Pyr-GC/MS consists of a pyrolysis unit (Pyrola) with a resistive heating platinum filament coupled to a gas chromatograph (TRACE Ultra) with an ion trap quadrupole mass spectrometer (ITQ 1100 from Thermo Fisher Scientific). The capillary column was 30m (DB-5, 0.25 mm ID, 0.25 μm from Agilent).

The Pyrola unit was calibrated for the temperatures 250°C, 400°C, 600°C, 700°C, 900°C and 1000°C before start. The samples were run at 700°C. The specifications of the run can be seen below in table [3.2](#).

Table 3.2: Settings for the Pyrolysis Gas Chromatography Mass Spectrometry.

Unit	Parameter	Setting
Pyr	Chamber temperature	150°C
	Pyrolysis temperature	700°C
	Pyrolysis time	2 sec
GC	Carrier gas	Helium
	Inlet temperature	320°C
	Injection mode& ratio	Split(1:100)
	Injection flow	1 mL/min
	Temperature program	40°C (2 min) + 20°C/min (14 min) Hold 320°C (13 min)
	MS temperature	320°C
	Ionization technique	Electron (EI)
MS	Voltage and temperature	70 eV, 230°C
	Mass range	38 - 600 mz
	Scan mode	Full scan

Between each sample analysis, the filament and quartz glass were cleaned using a blow torch, and 1-3 blank Pyr-GC/MS runs were conducted to limit any contamination or carry-over. The samples were cut in the approximately size of 1 mm² with a scalpel on a glass surface over mm-paper before placement on the filament. The samples were applied in dry form. Peak areas were integrated using Xcalibur software (Thermo Fisher Scientific). Identification was achieved by comparison with reference spectra found in the Pyrolysis-GC/MS Data Book of Synthetic Polymers [\[120\]](#).

3.2 Weathering Study

An experiment to study the degradation impact UV light has on virgin plastic with and without an antioxidant additive (Vitamin E), in both powder and film form, was created.

3.2.1 Production of Samples for Weathering

Four powder samples and two films were produced from LLDPE for this experiment. In addition a commercial breadbag (LDPE) from the supermarket chain Meny was added for comparison.

To create the samples linear low density polyethylene (LLDPE) polymer material (Ineos 22D730) was used. In half an anti-oxidant, Vitamin E, was added to get the concentration of 100 ppm and the other half left without adding any additives. The vitamin E was incorporated into the LLDPE by extrusion (Prism 24 twin-screw extruder) compounding with a screw temperature of 190°C at 300 rpm. After compounding the polymer string was cooled in a water bath and pelletized. The additive free LLDPE was also extruded, cooled and pelletized to ensure equal processing.

The LLDPE film samples were produced through blown film processing (Collin line, with screw diameter of 25 mm and screw length of 25xD). The processing temperature was kept constant at 190°C and extruder RPM was adjusted to obtain a stable bubble for film production. Both additive-free LLDPE and LLDPE with 100 ppm Vitamin E antioxidant were processed into film samples. The films were made 45 μm thick. The two produced films, and the commercial bread bags thickness profiles were measured before start. This was done on a cross section taken out from the blown film using a GPA-Cap which is equipped with two sensors, one capacitive without contact, the other a micrometer (MAC 100 GPA from Octagon Process technology).

The remaining of the polymer samples were milled (PK-18 laboratory mill from Powder King). The powder was separated into the sizes of 200-425 μm and 425-600 μm using sieves, and the remaining particle sizes were discarded.

In summary this means 7 samples were produced:

1. Virgin LLDPE grinded to 200-425 μm .
2. LLDPE with additive grinded to 200-425 μm .
3. Virgin LLDPE grinded to 425-600 μm .
4. LLDPE with additive grinded to 425-600 μm .
5. Virgin LLDPE made into a film with 45 μm thickness.
6. LLDPE with additives made into a film with 50 μm thickness.
7. A commercial plastic bread bag, bought at the supermarket chain Meny.

3.2.2 Weathering in UV-Chamber

The degradation took part in an UV chamber (ATLAS Suntest XLS+) fitted with a xenon lamp (1500 W) and a daylight filter to simulate daylight. The instrument was used at maximum irradiance. The intensity of the UV radiation were recorded for 3 specific wavelengths (UV-A (351 nm) = 2.90 W/m², UV-A (340 nm) = 1.95 W/m², and UV-B (313 nm) = 2.81 W/m²) and the temperature was on a constant 93°C. Each of the four powder samples were placed in 3 petri-dishes, one larger (2g sample) and 2 smaller (1g sample) adding up to a total of 12 dishes in the chamber. During the experiment the samples were stirred to ensure a more homogeneous degradation of the samples. The 3 film samples were cut out and wrapped around metal holders to be placed horizontal in the chamber. All samples fitted into the UV chamber before starting the experiment can be seen in figure [3.4](#).

The black standard temperature (BST) sensor which is embedded into the UV chamber, whose purpose is to estimate and control the temperature obtained by the samples, was placed at a lower level than the samples due to a chord limitation. An external thermometer was therefore placed in the height of the samples. An external UV(A+B) meter was also used to check the radiation on the samples. Samples were taken out before starting the chamber as reference. During different time intervals of the experiment

3. EXPERIMENTAL

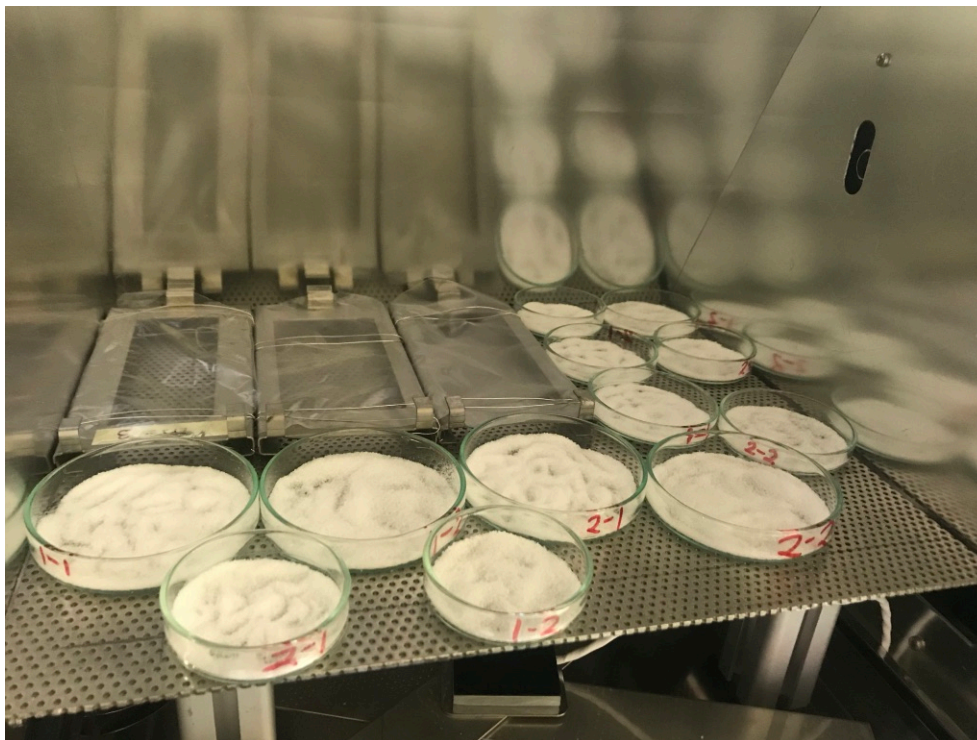


Figure 3.4: Samples placed in UV-chamber before starting degradation.

samples were collected (approximately every 2 weeks for 12 weeks), put into vials, labelled and stored in a cool, dark place. A summary of the samples and times can be seen in the table [3.3](#) below.

Table 3.3: Samples from the degradation in UV-chamber.

Description	Form	Size	Label	t1	t2	t3	t4	t5	t6
LLDPE	Film	45 μm	1	1-1	1-2	1-3	1-4	1-5	1-6
LLDPE + A	Film	45 μm	2	2-1	2-2	2-3	2-4	2-5	2-6
Bread bag	Film	20 μm	3	3-1	3-2	3-3	3-4	3-5	3-6
LLDPE	Powder	200-425 μm	1-1	1-1-1	1-1-2	1-1-3	1-1-4	1-1-5	1-1-6
LLDPE	Powder	425-600 μm	1-2	1-2-1	1-2-2	1-2-3	1-2-4	1-2-5	1-2-6
LLDPE + A	Powder	200-425 μm	2-1	2-1-1	2-1-2	2-1-3	2-1-4	2-1-5	2-1-6
LLDPE + A	Powder	425-600 μm	2-2	2-2-1	2-2-2	2-2-3	2-2-4	2-2-5	2-2-6

3.2.3 ATR FT-IR Analysis of Weathered Samples

For ATR FT-IR analysis the powder samples were made into films to ensure a homogeneous mixture. Circular holes of 1.2 cm in diameter was cut out on mylar film with 25 μm thickness, and the powder was then placed in the hole with teflon film under and over the mylar. Using a hotpress (Collin P 200 P) with the temperature of 170°C it went through the pressing program that can be seen below in the table [3.4](#).

Table 3.4: Pressing program used for making films.

	Heating				Cooling
Time (sec)	30	10	10	40	300
Pressure (bar)	0	30	70	250	250

The films were pushed out of the mylar and analysed by ATR-FTIR (Perkin Elmer FT-IR Spectrometer Spectrum Two with the ATR unit Specac Quest (diamond crystal)). This was done in the range of 4000 – 550 cm^{-1} . The film samples were analysed in the same way, but without any preparation.

For all spectra FT-IR background was recorded before start and re-recorded regularly during the analysis. The crystal was wiped off between each run, as well as cleaned with acetone and air-dried.

3.2.4 GPC Analysis of Weathered Samples

A selection of the degraded samples were further analysed by an expert at Norner AS using high temperature Gel Permeation Chromatography (HT-GPC) (GPC-IR5 from Polymer Char coupled with 7890B Gas Chromatograph System from Agilent Technologies) with a IR detector. Each run was performed using 10-12 mg of sample, and 1,2,4-Trichlorobenzene (TCB) as the mobile phase.

3.3 Adsorption of Metals in Microplastics

A study of the adsorption of 6 certain metals to degraded microplastic samples was done using 4 types of microplastic samples that had been degraded in an UV-chamber for 1200 hours (7 weeks) as described in section [3.2.2](#).

3.3.1 Exposure to Metals

16 Beakers (400 mL) of the same brand and make (VWR Borosilicate glass 3.3) were left for 24 hours with 0.1 mol HNO₃ (Ultrapure diluted with MilliQ water) to ensure proper cleaning. The same was done with a flask (5000 mL). All glassware was then rinsed with MilliQ water 8-10 times until pH paper (universalindikator from MERCK) showed the same pH as for the MilliQ water.

The flask was filled with MilliQ water (5000 mL), and NaCl was added (181.50 gram) to ensure a weight percentage equal of 3.5. Element standards with a concentration of 1000 +/- 3 ppm of the following elements: Cadmium, Chromium, Copper, Lead, Mercury and Zinc were added to the flask (25 μ L each) with a pipette (20-300 μ L) to ensure a concentration of 5 μ gr/L. The flask was then thoroughly mixed. 300 mL solution was distributed into each of the 16 beakers (400 mL). The 4 degraded microplastic samples (200-425 μ m without additive, 200-425 μ m with 100 ppm vitamin E additive, 425-600 μ m without additive and 425-600 μ m with 100 ppm additive) were weighed out (approx. 0.2 gram). For each of the 4 types of microplastics there was 3 parallels. This was added to 12 of the beakers, 4 were left without any microplastics as control. A magnet was added into each of the beakers, 12 with the size 30 x 6 mm and 4 with the size 20 x 6 mm. A summary of this can be seen in the table [3.5](#).

Table 3.5: Table showing the labelling of the adsorption experiment with 4 different microplastic particles, with 3 parallels and one control for each type.

Particle Size (μm)	200-425	200-425	425-600	425-600
Additive	No	Yes	No	Yes
0.2g Sample	1-1A	2-1A	1-2A	2-2A
	1-1B	2-1B	1-2B	2-2B
	1-1K	2-1K	1-2K	2-2K
Control (0g)	1-1C	2-1C	1-2C	2-2C
Magnet	30x6mm	30x6mm	30x6mm	20x6mm

The beakers were first wrapped with a layer of aluminium foil, and then a layer of parafilm was wrapped on top. All glasses were put on magnetic stirrers (Heidolph MR 3000) with the speed of 500 rpm in room temperature. They were left for 312 hours (13 days). After this time, all stirrers were shut off, and the sample glasses were collected and left for 5 hours to let the particles sediment. Solution was then taken out from the middle layer and filtered (VWR 25 mm Syringe Filter w 0.45 μm Polyethersulfone Membrane) with a 12 mL syringe and into centrifuge tubes (VWR metal free, 10 ml) and 3 drops Ultrapure concentrated HNO_3 was added, samples were then stored in fridge until ICP-MS analysis.

To separate the particles from the solution for analysis the 12 samples with microparticles were decanted. When the particles had sedimented, as much liquid as possible was removed using a glass pipette. MilliQ water (50 mL) was then added to the beakers to wash the particles and the solution was left for several hours until it again sedimented and repeated. It was done a total of 5 times to ensure the original liquid solution was flushed out. The remaining particles were put to dry in 50°C for 12 hours. References were also added by measuring out 0.2 gram sample for each of the 4 types of plastics and adding them to beakers (400 mL). 10% v/v concentrated HNO_3 (15 mL) was added to each of the 16 beakers and left for 24 hours in room temperature. The 16 samples were then filtered (VWR 25 mm Syringe Filter w 0.45 μm Polyethersulfone Membrane) and filled into centrifuge tubes (VWR metal free, 2.5-gram sample) and diluted (to 16.5-17 gram). The samples were then stored for ICP-MS analysis.

3.3.2 ICP-MS Analysis of Exposed Samples

The 16 samples from the seawater solution, and the 16 samples from the HNO₃ acid the particles were placed in were analysed by an expert at NTNU using the procedures established by the Department of Chemistry. The instrument was an Element 2 Inductively Coupled Plasma Mass Spectrometry (ICP-HR-MS) (Thermo Electronics). The sample was introduced to the system with an auto-sampler (SC2 DX). The instrument has a PFA-ST nebulizer (Elemental Scientific). The sampler is equipped with a dust cover with ULPA filter, and the samples are uncapped inside the cover with as little opening of the cover as possible. The gas flow was splitted, with 10% methane in argon.

The resolution of the analysis can be separated into low (400), medium (5500) and high (10 000). The detection limits for undiluted water samples for the 6 metals can be seen in the table [3.6](#) below.

Here the detection limit (LOD) is the absolute minimum concentration that can be detected. It is the best achievable value with a pure instrument (low background level and baseline). 25% means the concentration which gives relative standard deviation of 25%, and is uncorrected for baseline. QL-25% is found when LOD-25% is corrected for the baseline which gives is a more realistic quantification limit for Element 2 analysis.

Table 3.6: Detection levels of the 6 metals Cd, Cr, Cu, Hg, Pb and Zn for the HR-ICP-MS instrument Element 2 at NTNU. LOD is limit of detection, QL is LOD corrected for the baseline. 25% signifies the concentration in $\mu\text{g/L}$ that gives a rsd of 25%.

Sign	Isotope	Element	Resolution	LODs-25% ($\mu\text{g/L}$)	QL-25% ($\mu\text{g/L}$)
Cd	111/114	Cadmium	Lr	0.0004	0.0020
Cr	53	Chromium	Mr	0.0040	0.0200
Cu	63/65	Copper	Mr	0.0060	0.030
Hg	202	Mercury	Lr	0.0004	0.0020
Pb	208	Lead	Lr	0.000	0.0020
Zn	66	Zink-66	Mr	0.005	0.025

4 Results

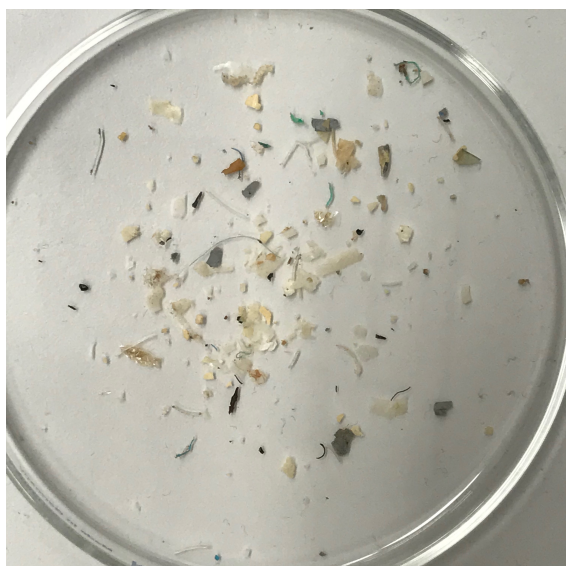
4.1 The Arctic Expedition

The Arctic Expedition ended with 11 samples, which were all weighed and measured. The results of this using the confirmed plastic samples can be found in the table [4.1](#) below. Here the distances of the trawl are also given, which are calculated based on the coordinates of the sailing that are given in the table [3.1](#) on page [35](#). The amount of sample per litre, m^2 and m^3 trawled sea is also given. A summary of the calculations can be seen in the appendix [A.1](#) on page [1](#).

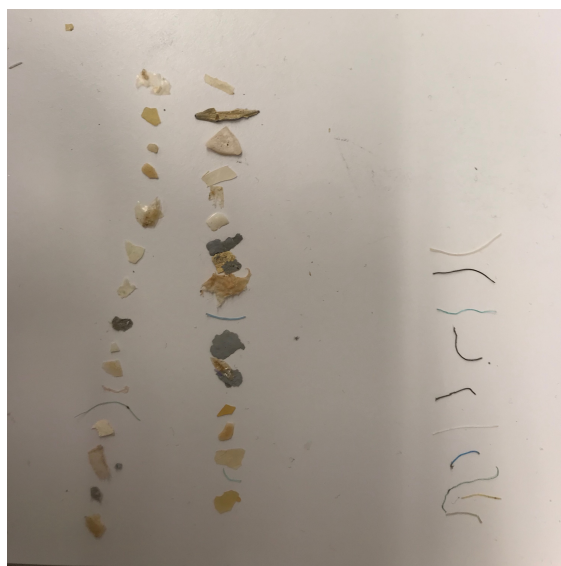
Table 4.1: Amount of particles, weight, weight/L, $\#/ \text{m}^3$, $\#/ \text{m}^2$ and water trawled on the Arctic Expedition.

Sample	Grams	#	Trawl (km)	$\mu\text{g/L}$	$\#/ \text{m}^3$	$\#/ \text{m}^2$
1	0.14	36	195	0.010	0.0026	0.00073
2	0.49	98	185	0.038	0.0075	0.0021
3	0.0017	118	10	0.0024	0.163	0.046
4	0.10	21	11	0.13	0.027	0.0076
5	0.15	34	18	0.12	0.027	0.0075
6	0.30	36	20.1	0.21	0.025	0.0071
7	0.014	4	28	0.0071	0.0020	0.00057
8	0.45	15	23	0.28	0.0091	0.0025
9	0.49	17	24	0.28	0.0099	0.0028
10	0.17	4	29	0.085	0.0020	0.00055
11	0.016	4	24	0.0093	0.0023	0.00066
Sum	2.3	387	567	0.11	0.025 (average)	0.0071

All samples were weighed and measured with a caliper in 2 directions (length and width). Physical characteristics like colour and type of each particle in all 11 samples were described. Type of sample were split into 2D/film, 3D and fibres. A summary of what types of samples were found in the bag can be seen in the table [4.2](#) below.



(a) Content of one sample.



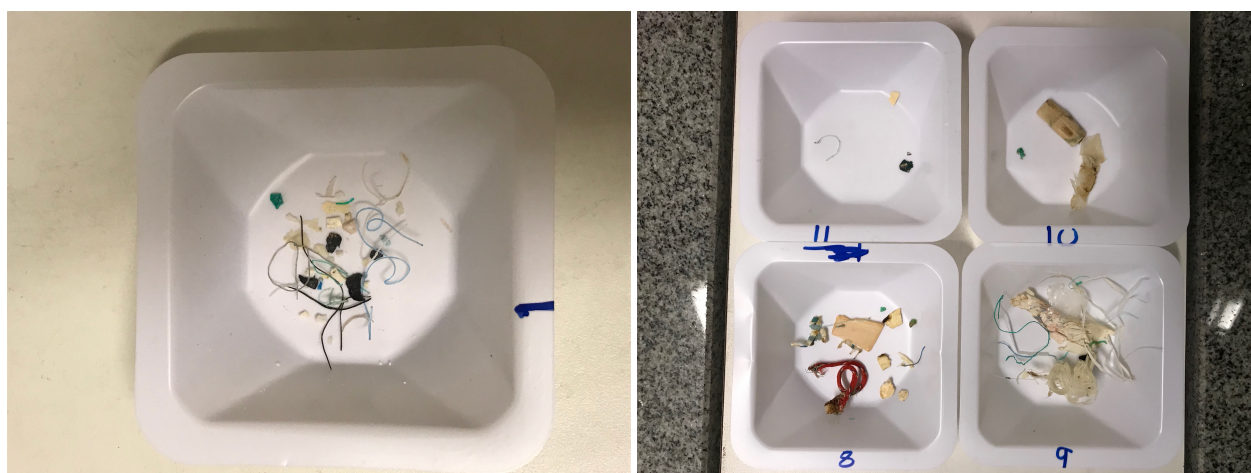
(b) Particles getting sorted and described.

Figure 4.1: Photos showing some examples of samples found on the Artic Expedition 2018

The total list of the particles and their identification with measurements can be found in the appendix section [B](#) that can be found on page [VIII](#).

Table 4.2: List of the types of samples. The particles were described as 2D, 3D or fibres.

#	Fiber	3D	2D
1	16	11	9
2	43	15	40
3	54	20	44
4	8	3	10
5	15	11	8
6	19	4	13
7	2	0	2
8	4	5	6
9	7	2	8
10	0	2	2
11	1	0	3
Sum	169	73	145
%	44	19	37



(a) Total particles in sample 1.

(b) Content of sample 8-11.

Figure 4.2: Photos showing the samples from 5/11 of the bags collected from S/Y Fairwinds on the Arctic Expedition 2018.

Table 4.3: Distribution of colours of the particles from the Arctic Expedition.

#	Blue	Green	White	Yellow	Black	Clear	Red	Orange	Grey	Brown
1	5	3	17	0	7	1	0	0	3	0
2	23	5	30	1	6	21	0	1	11	0
3	10	11	39	11	10	18	2	2	11	4
4	4	7	4	1	1	3	0	0	1	0
5	16	2	10	2	1	2	0	1	0	0
6	10	1	14	0	0	11	0	0	0	0
7	0	0	1	0	1	2	0	0	0	0
8	2	3	9	0	0	0	1	0	0	0
9	2	6	6	0	1	2	0	0	0	0
10	0	1	3	0	0	0	0	0	0	0
11	1	1	1	0	0	0	0	0	1	0
Sum	73	40	134	15	27	60	1	4	27	4
%	19	10	35	4	7	16	1	1	7	1

Images of typical samples can be seen in figure [4.1](#) where the contents of one sample was emptied onto a petri-dish before analysis and was sorted and described. As it can be seen

4. RESULTS

44% of the samples from the expedition were fibres samples, 37% were 2D particles and the remaining can be described as 3D samples. Of the samples 35% of the particles are white, 19% are blue and 15 % are clear, the total distribution of particle colours can be seen in the table [4.3](#).

A visual example of the different colours found in the samples can be seen in figure [4.2](#), where the total content of the samples 1, as well as sample 8 - 11 are shown.

4.1.1 ATR FT-IR Analysis

The reference transmittance FT-IR spectra of three of the most common polymers; low-density polyethylene (PE), polypropylene (PP) and polystyrene (PS) created using ATR FT-IR can be seen below in figure 4.3 [115]. On the figure there are markings that represent characteristic absorption bands for each polymer that can be used for identification.

The absorbance bands characteristic of the 3 respective polymers are assigned to molecular vibrations in Table 4.4 [138] [139].

Table 4.4: List of important vibration modes and assignments for the ATR FT-IR spectra for 3 of the polymers identified [140].

Polymer	Absorption band (cm^{-1})	Assignment
PE	(a) 2915	C-H stretch
	(b) 2845	C-H stretch
	(c) 1467	CH_2 bend
	(d) 1462	CH_2 bend
	(e) 1377	CH_3 bend
	(f) 730	CH_2 rock
	(g) 717	CH_2 rock
PP	(a) 2950	C-H stretch
	(b) 2915	C-H stretch
	(c) 2838	C-H stretch
	(d) 1455	CH_2 bend
	(e) 1377	CH_3 bend
	(f) 1166	C-H bend, CH_3 rock, C-C stretch
	(g) 997	CH_3 rock, CH_3 bend, CH bend
	(h) 972	CH_3 rock, C-C stretch
	(i) 840	CH_2 rock, C- CH_3 stretch
	(j) 808	CH_2 rock, C-C stretch, C-CH stretch
PS	(a) 3024	Aromatic C-H stretch
	(b) 2847	C-H stretch
	(c) 1601	Aromatic ring stretch
	(d) 1492	Aromatic ring stretch
	(e) 1451	CH_2 bend
	(f) 1027	Aromatic CH bend
	(g) 694	Aromatic CH out-of-plane bend
	(h) 537	Aromatic ring out-of-plane bend

All 387 particles taken from the 11 sampling bags from the Arctic Expedition were

4. RESULTS

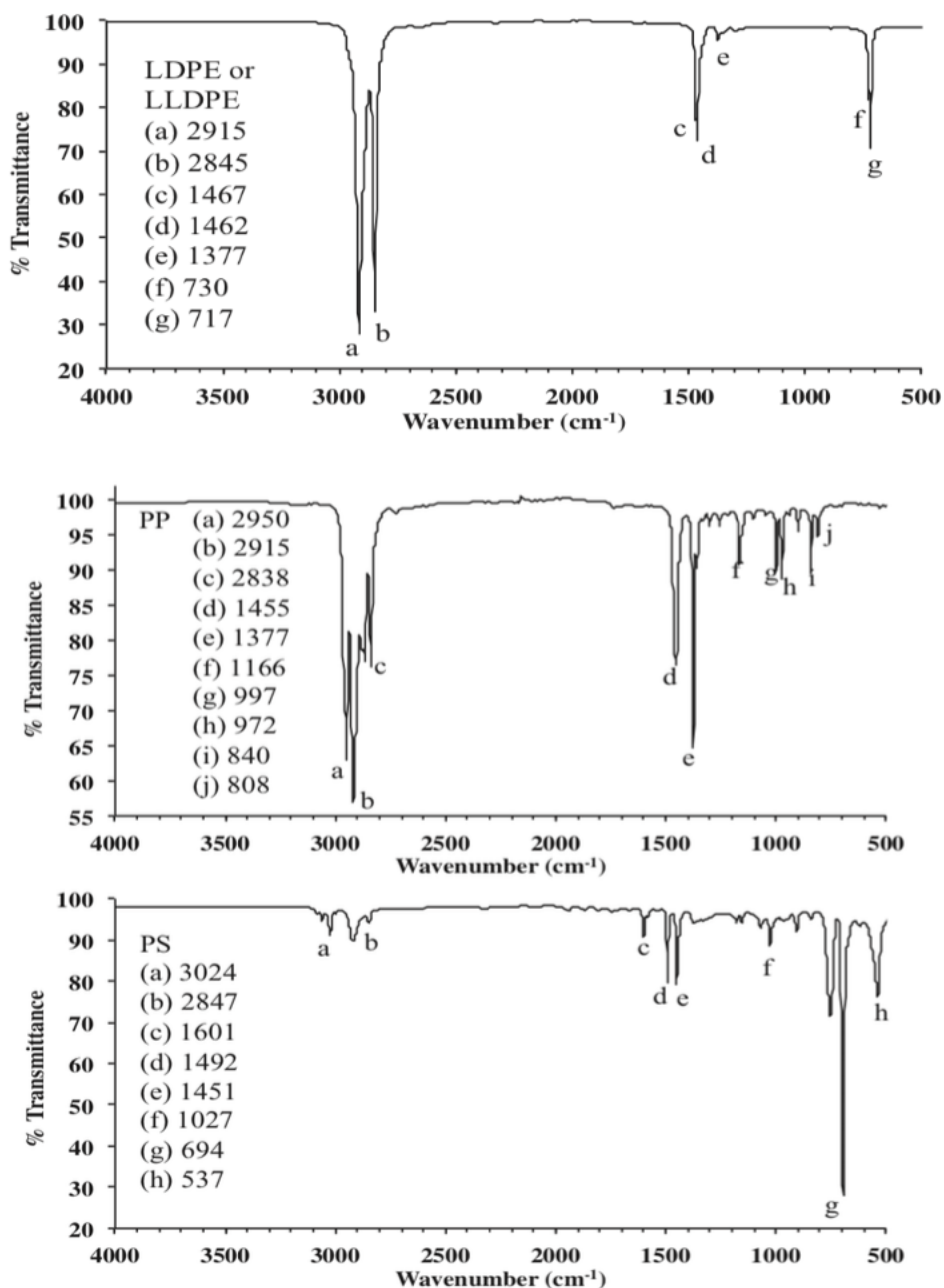


Figure 4.3: Reference spectra from 3 types of plastics; PE, PP and PS. Letters represent characteristic absorption bands used to identify each polymer [137]

analysed by ATR FT-IR. 365 of the particles were identified using the library search and the absorption bands listed in table 4.4 that are representative of vibrations critical for polymer identification. Out of the 365, 3 were identified as being organic particles. A total of 362 of the 387 were identified as synthetic polymers. The total list of the particles and

their identification with the quality index can be seen in the appendix section [B](#) that can be found on page [VIII](#).

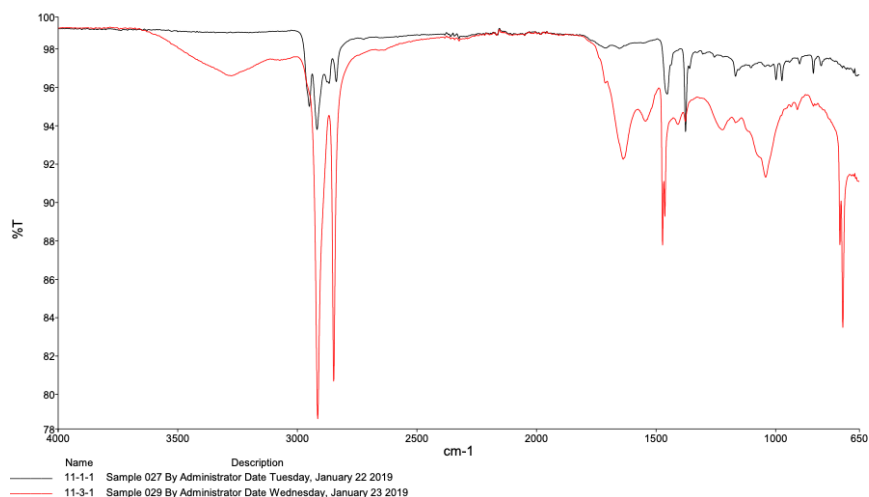


Figure 4.4: Sample 11-1 (black) identified as PP and 11-3 (red) identified as being PP.

The identification of different types of polymers is also very apparent visually. In the figure [4.4](#), sample 11-3 identified PE is put on top of sample 11-1 identified as PP. Here the distinctive bands as illustrated in the reference spectra from figure [4.3](#), and listed in table [4.4](#) can be seen. The black spectra (11-1, PP) has the distinctive three bands in the area $2950 - 2838 \text{ cm}^{-1}$ marked as PP (a), (b) and (c). The red spectra (11-3, PE) has the distinctive two bands in the area $2915 - 2845 \text{ cm}^{-1}$ marked as PE (a) and (b).

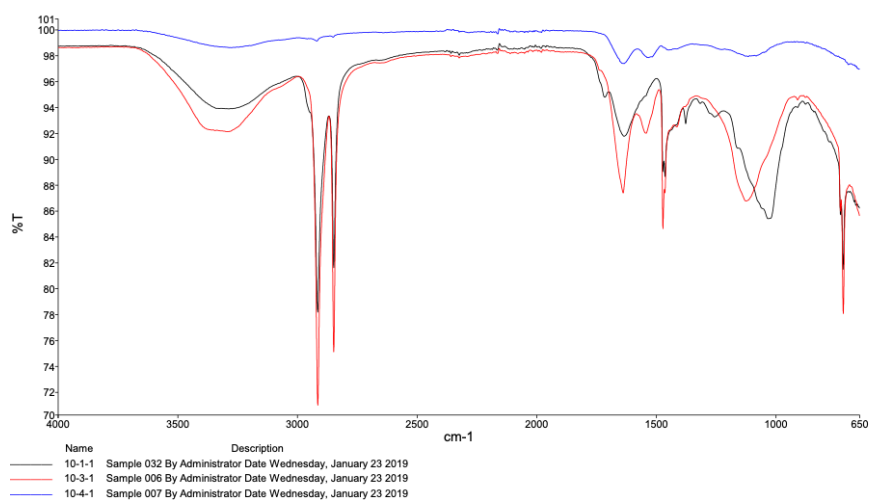


Figure 4.5: Sample 10-1 (black), 10-3 (red) and 10-4 (blue) which were all identified as being polyethylene.

In figure 4.5, an example is shown where the spectra from three samples from sample 10 that all were identified as being PE are shown on top of each other to show how different they could look. As is seen, some samples gave weaker signals, but sample 10-4 was still identified by the software with a quality index of 0.92.

4.1.2 Pyr-GC/MS Analysis

Comparison with reference pyrolysis gas chromatography mass spectrometry spectra from literature was used for identification [120]. Three of the most common polymers; high-density polyethylene (PE(HDPE)), polypropylene (isotactic) (iso-PP) and polystyrene (PS) are illustrated and described below. The reference pyrograms for the 3 polymers can be seen in figure 4.6.

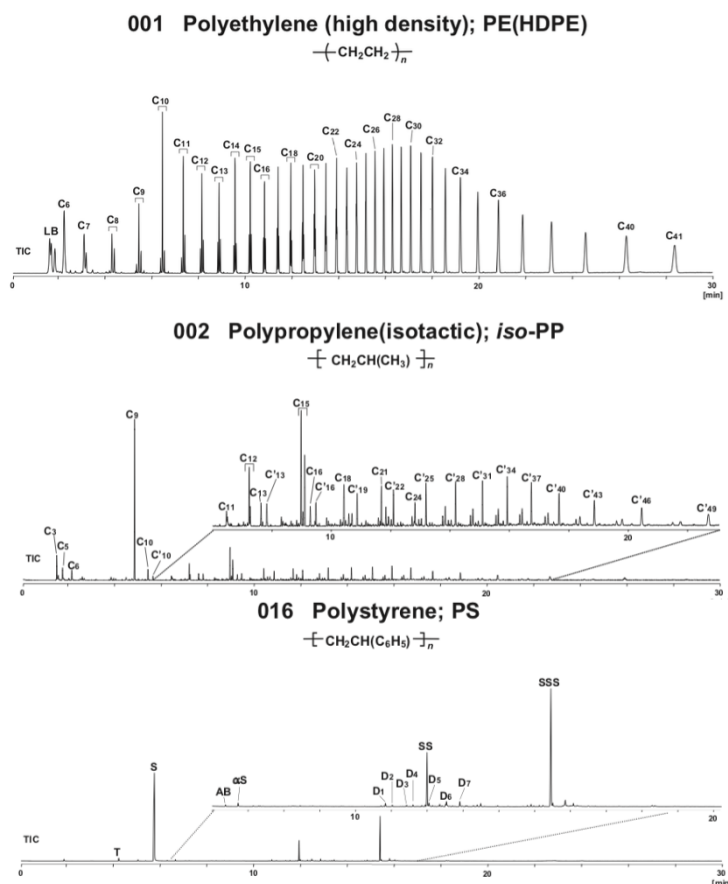


Figure 4.6: Major pyrolyzates for 3 typical homopolymer samples; HDPE, iso-PP and PS. [120]

On the figure 4.6 there are markings on each of the 3 polymers, which is the assignment of

the main peaks. More details of some of these assignment peaks with their notation, molecular weight, and relative intensity can be see in the table [4.5](#).

Table 4.5: Assignment for HDPE, iso-PP and PS with molecular weight and relative intensity [\[120\]](#).

	Notation	Assignment	M_w (Da)	RI
HDPE	C ₇	1-heptene ($\text{CH}_3(\text{CH}_2)_5\text{CH}_3$)	98	42.4
	C ₇	1-heptene ($\text{CH}_2=\text{CH}(\text{CH}_2)_4\text{CH}_3$)	100	19.3
	C ₁₀	1-decene ($\text{CH}_2=\text{CH}(\text{CH}_2)_7\text{CH}_3$)	140	64.2
	C ₁₁	1-undecene($\text{CH}_2=\text{CH}(\text{CH}_2)_8\text{CH}_3$)	154	49.8
	C ₁₄	1-tetradecene($\text{CH}_2=\text{CH}(\text{CH}_2)_{11}\text{CH}_3$)	196	49.2
	C ₂₀	1-eicosene($\text{CH}_2=\text{CH}(\text{CH}_2)_{17}\text{CH}_3$)	280	38.0
	C ₃₀	1-triacontene($\text{CH}_2=\text{CH}(\text{CH}_2)_{27}\text{CH}_3$)	420	100.0
	C ₄₀	1-tetracontene($\text{CH}_2=\text{CH}(\text{CH}_2)_{37}\text{CH}_3$)	560	94.1
	C ₄₁	1-hentetracontene($\text{CH}_2=\text{CH}(\text{CH}_2)_{38}\text{CH}_3$)	574	82.8
iso-PP	C ₅	n-pentane	72	10.0
	C ₆	2-methyl-1-pentene	84	8.1
	C ₉	2,4-dimethyl-1-heptene	126	100.0
	C ₁₀	2,4,6-trimethyl-1-heptene	140	6.8
	C ₁₂	2,4,6-trimethyl-1-nonene (meso)	168	9.5
	C ₁₅	2,4,6,8-tetramethyl-1-undecene (isotactic)	210	18.5
	C ₁₅	2,4,6,8-tetramethyl-1-undecene (syndiotactic)	210	10.6
	C ₃₄ '	2,4,6,8,10,12,14,16,18,20,22-undecamethyl-1,22-tricosadiene (isotactic)	476	9.7
	PS	T	toluene	92
S		styrene	104	100.0
α S		α -methylstyrene	118	0.7
D ₁		1,2-diphenylethane (C(Ph)-C-Ph)	182	0.6
SS		3-butene-1,3-diylidibenzene (C=C(Ph)-C-C-Ph)	208	10.2
D ₆		(<i>E</i>)-1-butene-1,4-diylidibenzene (C(Ph)=C-C-C-Ph)	208	1.2
SSS		5-hexene-1,3,5-triyltribenzene (C=C(Ph)-C-C(Ph)-C-C-Ph)	208	10.2

All reference pyrograms were created at 600°C, and the 30 min Gas Chromatography program was exactly the same as for the samples. This ensured easy identification as the peaks appeared close in time as the references.

As can be seen in the figure [4.6](#) the different types of polymers have quite distinct pyrograms. To ensure proper identification the mass spectrometry data [\[120\]](#) for relevant peaks was also compared.

4. RESULTS

Of the 387 samples that were analysed by ATR-FTIR, 50 samples were selected for analysis by pyr-GC/MS for method verification. 8 of the 50 samples did not result in identification, and 3 of the 50 analysis' gave a different identification than what was obtained with FT-IR. The total list of the 50 samples, and their identification can be seen in the appendix, in section [B](#) which can be found on page [XVII](#).

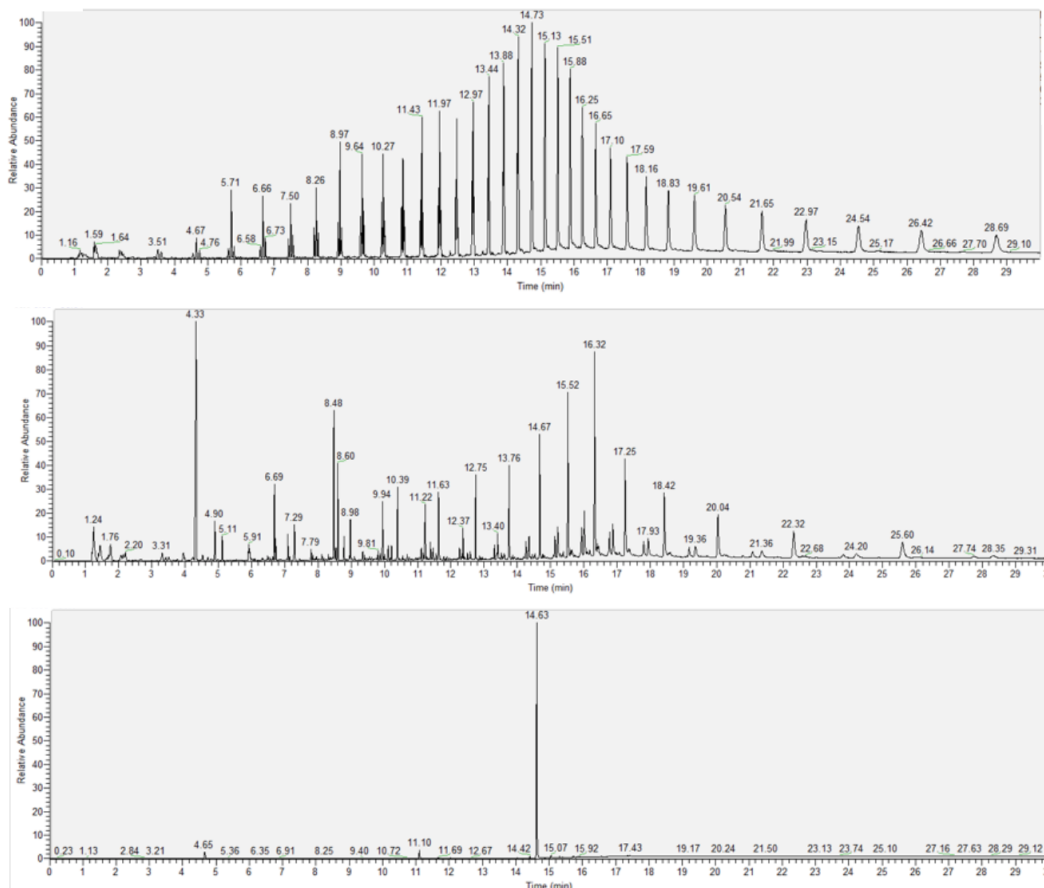


Figure 4.7: Identified samples from the arctic expedition. On top sample 2-59: PE, middle is sample 11-1: PP, and bottom is sample 6-30: PS.

An example of identification of samples from the expedition can be seen in figure [4.7](#). Here sample 2-59 was identified as PE, 11-1 as PP and 6-30 as PS. The spectra were compared with the table [4.5](#) for identification of the significant peaks. An example on how the reference MS-spectra looks can be seen in figure [4.8](#) where the literature mass spectra for some assigned peaks are given for PP in the m/z range of 29-600 amu [\[120\]](#).

The comparison to the sample 11-1 from the arctic expedition can be done to the reference shown in figure [4.8](#). Here the mass spectra for four peaks, given the notation C₉ (4.33

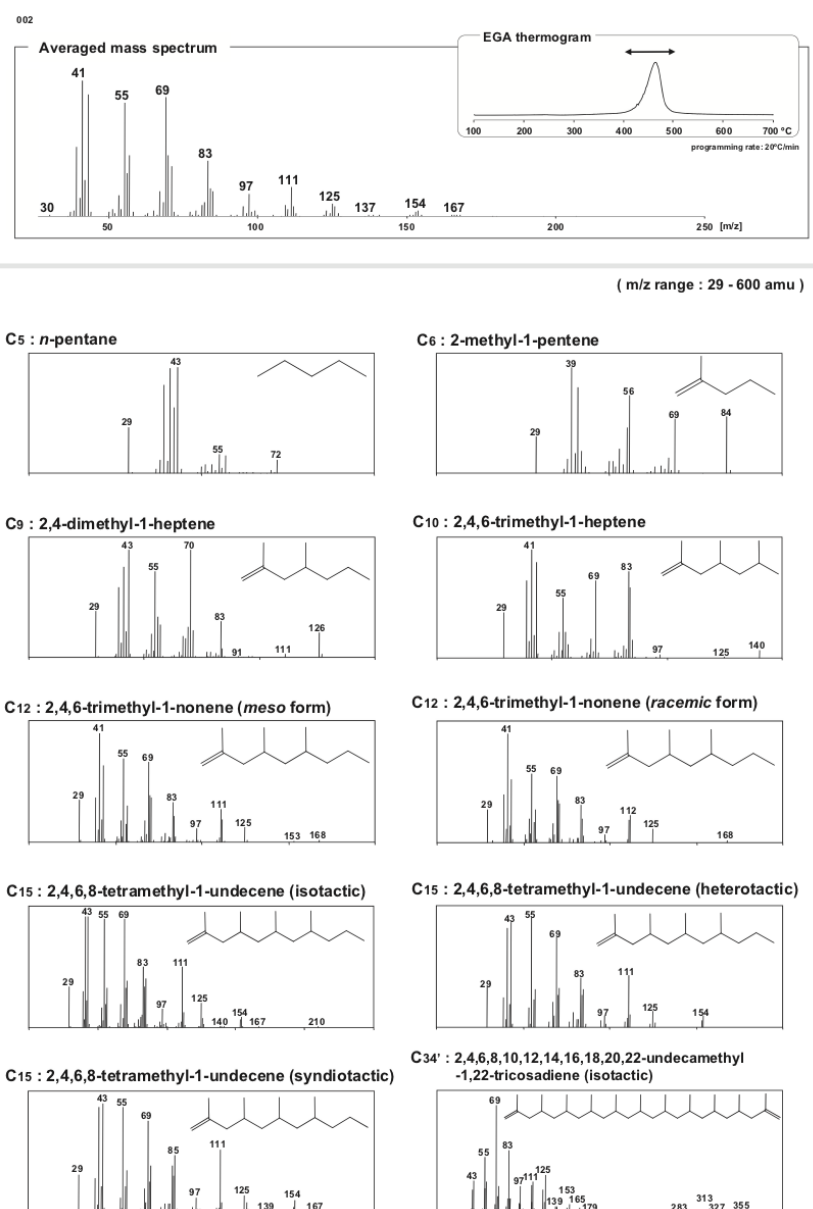


Figure 4.8: Reference mass spectra for polypropylene (isotactic) [120].

min), C₁₀ (4.90 min), C₁₅ (8.48 min) and C_{34'} (16.32 min) that can be seen in table 4.5 are shown. The mass spectra confirm the identification as PP.

4. RESULTS

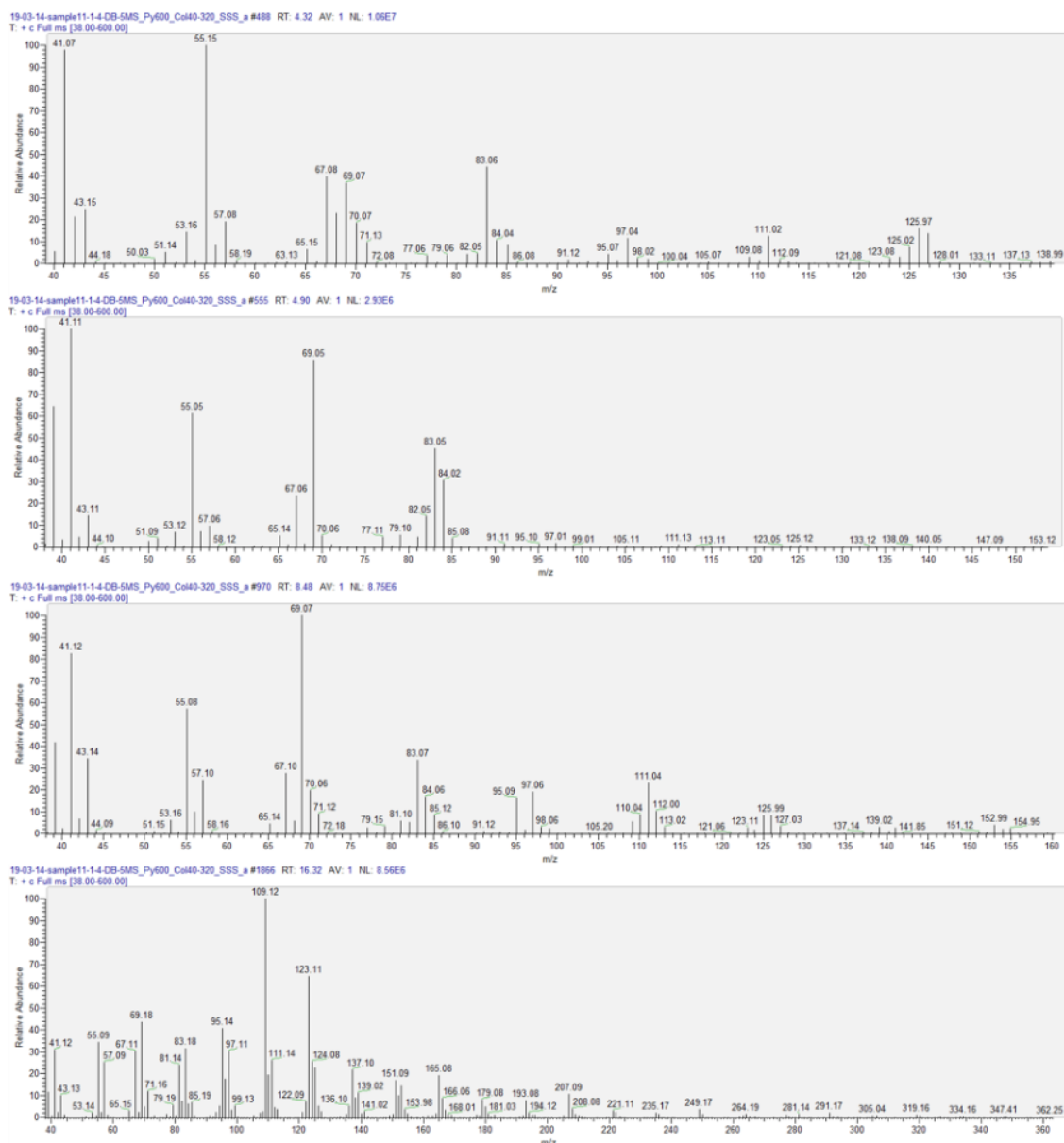


Figure 4.9: Mass spectra for the peaks C₉ (4.33 min), C₁₀ (4.90 min), C₁₅ (8.48 min) and C₃₄' (16.32 min) for sample 11-1 from the arctic expedition.

4.1.3 Summary of Results From the Arctic Expedition

After combining the results from ATR FT-IR with the pyr-GC/MS 57% of the samples were identified as polyethylene and 29% as polypropylene. The total distribution of synthetic polymers that were characterised are shown below in the table [4.6](#). Of the 50 samples analysed with pyr-GC/MS 39 out of 50 gave the same results as the analyses by FT-IR. This means that the two methods are 78% reproducible.

Table 4.6: Distribution of characterised polymers from the Arctic Expedition. Mix means mixture between PP and PE, unknown represent unidentified samples and 'org' is for substances identified as being organic.

#	PP	PE	Mix	Unknown	EVA	Org	PS	PET	Nylon 12	Nylon 6
1	2	30	4	0	0	0	0	0	0	0
2	10	86	0	2	0	0	0	0	0	0
3	55	56	0	6	0	1	0	0	0	0
4	3	11	0	5	0	0	1	1	0	0
5	8	18	0	2	1	0	2	0	3	0
6	17	0	0	6	0	1	0	0	6	6
7	2	1	0	0	0	0	0	1	0	0
8	5	6	0	1	0	0	3	0	0	0
9	7	10	0	0	0	0	0	0	0	0
10	0	3	0	0	0	1	0	0	0	0
11	3	1	0	0	0	0	0	0	0	0
Sum	112	222	4	22	1	3	6	2	9	6
%	29	57	1	6	0	1	2	1	2	2

4.2 Weathering of LLDPE

The artificial weathering was done on 4 powder samples (200-425 μm without additive, 200-425 μm with 100 ppm vitamin E additive, 425-600 μm without additive and 425-600 μm with 100 ppm additive) and 3 film samples (without additive, with 100 ppm vitamin E additive and a commercial LDPE bread bag). The thickness profiles of the film samples were measured before the experiment and the full profile can be seen in section [B](#) on page [XIX](#). A summary of the results can be seen in the table [4.7](#).

Table 4.7: Measured thickness of all film samples before degradation. A stands for samples with additive, here 100 ppm vitamin E.

Film	Set	Measured thickness	Tolerance
LLDPE	45 μm	44.3 μm	7.3%
LLDPE + A	45 μm	42.8 μm	7.9%
Bread Bag	20 μm	19.9 μm	25.7%

Samples were taken out of the UV degradation chamber at 360, 720, 960, 1200 and 1600 hours. The table [4.8](#) shows all samples in the chamber, and the labelling it was given.

Table 4.8: Samples from the degradation in UV-chamber. A represents the presence of an additive, 100 ppm Vitamin E.

Description	Form	Size	Label	0h	360h	720h	960h	1200h	1600h
LLDPE	Film	45 μm	1	1-1	1-2	1-3	1-4	1-5	1-6
LLDPE + A	Film	45 μm	2	2-1	2-2	2-3	2-4	2-5	2-6
Bread bag	Film	20 μm	3	3-1	3-2	3-3	3-4	3-5	3-6
LLDPE	Powder	200-425 μm	1-1	1-1-1	1-1-2	1-1-3	1-1-4	1-1-5	1-1-6
LLDPE	Powder	425-600 μm	1-2	1-2-1	1-2-2	1-2-3	1-2-4	1-2-5	1-2-6
LLDPE + A	Powder	200-425 μm	2-1	2-1-1	2-1-2	2-1-3	2-1-4	2-1-5	2-1-6
LLDPE + A	Powder	425-600 μm	2-2	2-2-1	2-2-2	2-2-3	2-2-4	2-2-5	2-2-6

4.2.1 Weathering of Samples

The photo-degradation could be seen by visual inspection of the samples, the powder samples became slightly yellow in colour over time. The film samples started breaking early in the experiment and this is illustrated in the figure [4.10](#). After just 2 weeks the films shows large tearing, after 4 weeks it was largely fragmented.

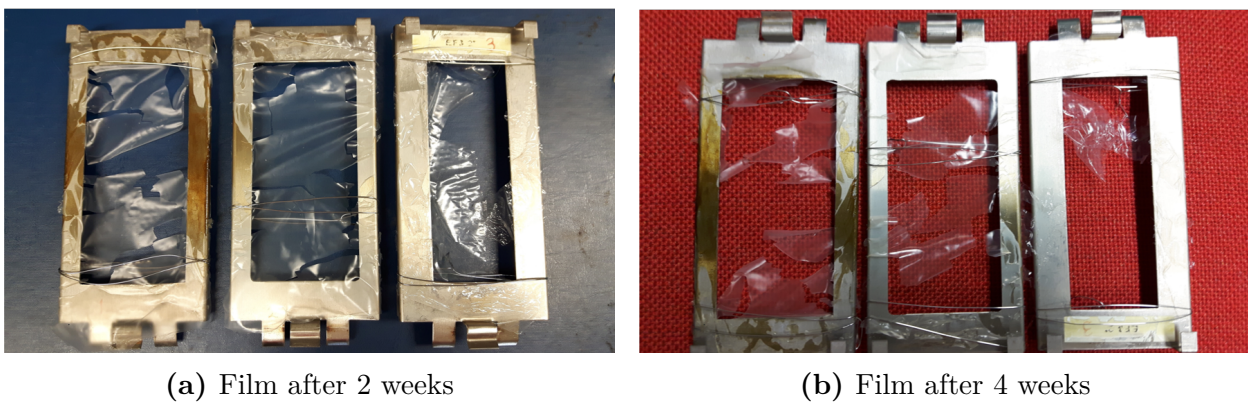


Figure 4.10: Films after 2 and 4 weeks in the UV chamber. Samples labeled 1, 2 and 3 respectively from left to right.

The UV-chamber gives the opportunity to accelerate aging by exposing samples to large doses of artificial light to stimulate a longer time period in nature. Using the estimate for mean European UV irradiance, which is $60 \text{ kWh}/(\text{m}^2\text{year})$ the times in chamber were calculated to stimulated time [\[73\]](#).

To do this several assumptions are made, as explained in the theory section. The simulated ageing was calculated in 4 ways and the complete calculation is described in appendix [A.2](#) on page [III](#).

The results of the conversion from hours in UV chamber to time in normal outdoor nature using the two different measurements of irradiation in the chamber and the 2 different ways of calculating the impact of the temperature can be seen below in table [4.9](#).

Table 4.9: Time in UV chamber converted to time in nature, given the European annual irradiation estimate of 60 kWh/(m²year). Method 1 is using UV-A(340) = 1.95 W/m² + T_c = 64. Method 2 is using UV-A(340) = 1.95 W/m² + T_c = 6.49. Method 3 is using UV(A+B) = 48.2 W/m² + T_c = 64. Method 4 is using UV(A+B) = 48.2 W/m² + T_c = 6.49. T_c means temperature coefficient.

Method	Time (simulated)	360h	720h	960h	1200h	1600h
1	Days	27331	54662	72883	91104	121472
1	Years	75	150	200	250	333
2	Days	2773	5546	7395	9244	12325
2	Years	8	15	20	25	34
3	Days	6756	13511	18015	22519	30025
3	Years	18.5	37.0	49.4	61.7	82.3
4	Days	685	1371	1828	2285	3046
4	Years	1.9	3.8	5.0	6.3	8.3

4.2.2 ATR FT-IR Analysis

The degraded samples were analysed by ATR FT-IR after exposure in the UV chamber. The times and labelling of the samples can be seen in table [4.8](#). The scales are here switched to absorbance but all of them were recorded on transmittance.

Spectra were placed onto each other to compare the changes in them as a results of the weathering they were exposed to. In the figure [4.11](#) below, a spectrum for each time interval of the experiment for powder sample one (LLDPE powder 200-425 μm, without additives) are placed on top of each other.

To ensure a more measurable view of the spectra, all were scaled using the two characteristic polyethylene peaks that are found in the interval 2700-3000 cm⁻¹. This is illustrated in figure [4.12](#) where values on the y-axis (absorbance (A)) disappear as a result of the scaling.

The biggest change in the spectra can be observed in the wavelengths of approximately 1600-1800 cm⁻¹, where one can see that the peak appear larger the more degraded the

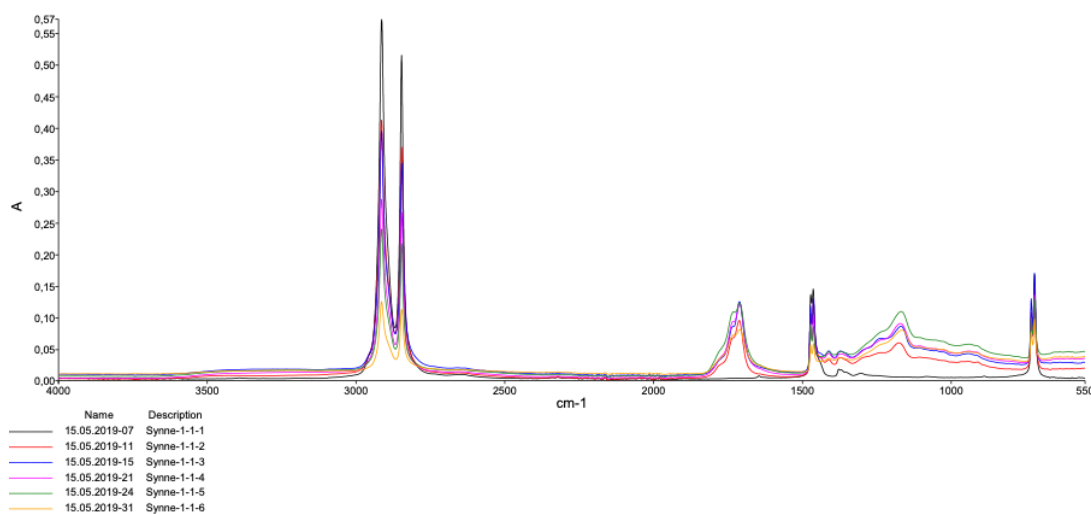


Figure 4.11: Powder sample 1-1 (200-425 μm , without additives) in all time intervals of degradation.

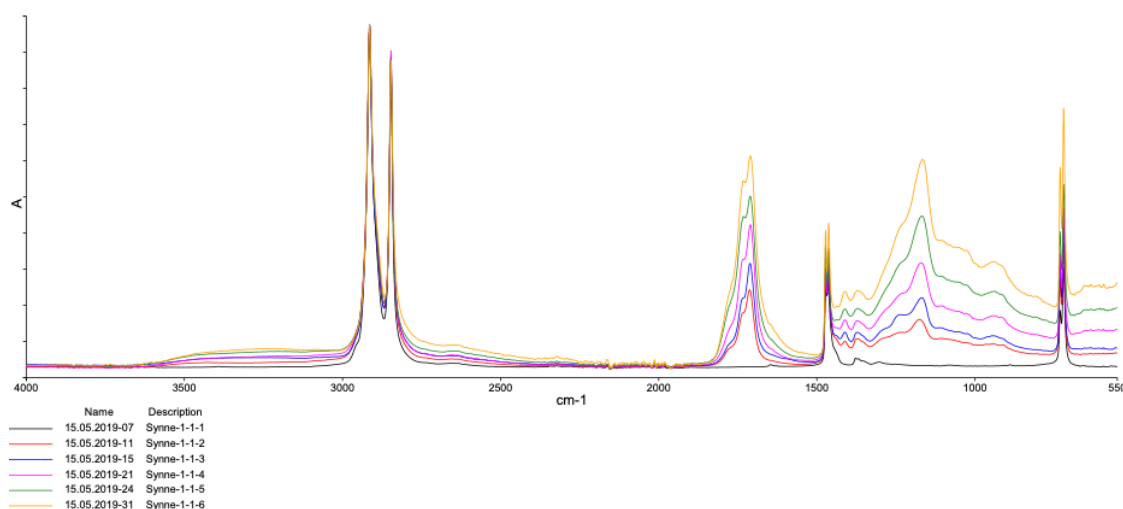


Figure 4.12: Powder sample 1-1 (200-425 μm , without additives) in all time intervals of degradation scaled.

sample is. This trend is observed on all samples as a function of their degradation. This is the carbonyl band area (due to C-O stretching at around 1720cm^{-1}). This can be observed in figure [4.13](#).

These differences in the spectra can also be observed from one type of sample to another. An example is posing sample 1-1 (200-425 μm , without additives) onto 1-2 (425-600 μm , without additives) at different intervals of the sampling, and scaling them.

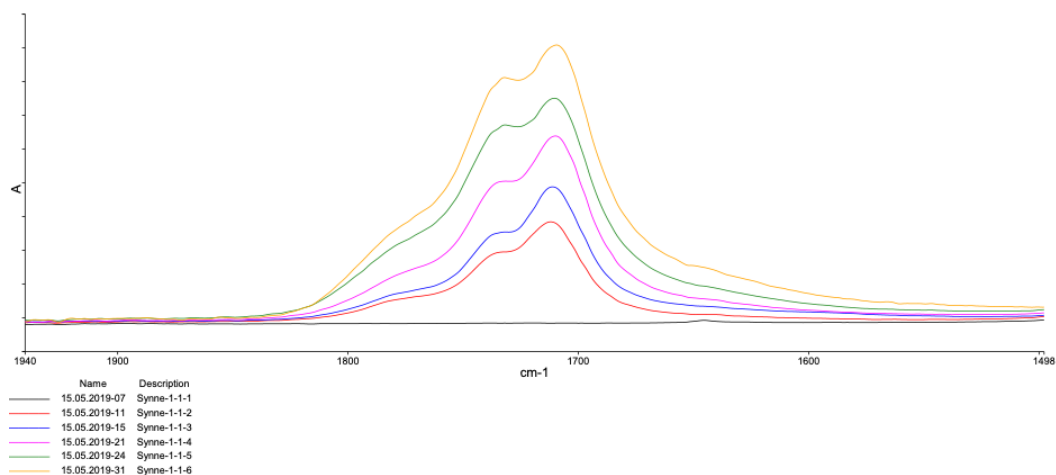


Figure 4.13: Powder sample 1-1 (200-425 μm , without additives) in all time intervals of degradation, scaled and zoomed in to 1500-1900 cm^{-1} .

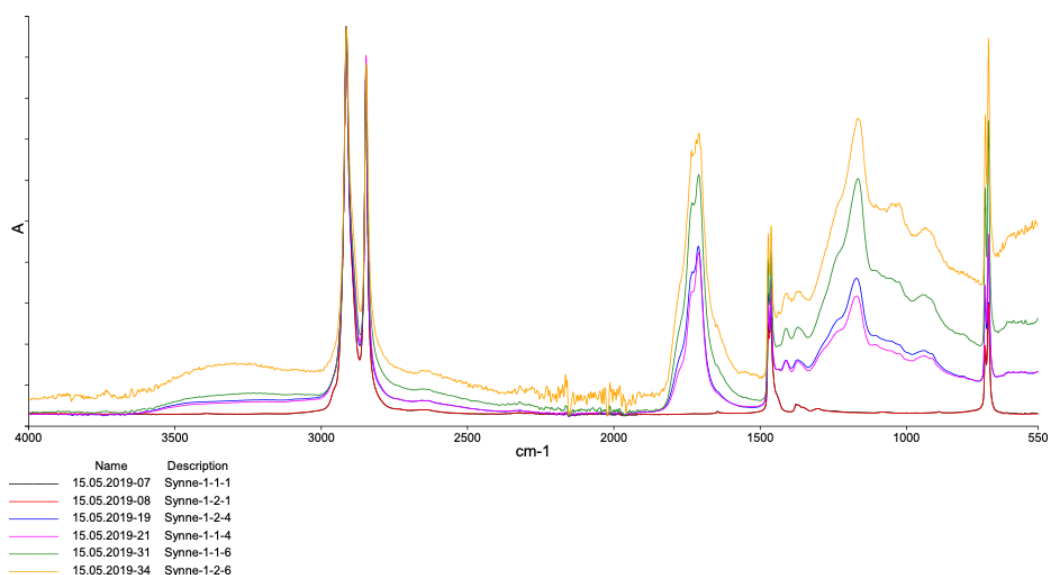


Figure 4.14: Powder sample 1-1 (200-425 μm , without additives) and 1-2 (425 - 600 μm , without additives) in time intervals of degradation scaled.

This is done in figure [4.14](#) using the reference from before the UV chamber, after 720 and 1600 hours. The spectrum suggests that the samples in the size 425-600 μm was to a larger extent degraded during the experiment than the samples with smaller particle size.

The effect of the anti-oxidant, the additive Vitamin E which was added to half of the samples, can also be compared in this manner. In figure [4.15](#) sample 1-2 (425-600 μm , without additives) is put on top of sample 2-2 (425-600 μm , with the additive).

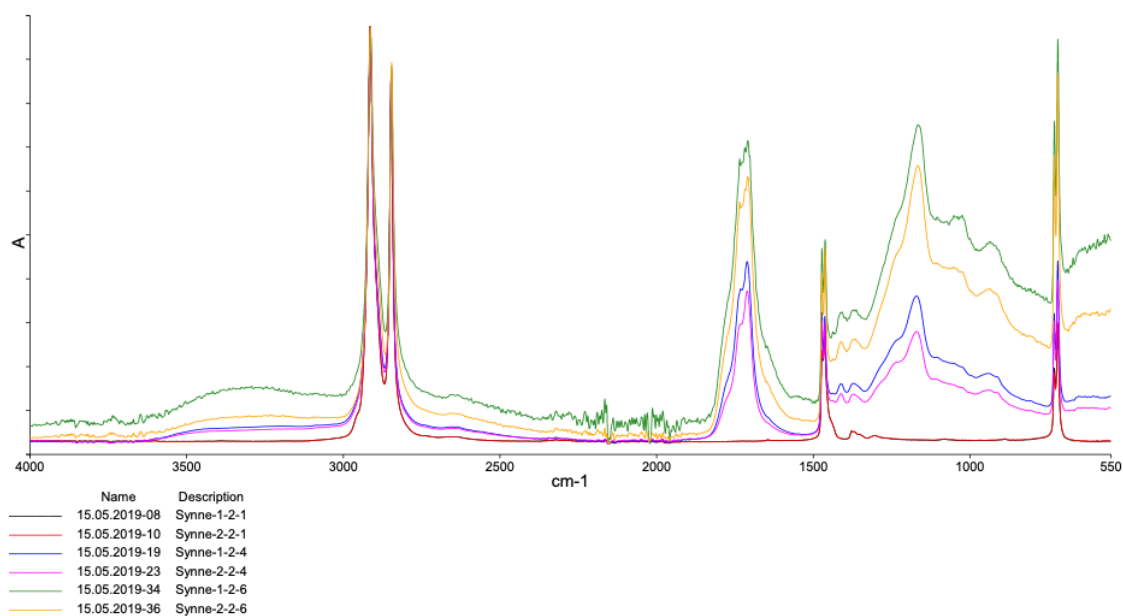


Figure 4.15: Sample 1-2 (425-600 μm , without additives) with sample 2-2, (425-600 μm , with Vitamin E additive) scaled. At 0, 720 and 1600 hours.

Here sample 1-2 has an higher increase in the carbonyl area than sample 2-2, which can be seen in figure [4.15](#). 2-2 has a lower rise in the C-O stretching bonds which show that the anti-oxidant slows down the weathering process.

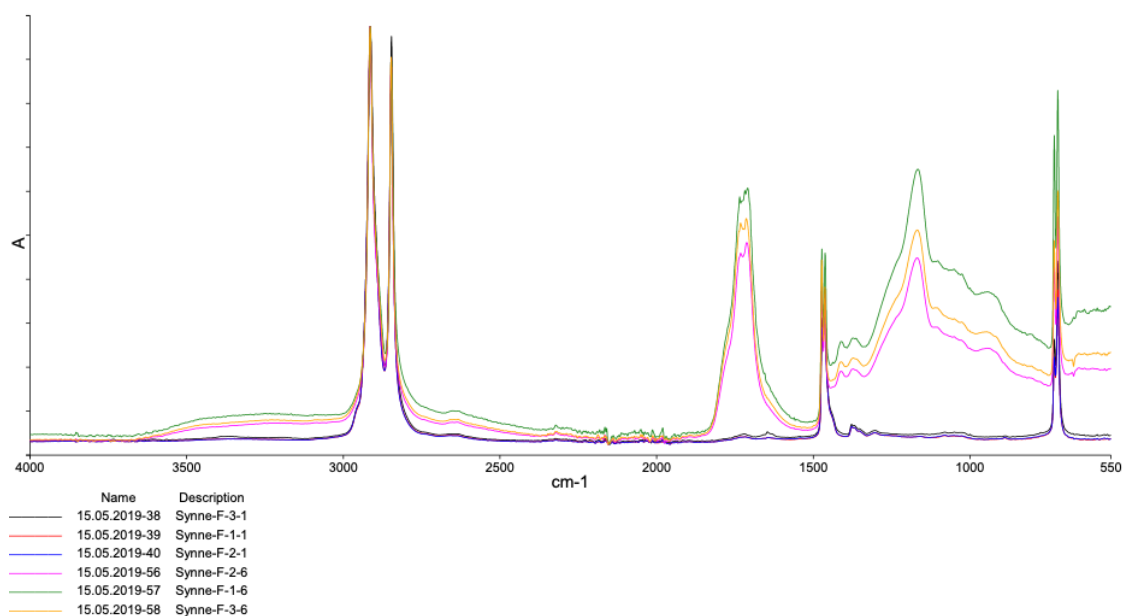


Figure 4.16: Film samples 1, 2 and 3 before start and after 1600 hours in the UV chamber.

The last film samples became very degraded and fragile, but there were no problems

recording spectra for them. The film sample 1 is the LLDPE without any additives and looks like the most degraded sample out of them all. For the commercial bread bag, film sample labelled 3, this was purchased at Meny and there is no knowledge of what possible additives are present. The commercial breadbag is also a considerable thinner film ($20 \mu\text{m}$ thickness) than film samples 1 and 2 (approximately $45 \mu\text{m}$ thickness). The spectra of the 2 films that were made with LLDPE can be seen in figure 4.17. The peaks of the commercial breadbag seems to be in-between the LLDPE with 100 ppm vitamin E (film sample 2) and LLDPE without any additives (film sample 1).

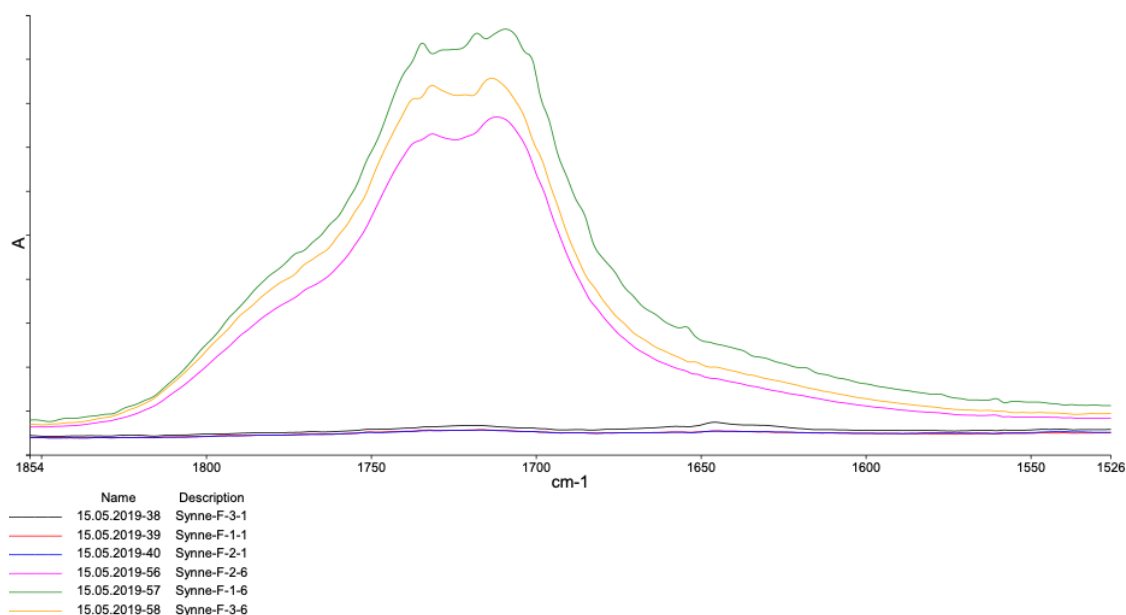


Figure 4.17: Film sample 1 and 2 at 3 different times of degradation, scaled and zoomed in to $1500\text{-}1900 \text{ cm}^{-1}$

4.2.3 Carbonyl Index

As described, the carbonyl band area around 1720cm^{-1} is where the largest effect of weathering can be observed. Therefore a model was created to give comparable values of the area for all samples. An algorithm was built that calculated a ratio of two peak areas (carbonyl/reference) in the samples. The specific bandwidth chosen can be seen in the table 4.10. The correlation to the model and error compared to Beer's Law can be seen in section B on page XXII.

Table 4.10: Parameters chosen for areas calculated

Peak name	Start	Stop	Base 1	Base 2
Carbonyl	1838 cm^{-1}	1552 cm^{-1}	1880 cm^{-1}	1560 cm^{-1}
Reference	3043 cm^{-1}	2737 cm^{-1}	3095 cm^{-1}	2699 cm^{-1}

These areas were built on Sample 1-1-6, which can be seen in figure [4.18](#) and implemented on all samples.

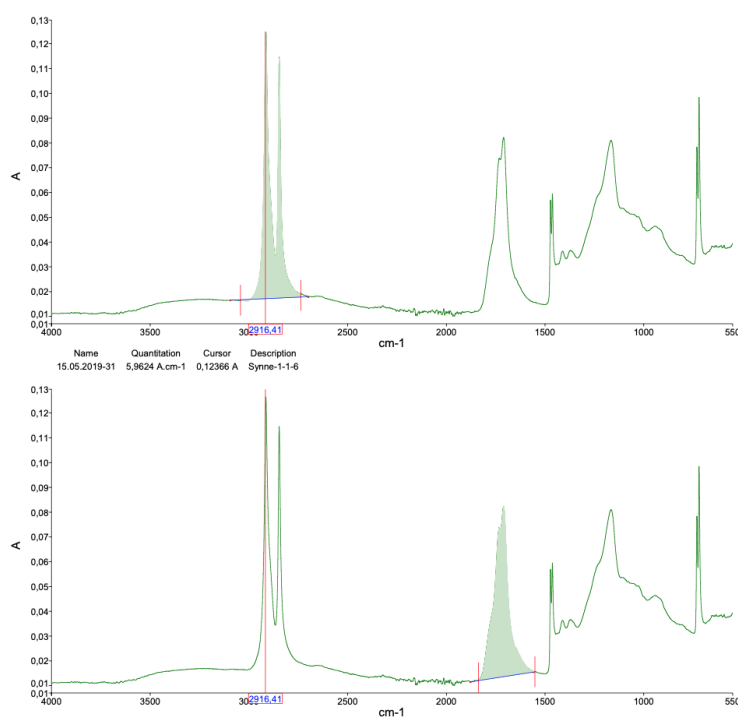


Figure 4.18: Film sample 1 and 2 at 3 different times of degradation, scaled and zoomed in to $1500\text{-}1900\text{ cm}^{-1}$

The calculated ratios (Carbonyl Index area/Reference area) that give the relative area of the 1720cm^{-1} over the characteristic reference peaks that are found in the interval $2700\text{-}3000\text{ cm}^{-1}$ can be seen in table [4.11](#).

4. RESULTS

Table 4.11: Carbonyl Ratio (Carbonyl group area/Reference area) for all samples.

Sample	Ratio (Cabonyl/Reference)	Sample	Ratio (Cabonyl/Reference)
1-1-1	0.0014	F-1-1	0.019
1-1-2	0.26	F-1-2	0.18
1-1-3	0.37	F-1-3	1.3
1-1-4	0.54	F-1-4	0.80
1-1-5	0.80	F-1-5	0.99
1-1-6	0.99	F-1-6	1.0
1-2-1	0.00041	F-2-1	0.016
1-2-2	0.37	F-2-2	0.22
1-2-3	0.56	F-2-3	0.57
1-2-4	0.67	F-2-4	1.0
1-2-5	0.83	F-2-5	1.4
1-2-6	1.2	F-2-6	0.83
2-1-1	0.0023	F-3-1	0.024
2-1-2	0.32	F-3-2	0.13
2-1-3	0.45	F-3-3	0.21
2-1-4	0.68	F-3-4	0.60
2-1-5	0.87	F-3-5	0.71
2-1-6	0.93	F-3-6	0.91
2-2-1	0.66		
2-2-2	0.18		
2-2-3	0.45		
2-2-4	0.52		
2-2-5	0.74		
2-2-6	1.0		

4.2.4 GPC Analysis

20 of the 42 samples were analysed using GPC. 11 of these were powder samples. Of the 1-1 powder samples (200-425 μm , without additives) it was tested for all time intervals (1-1-1 to 1-1-6). For the 2-1 powder samples (200-425 μm , with vitamin E additive) three of the samples were analysed (0, 720 and 1600 hour degraded). For the larger powder particles (1-2 and 2-2) only one of each was tested. The samples after 1600 hours in the UV chamber, 1-2-6 and 2-2-6. The full list can be seen in the table [4.12](#) below. The distribution of mass fraction plotted against the logarithm molar mass of the samples can be seen in the figure [4.19](#).

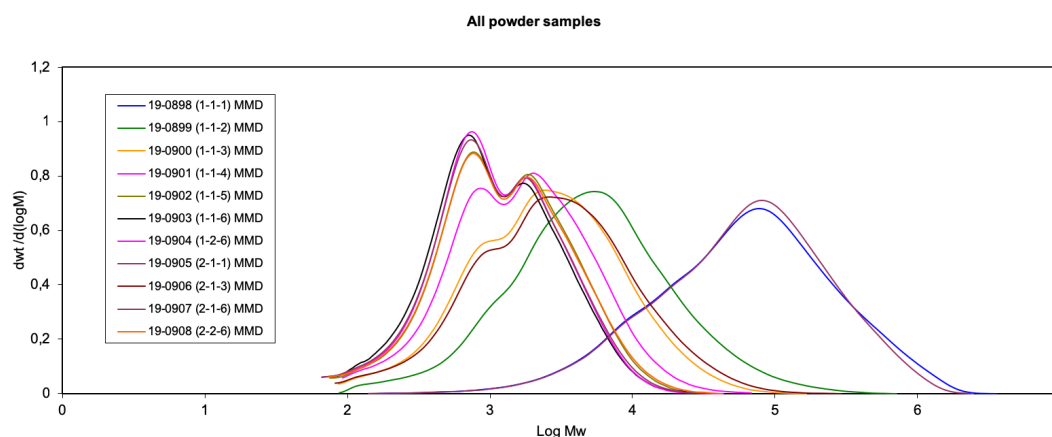


Figure 4.19: The mass distribution shown as mass fraction is plotted against the logarithm molar mass of the all powder samples analysed by GPC.

For all samples the polydispersity index (PDI), or molecular weight distribution, was calculated. This is the ratio of the weight-average molecular weight to the number-average molecular weight. For a monodisperse polymer the PDI is 1 [\[115\]](#). The polydispersity index increases as the polymer distribution broadens. The values obtained for the powder samples, as well as the average number of random chain scissions (n_t), can be seen in the table [4.12](#).

4. RESULTS

Table 4.12: Summary of results from GPC on selected degraded powder samples. M_n is the number-average molecular weight, M_w is the weight-average molecular weight, the ratio between them also known as PDI and average number of random chain scissions (n_t).

Sample name	Mw (g/mol)	Mn (g/mol)	Mw / Mn	(n_t)
1-1-1	151200	18100	8.3	-
1-1-2	12500	2100	6.0	$4.21 \cdot 10^{-4}$
1-1-3	5100	1200	4.3	$7.78 \cdot 10^{-4}$
1-1-4	3000	900	3.3	$1.31 \cdot 10^{-3}$
1-1-5	2100	700	2.9	$1.37 \cdot 10^{-3}$
1-1-6	1800	700	2.7	$1.37 \cdot 10^{-3}$
1-2-6	1800	700	2.8	-
2-1-1	134100	18400	7.3	-
2-1-3	6000	1200	5.0	$7.79 \cdot 10^{-4}$
2-1-6	1900	700	2.8	$1.37 \cdot 10^{-3}$
2-2-6	2200	700	3.0	-

For sample 1-1 all times of the degraded samples were analysed, making it possible to illustrate the loss of molecular weight as a function of the time passed. This can be seen in figure [4.20](#). After more time has passed in the UV chamber, the more the curve moves to the left of the figure.

Looking at the effect of the antioxidant, the 100 ppm Vitamin E additive, by comparing the samples 1-1 (200-425 μm , without additives) to 2-1(200-425 μm , with additive) at different times of degradation it can be seen that the sample 1-1 without additives has a slightly bigger loss of M_w as time passes in the chamber, but the exact same values for M_n . An illustration of this can be seen in figure [4.21](#).

As expected the particle sizes does not appear to affect the degree of degradation. When all the 4 powder samples (1-1, 1-2, 2-1 and 2-2) are compared at the end of degradation it can again be observed that all samples that have the additive in them (sample 2-1 and 2-2) get a slightly higher M_w after 1600 hours than for the other two samples. No such difference in

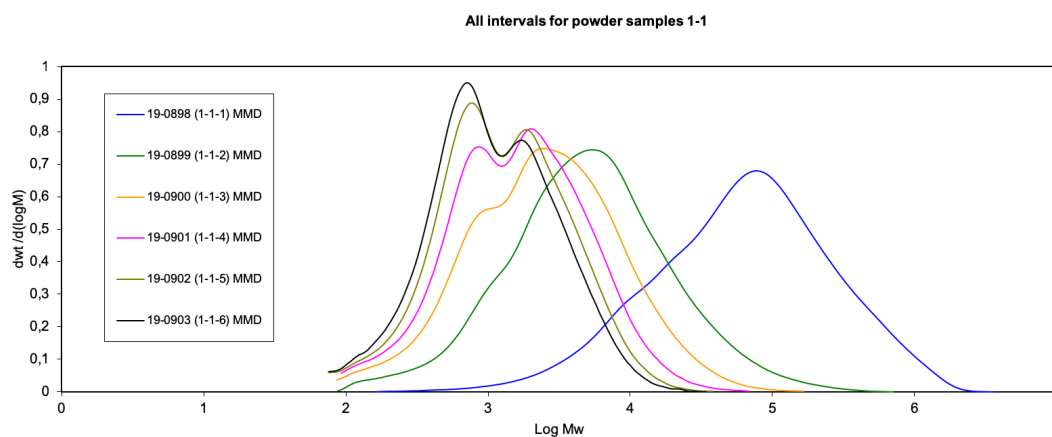


Figure 4.20: The mass distribution shown for powder samples 1-1 for all time intervals of the experiment as mass fraction is plotted against the logarithm molar mass of the all powder samples analysed by GPC.

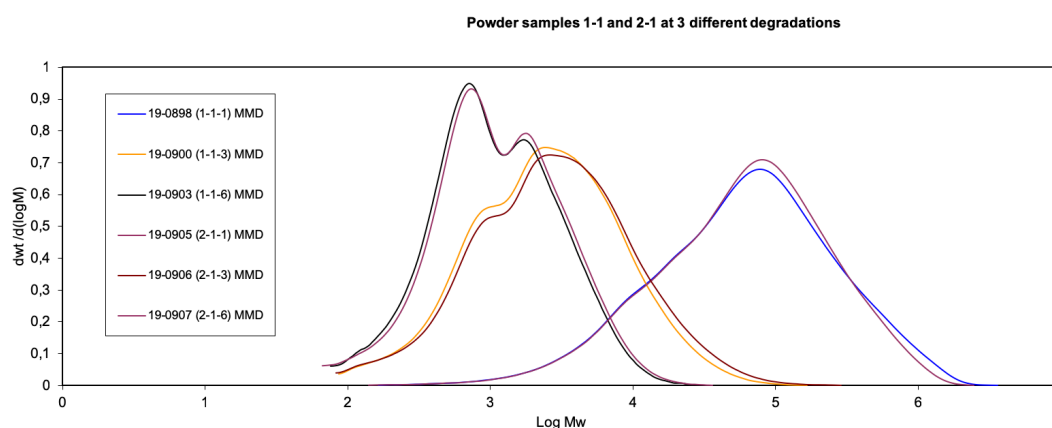


Figure 4.21: The mass distribution shown for powder samples 1-1 for all time intervals of the experiment as mass fraction is plotted against the logarithm molar mass of the all powder samples analysed by GPC.

observed between sample 1-1 (200-425 μm , without additives) and 1-2 (425-600 μm , without additives), nor between sample 2-1 (200-425 μm , with additive) and 2-2 (425-600 μm , without additive), so starting particle size does not effect the rate of loss in M_w for the samples. The M_n is equal at the end of the degradation for all samples as is the PDI.

4. RESULTS

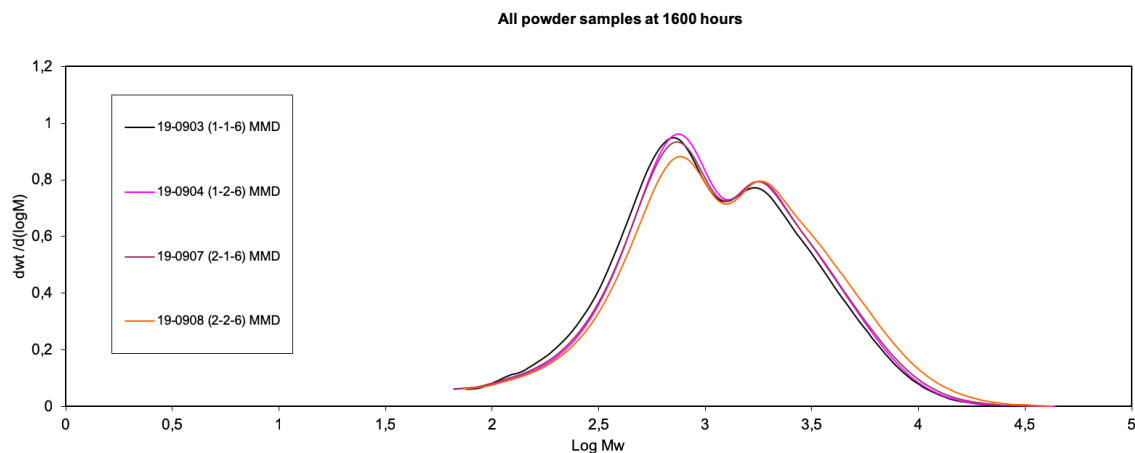


Figure 4.22: The mass distribution shown for all 4 powder samples at the end of the experiment as mass fraction is plotted against the logarithm molar mass of the powder samples analysed by GPC.

For the 3 types of films 9 of the total 18 samples were analysed with GPC. All 3 films were analysed at the times 0, 720 and 1600 hours. The full list of results can be seen in the table [4.13](#) below. The distribution of mass fraction plotted against the logarithm molar mass of the samples can be seen in the figure [4.23](#).

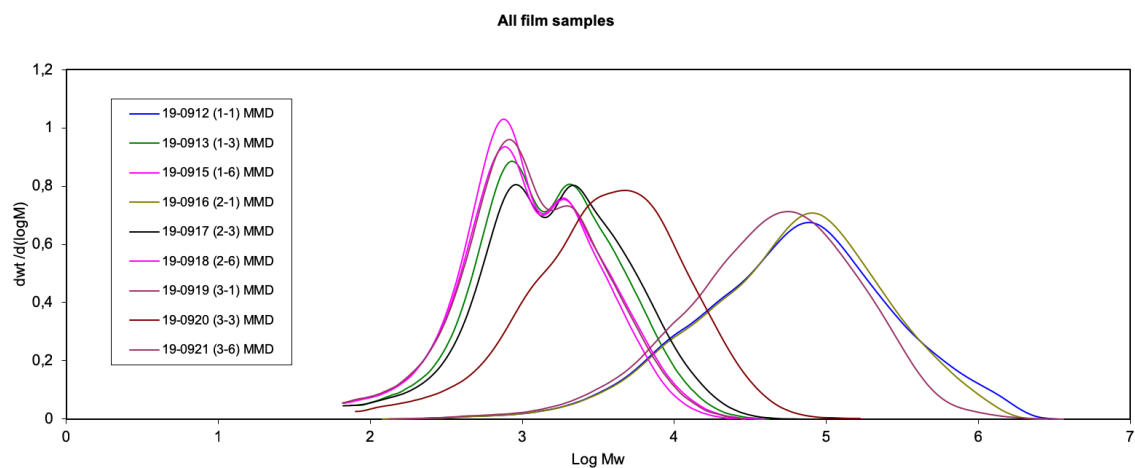


Figure 4.23: The mass distribution shown for all 3 film samples at the times 0, 720 and 1600 hours as mass fraction is plotted against the logarithm molar mass of the powder samples analysed by GPC.

For all samples M_n is the number-average molecular weight, M_w is the weight-average molecular weight and the polydispersity index (PDI), or molecular weight distribution, was calculated. This is the ratio of the weight-average molecular weight to the number-average

molecular weight. The average number of random chain scissions (n_t) was also calculated. The values obtained for the film samples can be seen in the table [4.13](#).

Table 4.13: Summary of results from GPC on selected degraded film samples. M_n is the number-average molecular weight, M_w is the weight-average molecular weight, the ratio between them also known as PDI and average number of random chain scissions (n_t).

Sample name	Mw (g/mol)	Mn (g/mol)	Mw / Mn	n_t
1-1	159900	17200	9.3	-
1-3	2500	800	2.9	$1.19 \cdot 10^{-3}$
1-6	1800	700	2.7	$1.37 \cdot 10^{-3}$
2-1	137800	16900	8.1	-
2-3	3000	900	3.4	$1.05 \cdot 10^{-3}$
2-6	2000	700	3.0	$1.37 \cdot 10^{-3}$
3-1	93800	14100	6.7	-
3-3	6600	1600	4.1	$5.54 \cdot 10^{-4}$
3-6	2000	700	2.9	$1.36 \cdot 10^{-3}$

Looking at the effect of the antioxidant, the 100 ppm Vitamin E additive, by comparing the samples 1 without additives to sample 2 with additive at the different times of degradation it can be seen that the sample 1 without additives has a slightly bigger loss of M_w as time passes in the chamber, but the exact same values for M_n . So the loss of weight is slightly slower with the additive.

The commercial LDPE plastic bag from Meny, film sample 3, has a lower starting M_w than the other samples, but all samples end with approximately the same M_w values at the end of the experiment. After 720 hours the commercial bread bag has retained a higher M_w than the two LLDPE films. All samples end with the same recorded M_n at the end of the experiment.

The distribution of mass fraction plotted against the logarithm molar mass of the 3 film samples at the start, and of the end of the experiment can be seen to follow very similar trends in the figure [4.24](#).

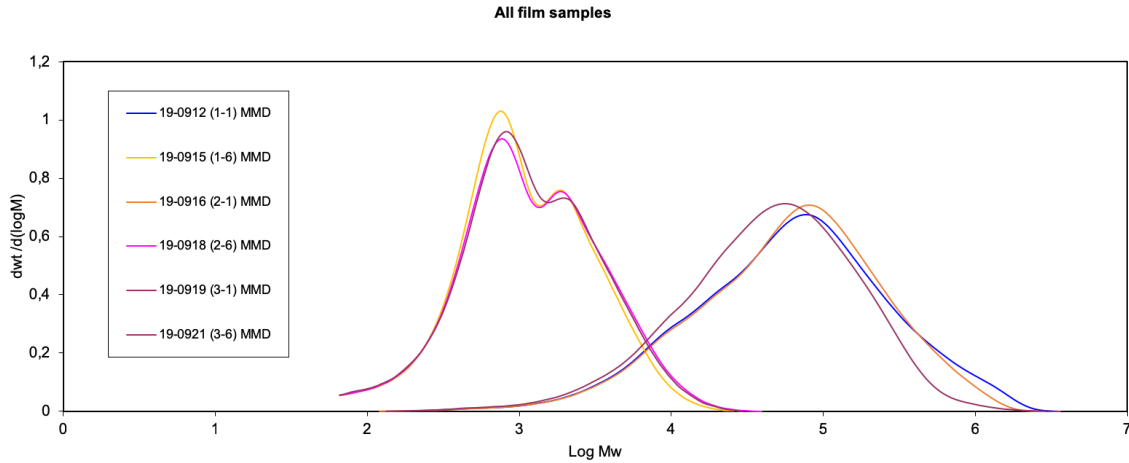


Figure 4.24: The mass distribution shown for all 3 film samples at the times 0 and 1600hours as mass fraction is plotted against the logarithm molar mass of the powder samples analysed by GPC.

4.3 Microplastic Adsorption of Metals

32 samples were tested for levels of six metals by ICP-MS. For the experiment 5L water was mixed with 181.5 gram NaCl which gives a weight percentage of 3.5% salt.

The density of water with 3.5% NaCl is 1.035g/cm^3 . This gives a total volume of 5.0063L. For each of the metals Cadmium (Cd), Chromium (Cr), Copper (Cu), Lead (Pb), Mercury (Hg) and Zinc (Zn) $25\mu\text{g}$ was added to the sample water. This gives an approximate concentration of $4.99\mu\text{g/L}$ for each of the metals in the solution.

Based on the results the partition coefficients (K_{pw}) were calculated for each case [16]. The formula is given by:

$$K_{pw} = \frac{[MeP]}{[MeW]} \quad (4.1)$$

where $[MeP]$ is the concentration of the respective metal on the surface of the plastic indicating the adsorption in $\mu\text{g/g}$ and $[MeW]$ is the concentration of the metal in the surrounding seawater of the respective experimental unit in $\mu\text{g/L}$.

4.3.1 ICP-MS Analysis

Sample 1-16 are the solution water which had degraded plastic particle suspended in for 13 days. The solution was filtered, and analysed by ICP-MS. A summary of the results can be found in the table [4.14](#)

Table 4.14: Results from ICP-MS of the solution. Cadmium (Cd), Chromium (Cr), Copper (Cu), Lead (Pb), Mercury (Hg) and Zinc (Zn) are all given in $\mu\text{g/L}$

ICP-MS label	Sample	Gram	Cd	Cr	Cu	Hg	Pb	Zn
1	W1-1A	0.201	5.30	5.31	7.63	2.92	5.01	9.57
1	W1-1A	0.201	5.47	5.61	7.74	2.36	5.13	8.79
2	W1-1B	0.209	5.46	5.22	10.1	2.55	5.19	7.80
3	W1-1C	0.205	5.22	5.05	7.82	2.38	4.97	6.27
5	W1-2A	0.202	5.19	5.25	8.32	2.25	4.98	6.43
6	W1-2B	0.204	4.81	4.74	6.88	1.94	4.56	7.22
7	W1-2C	0.208	5.12	4.83	29.9	2.19	4.83	7.43
9	W2-1A	0.206	4.89	5.03	6.32	2.11	4.62	6.68
10	W2-1B	0.204	4.64	4.46	6.23	2.16	4.54	5.36
11	W2-1C	0.203	4.81	4.44	5.89	1.90	4.51	5.40
13	W2-2A	0.203	4.72	4.55	16.3	2.13	4.74	5.65
14	W2-2B	0.206	4.73	4.56	133	2.75	4.59	5.56
15	W2-2C	0.203	4.63	4.42	17.5	2.30	4.46	4.82
Average	-	0.204	5.00	4.88	20.3	2.30	4.78	6.69
Median	-	0.204	4.89	4.83	7.82	2.25	4.74	6.43
4	1R	-	5.28	5.67	9.43	3.89	8.92	6.72
8	2R	-	5.13	4.80	6.04	3.59	6.36	5.40
12	3R	-	4.72	4.75	5.89	3.38	4.66	4.53
16	4R	-	4.66	4.51	9.86	3.10	4.68	5.36
Average	-	-	4.95	4.93	7.81	3.49	6.16	5.50
Median	-	-	4.93	4.78	7.74	3.49	5.52	5.38
K_{pw}	-	-	0.00811	-0.0105	-0.0103	0.355	0.141	-0.195

The complete list of results with error margins can be found in the appendix, in section [B](#) on page [XXV](#). Each sample had 4 parallels, where one was left without any plastic as a reference. Therefore if the particles have adsorbed any metals the control should show a higher concentration than the remaining samples. Only for mercury does it appear to have a consistently higher concentration in the control samples than the samples with degraded particles as can be seen by the higher coefficient (K_{pw}). For zinc there might be some interaction, as the reference samples without particles show a slightly lower value. For cadmium, chromium and lead it appears on these data alone that no interaction has occurred with the particles as the values are consistent for all samples, and the values are in the range of what was added to the solution. No trend between the different types of plastic particles can be seen.

For sample 17-32, the particles were left in the beakers as the solution was removed. The samples were washed several times with water before being left in a 10% HNO_3 solution for 24 hours. As HNO_3 is a strong oxidization acid it was used to achieve elution between the particles and the solution. It was expected that after 24 hours the H^+ will switch place with the metal ions so that they would be present in the acid solution.

Here the reference samples were the same degraded plastic samples and were also left for 24 hours in HNO_3 , but they were never exposed to a metal solution beforehand. A summary of the results can be seen in table [4.15](#), while the full results with error can be seen in section [B](#) on page [XXV](#). The (K_{pw}) for the elements are also in the table, also here it is calculating using the median of the values found for the solution without particles (sample 1R-4R) found in table [4.14](#) for the estimate of concentration in the seawater.

The reference samples were never put in the seawater and metals solution, and is therefore a good indicator of what metals were already present before starting the experiment. Here it can be seen that the samples had practically no levels of cadmium and mercury before start. There are some levels of chromium, and higher levels of copper, lead and zinc in the plastic particles. The mercury levels are around the same values for all samples (except the references), indicating that a stable level of adsorption occurred.

Table 4.15: Results from ICP-MS after washed particles were left in acid for 24 hours. Cadmium (Cd), Chromium (Cr), Copper (Cu), Lead (Pb), Mercury (Hg) and Zinc (Zn) are all given in $\mu\text{g/L}$

ICP-MS label	Sample	Gram	Cd	Cr	Cu	Hg	Pb	Zn
17	P1-1A	0.201	2.40	28.1	56.0	3.17	16.2	24.1
17	P1-1A	0.201	2.63	26.6	50.5	3.21	17.0	22.9
18	P1-1B	0.209	3.59	17.1	49.4	4.80	15.3	17.9
19	P1-1C	0.205	3.75	32.7	73.0	5.29	18.4	40.0
21	P1-2A	0.202	0.466	8.5	20.9	2.13	5.8	20.2
22	P1-2B	0.204	1.66	22.6	27.2	2.96	7.8	8.8
23	P1-2C	0.208	1.19	18.8	35.9	2.50	9.4	13.8
25	P2-1A	0.206	1.53	13.0	35.2	2.67	10.4	10.4
26	P2-1B	0.204	2.38	18.7	44.5	2.53	11.3	25.8
27	P2-1C	0.203	1.74	10.9	32.0	2.66	11.0	24.3
29	P2-2A	0.203	1.15	11.5	43.7	2.59	7.3	9.64
30	P2-2B	0.206	0.437	11.7	160	2.38	4.8	12.8
31	P2-2C	0.203	0.974	11.6	40.2	2.39	5.7	8.7
Average	-	0.204	1.84	17.8	51.4	3.02	10.8	18.4
Median	-	0.204	1.66	17.1	43.7	2.66	10.4	17.9
20	P1-1R	0.202	0.0904	3.31	22.2	-0.158	10.9	9.47
24	P1-2R	0.203	0.0539	2.02	15.5	-0.111	3.28	10.1
28	P2-2R	0.202	0.00640	0.970	13.2	0.137	6.49	8.01
32	P2-2R	0.205	-0.00252	1.64	16.4	-0.115	3.15	18.3
32	P2-2RR	0.205	0.00586	2.13	13.8	0.00458	2.85	17.4
K_{pw}	-	-	0.337	3.58	5.65	0.762	1.89	3.33
Average	-	0.204	0.0308	2.01	16.2	-0.0485	5.33	12.7
Median	-	0.204	0.00640	2.02	15.5	-0.111	3.28	10.1

4.3.2 Principle Component Analysis

On the ICP-MS results the statistic operation principal component analysis (PCA) was executed. PCA can be seen as an ordination technique that constructs the theoretical variable that reduces the total residual sum of squares after fitting a straight line to the data for each species. PCA reduces the dataset into major components representing the correlation of the elements. Since the nature of the experiment was that if there are no change in levels compared to reference then no adsorption had taken place, if there is a lower level in the samples than reference this will indicate that the particles had adsorbed parts of the solution and if the levels are higher than the reference that the particles had released metals to the solution.

The data was pre-processed before PCA was executed on them. This was done by subtracting the median reference value from all values. The PCA was executed in the software PAST [141]. It was verified using a MATLAB code that can be seen in the appendix in section B on page 33. The factor loadings or component loadings are the correlation coefficients between variables and factors. Factor loadings of these elements onto the principal components PC1-PC4 with eigenvalues and explained variances are found for sample 1-16 in table 4.16 and for sample 17-32 in table .

Table 4.16: Principal component loadings for Cadmium (Cd), Chromium (Cr), Copper (Cu), Lead (Pb), Mercury (Hg) and Zinc (Zn) on sample 1-16. Pre-processed by subtracting the median of the reference samples

Element	PC1	PC2	PC3	PC4
Cd	-0.27	0.80	0.37	0.32
Cr	-0.29	0.81	0.32	0.35
Cu	1.0	0.00054	-4.6E ⁻⁵	4.9E ⁻⁵
Hg	0.43	0.62	0.52	-0.40
Pb	-0.24	0.74	0.49	0.28
Zn	-0.25	0.97	-0.067	-0.017
Eigenvalue	319	0.73	0.031	0.012
% Variance	99.8	0.23	0.0096	0.0061

The number of significant principal components were estimated on the basis of the Kaiser criterion with eigenvalue higher than 1 [97]. According to this criterion, for sample 1-16 only the first principal component should be retained because subsequent eigenvalues are

all less than one.

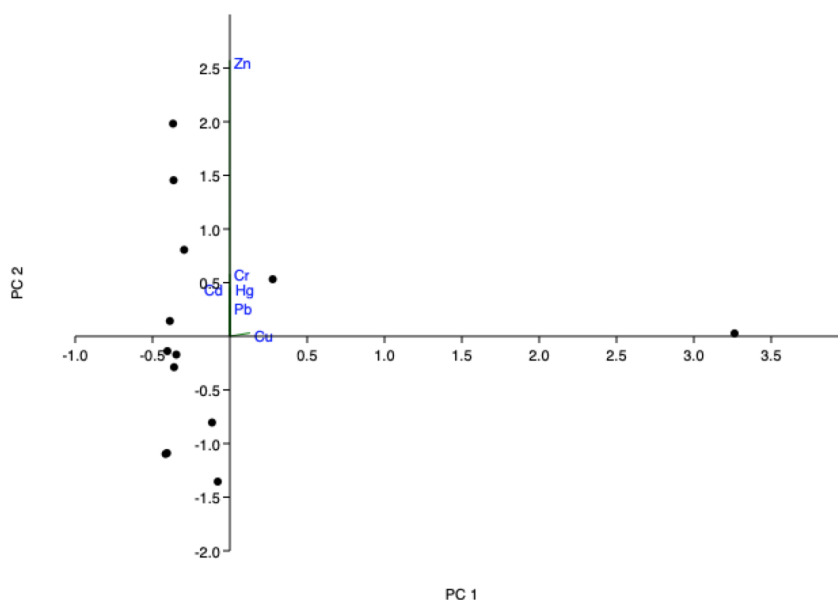


Figure 4.25: Principal component analysis (PC1 vs PC2) loading plots for sample 1-16.

The variables of sample 1-16 are correlated with one principal components in which 99.75% of the variance in the data is found. However, for illustrative purposes 2 principle component were kept. The second has an eigenvalue of 0.73 retaining it keeps a total variance of 99.98%. A spatial representation of the two components is shown in [4.25](#). Where a positive score means that the concentration of variables increases along the PC axis, a negative score suggests that the concentration of variables decreases along the axis and a score near 0 means that the concentration is poorly related to the PC axis. The direction of the variable arrows indicates the direction in which the concentration of the corresponding species increases most.

For sample 17-32, 4 principle components have an eigenvalue above 1, with PC 1 having a considerable higher value than the other. Hence, reduced dimensionality of the descriptor space is four. The variables with the 4 PC's have retained 99.96% of the total variance. In PC1 Cu shows with a particularly high loading. In PC 2 Cr, Zn and and Cr have higher loadings that the remaining variables. This indicates a correlation between these metals. A spatial representation of the two components PC 1 and PC 2 is shown in figure [4.26](#).

4. RESULTS

Table 4.17: Principal component loadings for Cadmium (Cd), Chromium (Cr), Copper (Cu), Lead (Pb), Mercury (Hg) and Zinc (Zn) on sample 17-32. Pre-processed by subtracting the median of the reference samples.

Element	PC1	PC2	PC3	PC4
Cd	-0.0024	0.076	0.033	0.20
Cr	0.013	0.57	0.74	-0.36
Cu	0.99	-0.018	0.0048	0.016
Hg	0.0027	0.059	0.027	0.15
Pb	-0.0093	0.36	0.15	0.88
Zn	0.019	0.73	-0.66	-0.18
Eigenvalue	1247	31.0	27.6	4.7
% Variance	88	9.3	2.0	0.33

It can be seen that most of the samples are oriented on the negative side of the PC 1 axis, with 3 exceptions. Sample 30 (P2-2B) is found high on the PC 1 axis, and sample 19 (P1-1C) high on the PC 2.

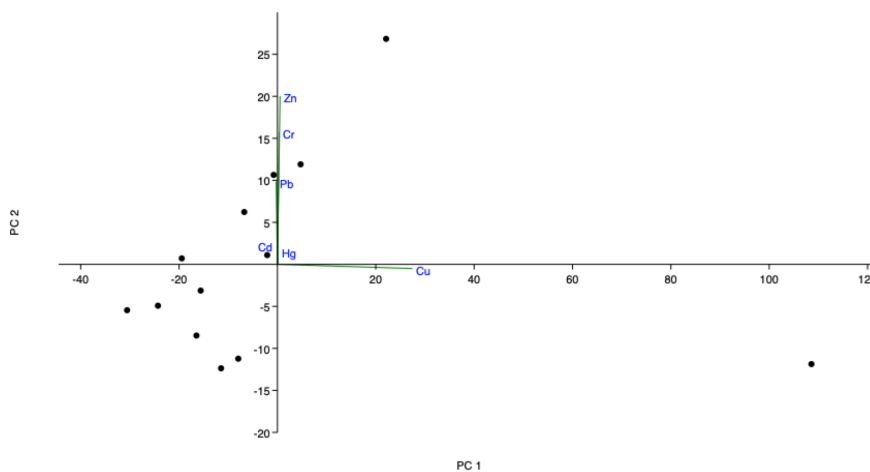


Figure 4.26: Principal component analysis (PC1 vs PC2) loading plots for sample 17-32.

A spatial representation of the two components PC 2 and PC 3 is shown in [4.27](#). The direction of the variable arrows indicates the direction in which the concentration of the corresponding species increases most, and the length of the arrows equals the rate of change in that direction.

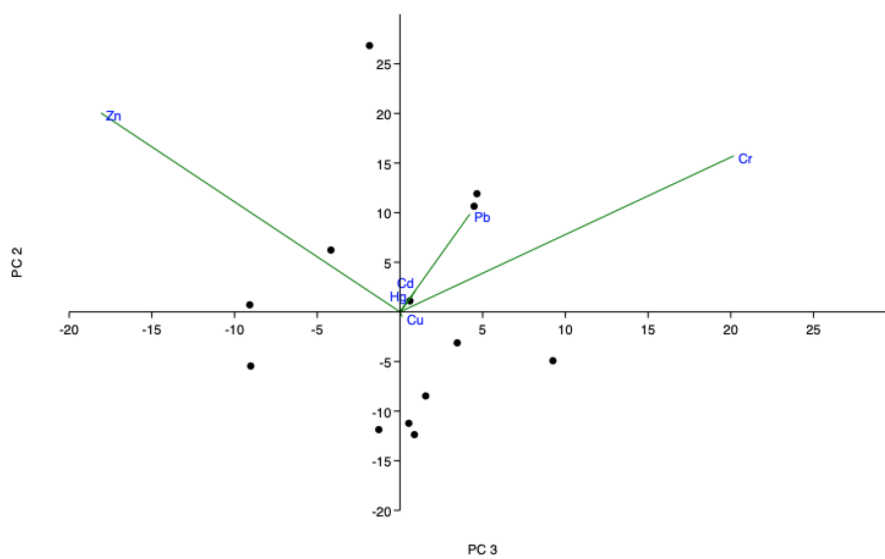


Figure 4.27: Principal component analysis (PC2 vs PC3) loading plots for sample 17-32.

5 Discussion

5.1 Samples from The Arctic Expedition

All 11 trawls conducted on the S/Y Fairwinds for the arctic expedition resulted in samples containing plastics. Due to the mesh size of the plankton net used it limited the acquisition to macroplastics, and microplastics in the size of 300 – 5000 μm . The distances trawled ranged from 195.5 to 10.2 km in the North Atlantic Ocean. The expedition started with the first 2 samplings on the west-coast of Bermuda, followed with 1 outside Nova Scotia, 3 in the Gulf of Saint Lawrence bounded by the Newfoundland and Canada, 4 on the east coast of Greenland and ending with one on the west coast of Iceland. 387 particles were visually identified in the 11 samples. The types of particles were identified as either 3D, 2D/film and fibre. Fibres were most abundant with 44%, followed by film/2D at 37% and the remaining 19% being 3D. This compares well with other studies that also found fibres as the main type microplastic [91]. The colours were also characterised showing that 35% of the particles were white, 19% blue and 16% clear.

With the assumption that half the trawl was lowered in the seawater, meaning that the samples were collected on the top 28 cm of the water surface, concentrations were calculated. The abundance of microplastics ranged between 0.002 to 0.1630 particles per m^3 , and was averaged on 0.0252 per m^3 . The highest abundance was found in sample 3, outside Nova Scotia. The lowest abundance was found on the east coast of Greenland (sample 7 and 10).

Compared to published studies these levels are low. Older estimates in the Northwest Atlantic have been 3 particles per m^3 (costal, 1972) to 67 particles per m^3 (offshore, 1974) [142]. Average plastic abundance in the Northeast Atlantic was estimated to be 2.46 particles/ m^3 in 2014 [143], and an average microplastic abundance in the sub-surface waters of the Atlantic Ocean was found to be 1.15 particles/ m^3 in 2016 [144]. This could indicate that the assumption that half the trawl was below the sea surface could be incorrect, the depth should be more accurately measured and recorded for a better study.

Previous studies conducted on the east coast of Greenland observed average abundances of 0.99 ± 0.62 microplastics per m^3 and 2.38 ± 1.11 microplastics per m^3 in 2005 and 2014, respectively [145]. The 2005 study was executed with a mesh size of $500 \mu\text{m}$ and the 2014 with a $100 \mu\text{m}$. This is also considerable higher numbers compared to sample 7 to 10 ($0.02 - 0.099$ particles/ m^3) trawled on the east coast of Greenland during the arctic expedition. Based on the current estimates of growing plastic pollution one would expect that there would be a higher number of particles found in 2018 than in 2005, especially considering that the study was conductive with a mesh size $200 \mu\text{m}$ larger than in the arctic expedition.

There are few comparable studies to the sample 3, taken in the waters outside Nova Scotia. This was the sample with the highest result, with 0.1630 particles/ m^3 . There have been a study showing higher levels of microplastics in mussels farmed off the coast of Newfoundland and Labrador (close to where the trawling occurred) compared to what is found in wild mussels in the harbour in Halifax [146]. One potential explanation to this is the fact that the Gulf Stream passes and can carrying plastic pollution from southern latitudes in the North Atlantic Ocean known to have high concentrations of microplastics to the north into the Labrador Sea [45].

Samples 4, 5 and 6 were all taken trawled in the Gulf of Saint Lawrence. The three samples have very similar results with 0.0271 , 0.0268 and 0.0252 particles per m^3 . These three samplings were done in the timeframe of six days. As the area is relatively closed off for any big currents this seems likely to be an indication of a constant level of concentration of microplastics that can be found there.

A study conducted in the North Atlantic gyre ($29-31^\circ\text{N}$) found an average of 0.0041 particles/ m^3 ($20,328 \text{ km}^{-2}$) in 2010 [147]. This compares well to the samples 1 and 2 that were conducted at 30 to 31°N . Sample 1 found a concentration of 0.0025 particles per m^3 and sample 2 0.0075 per m^3 .

Few studies report on the microplastic pollution outside Iceland, but a study conducted in Arctic polar waters, south and southwest of Svalbard (Norway) found an averaged of 0.34 particles per m^3 where the particle composition showed 95% fibres [59]. This is thought to be a result of the North Atlantic Current that can disperse litter from the North Atlantic

gyre north to more remote areas. However, the values reported outside Svalbard is much higher than the found 0.0023 particles per m³ found in sample 11 taken outside Iceland.

Many studies have reported increasing numbers of micro and macroplastics towards centres of ocean gyres [57], this cannot be seen in these results. Surface currents, wind and boat movement can cause turbulence that would be expected to redistribute particles within the water column, possibly below the level of trawling. There have been reported in studies a difference with fewer particles in colder, less saline waters which could affect the results. The distances and conditions for the different trawls were reported to vary a lot. Executing several trawls in the same areas would have been preferred, to evaluate the finds through statistical analysis as well as keeping the trawls within similar distances.

5.1.1 ATR FT-IR Analysis

All 387 particles from the 11 samples were analysed using ATR-FT-IR or microscopy FT-IR. 365 of the particles were successfully identified, with 362 were identified as synthetic polymers, and 3 as organic particles. This gives a percentage of identification of 95%. The remaining 22 particles were too small to fit the crystal for proper ATR-FT-IR identification, and could also not be successfully identified using FTIR microscopy as the total adsorption appears in the high spectral range. Another issue was that the self-adsorption band on the filter superposes on the band around 1500 cm⁻¹, creating issues for the identification. To identify and to classify environmental microplastic particles, the complete mid-infrared spectrum including the fingerprint region must be available. Many of these unidentified samples were also described as ‘greasy’ that indicated contamination that could be disturbing the spectra, but were considered too fragile to be cleaned by anything else than distilled water.

Identification of FT-IR spectra are only possible with the comparison of reference samples for the polymers. Using polymer libraries most of the samples were easily identified, giving a quality index well above 0.7. To ensure the level of correct identification all polyethylene sample were identified as that, making no distinction between PE, HDPE, LLDPE and LDPE. HDPE and LDPE share the same major structural unit, functional groups and

most of the chemical bonds resulting in many identical bands for identification. However, there are some studies on using ATR FT-IR to distinguish them [140]. This can be done by comparing the band at 1377 cm^{-1} , as LDPE or LLDPE typically show a clear but small band here while it is absent or has a shoulder in HDPE. This is due to the higher branching in LDPE and LLDPE. However, aging and chemical weathering of the samples can modify their spectral features [7]. As the samples were expected to show some degree of weathering, and the uncertainty of their aging this was considered too difficult and the types of PE were not attempted differentiated.

It is known that aging, and photo-oxidation of synthetic polymers gives changes to the FT-IR spectrum. When the polymers react with oxygen, it leads to the formation of carbonyls (C=O) and vinyl ($\text{CH}_2=\text{CH}$) groups that can be identified. But, without a reference as a comparison for a specific sample it is impossible to use it as a measure of aging. Therefore FT-IR can be considered a good method of identification, but not much else information can reliably be extracted.

5.1.2 Pyr-GC/MS Analysis

A selection of 50 particles were analysed using Pyr-GC/MS to verify the results obtained through FT-IR. Here identification was unsuccessful for 8 of the 50 samples. 3 gave identifications that differed from the FT-IR, and 1 sample that was not possible to identify with FT-IR was identified.

Pyr-GC/MS shows great potential for weathered polymer samples, and each run requires only 5 - 200 μg of the sample [119]. However, the results are quite affected by the sample size, and it should be kept constant. Most samples had to be cut with a scalpel to the size of 1 mm^2 to give a good spectrum. Especially challenging were the fibre samples as they have a very low weight, a greater sample was needed, and when positioned on the pyrolysis filament they frequently were blown away by the helium gas before analysis. It is possible that pyr-GC/MS analysis of fibres would be better with another type of pyrolyzer unit like a continuous-mode one where the samples are placed into a closed furnace.

The remaining unidentified samples particles could not be classified due to either a lack of pyrolytic products formed, low pyrolytic product abundance, or the lack of a clear polymer match, and were subsequently categorised as unknown. A clear disadvantage of pyr-GC/MS is that it is destructive and for many of the microplastic particles there were not enough for a second or third run.

The significant carry-over and ghost peaks in the Pyr-GC/MS pyrograms might be explained by the decomposition of the polymer sample and deposition at an inadequate interface, like between the injector and column. This resulted in a constant background that caused problems, also the septum on the unit is made of rubber that could contaminate the sample. As such, the identification of the polymer was possible in most cases but the background was so large that no peaks for additives could be identified. Due to time and sample size limitations the samples were not re-run on a lower temperature, this has shown promising for additive identification but the temperature is too low for proper identification of the polymer itself [17].

Distinction between the different types of polyethylene and polypropylene should also be possible with pyr-GC/MS. The pyrograms should have noticeable different patterns due to the branching nature of LDPE and HDPE. However, the spectra obtained were often far from the reference ones, and the intensities much lower. This is most likely due to the weathering of the samples, which effects the pyrogram by reducing the amount of peaks and the intensities of them, so the usage of mass spectrometry is instrumental for correct identification.

In total pyr-GC/MS gave identification of 42 of 50 particles. This gives a percentage of reproducibility 84% and confirms pyr-GC/MS as an applicable analytical tool for microplastic polymer identification.

5.1.3 Comparison of Methods

Both methods of identification, FT-IR and py-GCMS, are well suited to characterise the chemical nature of microplastics. FT-IR gave a successful identification on 95% of the

particles and pyr-GC/MS on 85%.

ATR-FTIR has shown to be a reliable and fast identification of polymer type for most sizes of mass. It has the clear advantage of being non-destructive, and the same item can be repeatedly analysed to confirm the results. However, it does struggle when the size of the microplastic is too small to cover the crystal, here FT-IR microscopy is useful but also has some issues. The identification of FT-IR can also be hindered in the presence of organic and inorganic impurities as they can overlap the polymer bands in the IR spectra. This is not an issue for pyr-GC/MS as they are either not pyrolyzed (inorganic contaminants) or have discriminable different retention behavior and m/z values (organic contaminants).

Another considerable advantage of py-GC/MS is the simultaneous identification and specification of the synthetic polymer and then potentially associated additives when possible. But the method is considerably more time consuming for polymer identification. For comparison, for the 50 particles analysed with pyr-GC/MS 179 runs of 30 min was conducted (this is including runs for calibration of the pyrolysis and necessary blank runs to ensure no contamination between samples), and adding the time to prepare/cut samples and clean the filament between samples this adds up to around 2.5 hours per particle identification. Identification of an sample through FT-IR was a matter of minutes.

Pyr-GC/MS can still be considered a relatively new method, and only recently have standardisation of the instruments taken place making it possible to compare spectra. Because of this databases are still under development and therefore comparison to literature values is often needed. However, the method is has good sensitivity due to the MS and should theoretically be able to identify indicator ions even on trace levels.

Of the 387 particles from the 11 samples 362 were identified as synthetic polymers. Of this 57% were shown to be PE and 29% PP. This concurred well with what was expected to find on the sea-surface, considering the density of polymers. Both method of analysis give good identification but FT-IR is more developed, as well as bit easier and quicker than pyr-GC/MS.

5.2 Artificial Weathering of LLDPE

The weathering effects of the films were apparent after only 2 weeks as it had fragmented, and already after 4 weeks it was barely holding together and was extremely fragile. The powders could be observed to be yellowed in colour over the course of the experiment which is also insinuating weathering but not a definitive indicator. The UV light source was placed right above the samples, being placed flat in the chamber. The powder was stirred during the experiment to ensure homogeneous weathering, but constant stirring of a thinner layer might have been a better guarantee of it. It is also assumed that the lamp gave an equally strong irradiation to all corners of the chamber, but this seems unlikely, so samples were shifted a bit during the experiment within limitations as the chamber was filled to maximum capacity. As PE was the most common polymer (57%) found in the samples from the Arctic Expedition it seemed as the most natural polymer for the accelerated weathering experiment. As discussed, it was not possible to say which type of PE is most frequent as a plastic pollution but LLDPE was chosen so it could be compared to a commercial LDPE bread bag found in the local supermarket. A product most are familiar with, and which frequently appears in photos of plastic pollution in nature.

Accelerated tests are useful as the time scale for providing information about the weathering of products are too long. However, it is an issue to prove the validity of accelerated test and obtain correct correlation with natural exposure. Natural exposure or service trials are commonly executed for a comparison of weathering models, but as there are such a wide range of synthetic polymers with a range of adaptation (for example additives) that has proven difficult. Studies on the status of standard testing methods and procedures have shown that few international standards are totally adequate, but despite their limitations are necessary [148]. Therefore, accelerated tests show a number of intrinsic problems and careful consideration should be taken when designing the experiment, its analysis and especially when estimating the significance and limitation of the results.

Four estimations for the time in the accelerated UV-chamber to real-world exposure were conducted using different models. The irradiation was measured in two ways and the measurement done of the total UV(A+B) should be considered more reliable as when using

the approximation of the total irradiation based on the measurement for UV(340nm) several assumptions are made. A level of complexity was added to the experiment as real-world irradiation exposure in Europe is given under the conditions of an annual average temperature. In the chamber the temperature far exceeded this, being around 85°C for the duration of the weathering. Models estimating the exposure time taking into account an increase in temperature have shown to have many flaws, and the general rule of thumbs saying a 10 degree increase in temperature doubles the rate of degradation has been proven unreliable in several studies as one synthetic polymer might not react much to the temperature increase and another might. The addition of UV and thermal stabilizers to the polymers complicates the matter even further. Therefore, the estimation using the Arrhenius equation is valued as a better way of calculation, however it is depending on having the activation energy of the specific polymer for UV degradation which might differ from the global activation energy of a polymer that can be found in literature. As well as the impact possible additives would have. Therefore, the real-world time estimate of 1600 hours in the UV chamber using these two methods for temperature and the total UV(A+B) measured differs of almost a factor of 10. For 1600 hours in these 2 cases the simulated years in real-world would be 82.3 (rule of doubling) and 8.3 (Arrhenius with a literature value of the global activation energy for LLDPE). This does however show a tendency that the LLDPE films fragment much faster than what was expected, as plastic products are believed to be durable in their original state for many hundred years in nature. Real-world experiments would have to be conducted to verify which of the estimates are the best. For a more ideal accelerated weathering experiment it would be recommended holding a constant temperature equal to the real-world comparison as this would eliminate some of the complexity.

The samples were analysed using ATR FT-IR and GPC after exposure in the UV chamber. The powders were made into films using a hot press for ATR FT-IR analysis, this was done to try to ensure a homogenous film as the powders might have not been. The films were analysed as they were. There are three areas in the infrared spectra where degradation is commonly identified based on changes of the polymers, the presence of hydroxyl groups (peaks 3100 – 3700 cm^{-1} , centred around 3350 cm^{-1}), carbon double bonds/alkenes

(1600–1680⁻¹), and carbonyls (1690–1810 cm⁻¹), centered close to 1715 cm⁻¹. For all samples analysed there is an increase around 3100 – 3700 cm⁻¹, but as it was not one specific band but more of a flat-structured hump the hydroxyl groups were not used as a measure of weathering. The clearest peak that can be seen growing after time passes in the UV chamber is the carbonyl group which is centred around 1715-1720 cm⁻¹. The alkene bonds also seem to be increasing some, but not as clearly. The increase of the carbonyl group is expected as a result of LLDPE degradation, as the UV irradiation causes the formation of hydrogen radicals which are abstracted so the polymer reacts with oxygen leading to the formation of carbonyls (C=O). Scaling the spectra on top of each other, comparing the LLDPE samples with the anti-oxidant Vitamin E additive compared to the ones without, it can be seen that the increase of carbonyl groups is smaller over the time in the UV chamber with the anti-oxidant than those without. This can be seen to illustrate the stabilisation the vitamin E has on the polymer, delaying the reaction with oxygen leading to a slower rate of degradation. It was also seen that the smaller particle sized (200 – 425 μm) had a larger increase in the carbonyl group than particles with the larger size (425 - 600 μm) building up under the assumption that degradation goes faster as particle size decrease.

Based on the growth in the carbonyl group a carbonyl index model was built. By using the characteristic double peaks at around 2700 - 3000 cm⁻¹ as a reference for each sample the ratio between this and the carbonyl peak around 1552 - 1838 cm⁻¹ was calculated for each sample. The model was correlated across the different spectra and gave a calibration graph with a correlation of 0.99 and standard error of 0.0037, it was therefore estimated to be a good fit. The carbonyl index verified what was observed by visually inspecting the spectra and giving numbers to compare the increase in the group as time passed in the UV chamber. It gave a steady increase of the ratio for all samples as a function of time.

Analysis of the film samples showed that the carbonyl group increased faster without the anti-oxidant Vitamin E than with. There is no knowledge of possible additives in the commercial plastic bag, but is known to be LDPE and a bit over half as thin as the other LLDPE samples. The increase of carbonyl peaks as a function of time were in-between

what was observed for the other LLDPE films. This might indicate that there is some anti-oxidant or other additive present.

A selection of the samples was further analysed using HT-GPC. This was done to observe the possible decrease in the weight-average molar mass as a function of UV irradiation. As well as the number average of molecular weight (M_n), and the molecular weight distribution (M_w/M_n) also called PDI. An increased amount of material on the tailing end of the peaks corresponds to a lower M_w polymer. In GPC the longer retention time indicates that the polymer is smaller in size, and results confirmed that that was the case as a function of photodegradation of the polymers as both M_w and M_n is seen to increase. These observations indicate that chain scission have occurred, especially in the longer chains of the LLDPE. Chain scission might commonly occur in polymers to form polymer chains of medium size, but the end measurements of the M_w and M_n for the samples after 1600 hour in the UV chamber are very small that they are in the lowest end possible to measure by the HT-GPC instrument. This is confirmed as the M_n is the same in time 5 and 6, which seems unlikely due to the fact that the breakage of the polymers should increase as a function of UV irradiation. The decrease in the molecular weight distribution (PDI) indicates that the samples are more polydisperse than before exposure to the UV-light. The average number of chain scissions, or bond breakage number, was calculated for the possible samples and shows the same value for the samples with and without anti-oxidant additives at the time 1600 hours, however as it is based on the M_n it flattens out to this maximum value by the time 5.

All powder samples 1-1 (200-425 μm , without additives) were analysed at all time intervals (1-1-1 to 1-1-6) with GPC and 3 time intervals ($t = 1, 3$ and 6) of the 2-1 (200-425 μm , with vitamin E additive). The effect of the vitamin E anti-oxidant can also be observed here as the molar mass shifts slightly less to lower values as a function of time exposed to UV. For the larger particles only 1-2-6 and 2-2-6 (time 1600 hours) were analysed, and shows they end up with equivalent molecular weight as the samples, however the rate of loss cannot be said anything about. This selection was done due to the price of the analysis, and for a further study it would have been preferable to analyse all samples. The

film samples were all analysed at three times, before exposure, and at times 3 and 6. Also here the M_w and M_n for the samples after 1600 hour in the UV chamber are so small that they are in the lowest end possible for measurement. The end M_n and M_w values are the same as observed for the samples in powder form. The commercial plastic bread bag has a lower starting M_w than the other two, as well as being less polydisperse, but retains it better than the two LLDPE films at time 3. This can also be seen by having a much lower average number of chain scissions, or bond breakage number (n_t) than the other two at this time. Therefore it seems to indicate that an additive that works as a stabiliser from chain breakage is present.

Combining the results from ATR FT-IR and GPC shows the advantage of having an anti-oxidant present, to increase the resistance to chain breakage in LLDPE. Vitamin E is an anti-oxidant and can therefore be seen effective against the formation of carbonyl groups compared to having no additive present. The results indicate that the smaller particles will have a faster rate of chain breakage than larger particles. The commercial plastic bags appears to contain additive that prevented chain breakage compared to the LLDPE film without any, but not that had the same anti-oxidant properties as the 100 ppm Vitamin E additive. This is indicated in the fact that the increase in carbonyl groups for the commercial bread bag were faster as a function of time than for the LLDPE film with vitamin E.

The films fragmented faster than what is speculated for LLDPE in nature. It was visually in pieces after 360 hours in the UV chamber which is estimated to be between 1.9 – 18.5 years in real-world nature. It can be discussed if this is positive or negative. As the film, or commercial bread bags, fragments in nature the pollution is not as visually apparent however it will still be present as smaller particles, that can be fragmented into microplastics and impossible to clean up.

5.3 Metal Pollution in Microplastics

The particles that were not exposed to the metal containing solution, and were placed in HNO₃ for 24 hours as a reference were shown to contain levels of Cu (average of 16 µg/L), Zn (average 12.65 µg/L), some Pb (average 5 µg/L) and Cr (average 2 µg/L). However, no Cd or Hg were measured. This can be thought to come from the raw materials, production or the degradation process.

In this experiment the exchange between the solution and the particles were the main focus. Using a known concentration (4.99 µg/L) of the six metals (Cd, Cr, Cu, Hg, Pb and Zn) it was checked if the metals would interact with the particles in any way. The particles were suspended in solution for 13 days in artificially made seawater (milliQ with a 3.5 weight % NaCl). This was used over an actual seawater solution to limit possible interaction between the metals and other elements in the water. The interaction between the particles and solution seems to be quite small. For Cd, Cr and Pb it appears like there has been little effect with particles, the concentrations of solution without particles show about the same values as those with, this is confirmed by the calculated K_{pw} . It does appear that some zinc was released from the particles to the solution and some mercury have gone from the solution to the particles. 2 samples have very high level of Cu, but as 3 parallels were run for each one can assume this is something with the particular sample. Any differentiating interaction between the samples that had additives and without, or particle sizes cannot be observed. The reference samples done without particles also show that there is a lower level measured of mercury than what was added into the solution. It is possible that the element bonded to the glass, an interaction with NaCl occurred or possibly that it was not properly dissolved.

For the samples that were tested through cleaning of the particles and being left in acid (HNO₃) overnight the results show higher levels of all metals compared to particles that were not exposed to the solution. However, these results do not compare well with any of the others. This might be due to the fact that proper washing and cleansing of the particles was unsuccessful leaving solution to be dried with the particles, and therefore being dissolved in the acid so the samples do not properly show the concentration in

particles. As the particles sedimented very softly, extracting the solution showed difficult and more rounds of washing, sedimenting and extraction should have been done.

For the samples a principle components analysis (PCA) was done in an attempt to reduce the dataset into major components representing the correlation of the elements. Due to the nature of the experiment the values achieved by ICP-MS were not given as $\mu\text{g/L}$ metals adsorbed or released to solution but by remaining concentration in the seawater.

Therefore, the data was pre-processed before PCA was executed on the values. All values were subtracted the median of the element in reference to give the impact the particles have. It was assumed based on the ICP-MS results that particle size and vitamin E additive did not affect the polymers interactions with metals. The median values were chosen over the average as it is more reliant for possible outliers. The principle component analysis was done on sample 1-16 and then 17-32 separately due to the nature of their values. The operation was done using the variance-covariance, to find the eigenvalues and eigenvectors with the SVD algorithm, as all variables are measured in the same units.

For sample 1-16 2 PCA's were included into the chosen model, which gave a total variance of 99.98%. But the most variance is contained within the first PC as it has an eigenvalue 318.91 and variance of 99.75%. Here PC 1 loadings indicate that there are correlations between the concentration copper (Cu) and the Mercury (Hg). The loadings on Cu are especially high. As it can be seen the values from the ICP-MS, Cu are higher than that of the reference without plastic particles and Hg consistently lower than the reference. PC 2 gives some possible correlation with Zn having the biggest loading, but all the loadings are very close in numbers making them not very useful. No element can be written off by having a very low contribution to the PCA's if two are included. At the biplot it can be seen that Cd, Cdr Hg and Pb are grouped quite close and close to origin, while Cu and especially Zn are further away. This can indicate that there is good correlation of values across the samples for these elements.

The principle component analysis of sample 17-32, which were the particles washed, dried and put in acid for 24 hours gets some differencing results. Here the 4 first principle components have eigenvalues over 1. The PC 1 has the highest eigenvalue (1246.95) and

variance (88.4%). In PC1 the element Cu has the highest loading. In PC 2 (eigenvalue 30.95 and variance 9.28 %), the largest loadings are Zn (0.72), and Cr (0.57), indicating a correlation. In the biplot Cd and Hg are closely grouped to each other while Cu is further along the positive side of the PC 1 axis and in direction with the PC 2 Pb, Cr and Zn are placed. PC 2 plotted against PC3 shows again Cd, and Hg grouped in the middle close to zero while Cr, Pb and Zn are spread further out however only 1.95% of the variance is contained in PC 3.

The PCA results did not explicitly eliminate any variable (metal element) if the rule of eigenvalue over 1 is kept. However, it shows that Cu, Zn and Hg are the most interesting ones, and it is indicated that there is a correlation between the values of Zn and Hg while the Cu concentration is not correlated with the other elements. Based on the ICP-MS and these PCA results it seems like the elements interaction between the particles and the solution that is interesting are then Zn and Hg, while the correlation to the values of Cu cannot be concluded. It is seen that for the three parallels of each run the Cu concentration varies greatly, indicating a source of contamination or improper handling that affected only this element.

As mentioned in the theory section, studies have shown the ability to adsorb metals on aged plastic particles due to the modification of the surface. One study showed a significant interaction between these the copper (Cu) and zinc (Zn) to virgin polystyrene (PS) beads and aged polyvinyl chloride (PVC) after only 14 days [16]. Here the calculated K_{pw} ranged from 33 to 659, which is considerable higher than what was found in this experiment. There are several differences in the design of the experiment, like the source of the metals and the type of plastic particles even if there was just a 24 hour difference in the length.

These result does not strongly confirm the abilities of degraded particles to interact with metals as previous studies have but does imply that the particles bind to some mercury over any other metal. Another significant difference can be that this experiment was done using degraded LLDPE, which concurred well with the findings from the Arctic Expedition as 57% of the trawled particles were identified as PE, showing that these are more realistically the particles found in nature. They were exposed in the UV chamber for 1200h

5. *DISCUSSION*

which simulated is between 6 to 62 years in nature (depending on model used) be more realistic image of real-life particles. Further studies, over longer time should be executed to verify and build on these results preferably with different types of polymers.

6 Conclusion

387 particles from 11 samples from the Arctic Expedition in the North Atlantic Ocean was analysed using ATR FT-IR and was verified by analysing 50 by pyr-GC/MS. An average of 0.0252 particles per m³ was found, this is a bit below other reports of abundance. The majority of the samples were fibre (44%) and 2D/films (37%) over 3D. White (35%), blue (19%) and clear (16%) were the most common colours of the particles. 362 of the 387 particles were identified as synthetic polymers, PE (57%) and PP (29%) showed to be the most abundant types of plastics found. Pyr-GC/MS is a promising technique for analysing microplastics but is not as easy and well-developed as ATR FT-IR.

An accelerated weathering study was executed on LLDPE in both particle and film form, with and without 100ppm of the anti-oxidant Vitamin E additive. Two particle sizes were used 200-425 μm and 425-600 μm . An LDPE commercial bread bag was also tested with the other samples. It is found difficult to accurately estimate time in the UV chamber to time in real-life nature but 1600 hours in these conditions were estimated to be between 8.3 to 82.3 years. The weathered samples were analysed using GPC and ATR FT-IR, and showed that the anti-oxidant properties of vitamin E additive decreased the rate of chain breakage compared to LLDPE without, both for films and particles. A smaller particle size seems to increase the rate of chain breakage. The commercial LDPE bread bag from Meny appears to contain some type of additive as it has a slower chain-breakage than the other LLDPE films.

Using the weathered particles exposed to irradiation in the UV chamber for 1200 hours a study of the adsorption of six metals (Cd, Cr, Cu, Hg, Pb, Zn) in simulated seawater was done. ICP-MS was used to analyse the solutions and PCA was conducted on the results. It showed that the particles had some adsorption of Hg ($K_{pw} = 0.36$) but less than reported in other studies, and that the particles released Zn to the water ($K_{pw} = -0.20$). For the 4 other metals no interaction shown and there were no indication of particle size effecting adsorption.

7 Suggestions for Future Research

The characterisation of microplastic particles were limited to a size-range due to the mesh size of the net used (300 μm), repeating a trawl with a smaller net size would be desirable. Having several trawls from each location would be preferable, over the course of different weather conditions to ensure that the samples give a realistic image. Studies are still sparse for microplastic abundance in Arctic latitudes and more samples from these areas would be very interesting to trawl for.

The usage of FT-IR and pyr-GC/MS is well reported for identification of real marine microplastic samples. Running the pyr-GC/MS on both low and higher temperature could have given identification of some common additives if the time had allowed it. It would also be interesting to build a reference library for weathered samples for pyr-GC/MS.

The weathering of LLDPE showed significant chain-breakage but was difficult to convert into real-world exposure time. Repeating such an experiment while limiting the parameters affecting degradation would be preferable, for example having the temperature set to what it is in real-world conditions, and only stimulate accelerated weathering through UV-light. The accelerated weathering study should also be repeated with other types of polymers to compare the degradation to that of LLDPE. Not all samples from the weathering were tested using GPC, this would have been interesting to see how the size of the particles effected the loss of molecular weight. ATR FT-IR analysis was done on both the real-life exposed samples from the Arctic Expedition and the weathering study to see the pattern of degradation. It would also be very interesting to test the real-life samples with GPC to compare the molecular weight to times in the UV-chamber.

There is indication that mercury is adsorbed to weathered LLDPE particles, it would be interesting to repeat the experiment using a longer time frame, and a wider range of metals. The experiment could also have been done with a variety of synthetic polymers, and at different point of weathering to see if the absorbance is dependent on the plastic type or degradation.

References

- [1] Nichols M. *The Graduate* (film). United States: Embassy Pictures; 1967.
- [2] Halden R, North EJ. Plastics and environmental health: the road ahead. *Reviews on Environmental Health*. 2013;28(1):1–8.
- [3] Jambeck JR, Geyer R, Wilcox C, Siegler TR, Perryman M, Andrady A, et al. Plastic waste inputs from land into the ocean. *Science*. 2015;347(6223):768–771.
- [4] Gallo F, Fossi C, Weber R, Santillo D, Sousa J, Ingram I, et al. Marine litter plastics and microplastics and their toxic chemicals components: the need for urgent preventive measures. *Environmental Sciences Europe*. 2018 April;30(1):13.
- [5] Guzzetti E, Sureda A, Tejada S, Faggio C. Microplastic in marine organism: Environmental and toxicological effects. *Environmental Toxicology and Pharmacology*. 2018;64:164 – 171.
- [6] Gonowski M, Gerdes Z, Gorokhova E. What we know and what we think we know about microplastic effects – A critical perspective. *Current Opinion in Environmental Science Health*. 2018;1:41 – 46.
- [7] Song YK, Hong SH, Jang M, Ha GM, Gani M, Lee J, et al. A comparison of microscopic and spectroscopic identification methods for analysis of microplastics in environmental samples. *Marine Pollution Bulletin*. 2015;93(1):202 – 209.
- [8] Ceccarini A, Corti A, Erba F, Modugno F, La Nasa J, Bianchi S, et al. The Hidden Microplastics: New Insights and Figures from the Thorough Separation and Characterization of Microplastics and of Their Degradation Byproducts in Coastal Sediments. *Environmental Science & Technology*. 2018;52(10):5634–5643.
- [9] Science Advice For Policy By European Academies S. A scientific perspective on microplastics in nature and society; 2019.

- [10] Smith M, Love DC, Rochman CM, Neff RA. Microplastics in Seafood and the Implications for Human Health. *Current Environmental Health Reports*. 2018 September;5(3):375–386.
- [11] Boucher J, Friot D. Primary microplastics in the oceans : a global evaluation of sources. IUCN, Global Marine and Polar Programme. 2017;.
- [12] Duis K, Coors A. Microplastics in the aquatic and terrestrial environment: sources (with a specific focus on personal care products), fate and effects. *Environmental Sciences Europe*. 2016 January;28(1):2.
- [13] Klein S, Dimzon IK, Eubeler J, Knepper TP. In: Wagner M, Lambert S, editors. *Analysis, Occurrence, and Degradation of Microplastics in the Aqueous Environment*. Springer International Publishing; 2018. p. 51–67.
- [14] ter Halle A, Ladirat L, Martignac M, Françoise Mingotaud A, Boyron O, Perez E. To what extent are microplastics from the open ocean weathered? *Environmental Pollution*. 2017 August;227:167 – 174.
- [15] Seltenrich N. New Link in the Food Chain? *Marine Plastic Pollution and Seafood Safety*. *Environmental Health Perspectives (Online)*. 2015 02;123(2).
- [16] Brennecke D, Duarte B, Paiva F, Caçador I, Canning-Clode J. Microplastics as vector for heavy metal contamination from the marine environment. *Estuarine, Coastal and Shelf Science*. 2016;178:189 – 195.
- [17] Elke F, Dekiff J J Willmeyer, Nuelle M M Ebert, Remy D. Identification of polymer types and additives in marine microplastic particles using pyrolysis-GC/MS and scanning electron microscopy. *Environ Sci: Processes Impacts*. 2013;15:1949–1956.
- [18] Ma Y, Huang A, Cao S, Sun F, Wang L, Guo H, et al. Effects of nanoplastics and microplastics on toxicity, bioaccumulation, and environmental fate of phenanthrene in fresh water. *Environmental Pollution*. 2016;219:166 – 173.
- [19] Ram A. *Fundamentals of Polymer Engineering*. 233 Spring Street, New York, N. T. 10013: Plenum Press; 1997.

- [20] Goodship V. Introduction to Plastic Recycling. Shawbury, Shrewsbury, shropshire, SY4 4NR, UK: Smithers Rapra Technology Limited; 2007.
- [21] Thermoplastics, Resins, Polymers, Plastics, Performance Materials and Synthetic Rubber Manufacturing Industry (U.S.) Analytics, Extensive Financial Benchmarks, Metrics and Revenue Forecasts to 2025, NAIC 325210 Published November 25, 2018. Plunkett Research, Ltd; 2018.
- [22] Andrady AL. *Plastics and the Environment*. Hoboken, New Jersey: John Wiley and Sons; 2003.
- [23] Thompson RC, Moore C, vom Saal FS, Swan S. Plastics, the environment and human health: current consensus and future trends. *Philosophical transactions of the Royal Society of London Series B, Biological sciences*. 2009 July;364(1526):2153–66.
- [24] Vasile C. *Handbook of Polyolefins - Plastics Engineering*. New York, USA: Marcel Dekker Inc; 2000.
- [25] Deanin RD. Additives in Plastics. *Environmental Health Perspectives*. 1975 June;11(3):35–39.
- [26] Laermer SF, Zambetti PF. Alpha-Tocopherol (Vitamin E)—the Natural Antioxidant for Polyolefins. *Journal of Plastic Film and Sheeting*. 1992 July;8(3):228–248.
- [27] Yarsley VE, Couzens EG. *Plastics*. London, UK: Pelican Books / Penguin Books; 1941.
- [28] Jones MM, Benrubi ID. Poison politics: a contentious history of consumer protection against dangerous household chemicals in the United States. *American journal of public health*. 2013;103(5):801–812.
- [29] Thompson RC, Moore CJ, vom Saal FS, Swan SH. Our plastic age. *Philosophical transactions of the Royal Society of London Series B, Biological sciences*. 2009 July;364(1526):2153–66.
- [30] Geyer R, Jambeck JR. Production, use, and fate of all plastics ever made. *Science Advances*. 2017 July;3(7):2153–66.

- [31] Europe P. *Plastics – the Facts 2015*. An analysis of European plastics production, demand and waste data; 2015. Accessed 3rd June 2018.
https://www.plasticseurope.org/application/files/3715/1689/8308/2015plastics_the_facts_14122015.pdf.
- [32] Rochman C. Chapter 5 - The Complex Mixture, Fate and Toxicity of Chemicals Associated with Plastic Debris in the Marine Environment. In: Bergmann M, Gutow L, Klages M, editors. *Marine Anthropogenic Litter*. Marine Anthropogenic Litter. Springer Open; 2015. .
- [33] Pravettoni R. 'How microplastics are generated' in *Marine Litter Vital Graphics*; 2018. Accessed 3rd June 2018. <http://www.grida.no/resources/6929>.
- [34] Lebreton LCM, Greer SD, Borrero JC. Numerical modelling of floating debris in the world's oceans. *Marine Pollution Bulletin*. 2012 March;64(3):653 – 661.
- [35] Ojeda T, Freitas A, Birck K, Dalmolin E, Jacques R, Bento F, et al. Degradability of linear polyolefins under natural weathering. *Polymer Degradation and Stability*. 2011 April;96(4):703 – 707.
- [36] Cózar A, Echevarría F, González-Gordillo JI, Irigoien X, Úbeda B, Hernández-León S, et al. Plastic debris in the open ocean. *Proceedings of the National Academy of Sciences*. 2014;28(111):10239–10244.
- [37] Rillig M, Lehmann A, de Souza Machado AA, Yang G. Microplastic effects on plants. *New Phytologist*. 2019;0(0).
- [38] Dris R, Gasperi J, Mirande C, Mandin C, Guerrouache M, Langlois V, et al. A first overview of textile fibers, including microplastics, in indoor and outdoor environments. *Environmental Pollution*. 2017;221:453 – 458.
- [39] Hopewell J, Dvorak R, Kosior E. Plastics recycling: challenges and opportunities. *Philosophical Transactions of the Royal Society B: Biological Sciences*. 2009;364(1526):2115–2126.

- [40] Lahtela V, Hyvärinen M, Kärki T. Composition of Plastic Fractions in Waste Streams: Toward More Efficient Recycling and Utilization. *Polymers*. 2019;11(1).
- [41] Pravettoni R. 'How plastic moves from the economy to the environment' in *Marine Litter Vital Graphics*; 2018. Accessed 3rd June 2018. <http://www.grida.no/resources/6908>.
- [42] Hartley BL, Pahl S, Veiga J, Vlachogianni T, Vasconcelos L, Maes T, et al. Exploring public views on marine litter in Europe: Perceived causes, consequences and pathways to change. *Marine Pollution Bulletin*. 2018;133:945–955.
- [43] Parliament E. Parliament seals ban on throwaway plastics by 2021; 2019. Accessed 8rd June 2018. <http://www.europarl.europa.eu/news/en/press-room/20190321IPR32111/parliament-seals-ban-on-throwaway-plastics-by-2021>.
- [44] Zbyszewski M, Corcoran PL, Hockin A. Comparison of the distribution and degradation of plastic debris along shorelines of the Great Lakes, North America. *Journal of Great Lakes Research*. 2014 June;40(2):288 – 299.
- [45] Eriksen M, Thiel M, Lebreton L. Nature of Plastic Marine Pollution in the Subtropical Gyres; 2016.
- [46] Lebreton L, Slat B, Ferrari F, Sainte-Rose B, Aitken J, Marthouse R, et al. Evidence that the Great Pacific Garbage Patch is rapidly accumulating plastic. *Scientific Reports*. 2018;8(1):4666.
- [47] Di Mauro R, Kupchik MJ, Benfield MC. Abundant plankton-sized microplastic particles in shelf waters of the northern Gulf of. *Environmental Pollution*. 2017 November;230:798 – 809.
- [48] Williams AT, Simmons SL. The degradation of plastic litter in rivers: Implications for beaches. *Journal of Coastal Conservation*. 1996 January;2(1):63–72.
- [49] Eriksen M, Lebreton LC, M Carson HS, Thiel M, Moore CJ, Borerro JC, et al. Plastic Pollution in the World's Oceans: More than 5 Trillion Plastic Pieces Weighing over 250,000 Tons Afloat at Sea. *PLOS ONE*. 2014 12;9:1–15.

- [50] Seville E, Wilcox C, Lebreton L, Maximenko N, Hardesty BD, van Franeker JA, et al. A global inventory of small floating plastic debris. *Environmental Research Letters*. 2015 December;10(12):124006.
- [51] 'How much plastic is estimated to be in the oceans and where it may be' in *Marine Litter Vital Graphics*; 2018. Accessed 3rd June 2018.
<http://www.grida.no/resources/6907>.
- [52] Derraik J. The pollution of the marine environment by plastic debris: a review. *Marine Pollution Bulletin*. 2002;44(9):842 – 852.
- [53] Cheang C, Ma Y, Fok L. Occurrence and Composition of Microplastics in the Seabed Sediments of the Coral Communities in Proximity of a Metropolitan Area. *International Journal of Environmental Research and Public Health*. 2018;15(10).
- [54] Dartora PC, Santana RM, Moreira AC. The influence of long chain branches of LLDPE on processability and physical properties. *Polímeros*. 2015 December;25:531 – 539.
- [55] Gewert B, Plassmann MM, MacLeod M. Pathways for degradation of plastic polymers floating in the marine environment. *Environ Sci: Processes Impacts*. 2015 July;17:1513–1521.
- [56] Trevail AM, Gabrielsen GW, Kühn S, Van Franeker JA. Elevated levels of ingested plastic in a high Arctic seabird, the northern fulmar (*Fulmarus glacialis*). *Polar Biology*. 2015 Jul;38(7):975–981.
- [57] van Franeker JA, Law KL. Seabirds, gyres and global trends in plastic pollution. *Environmental Pollution*. 2015;203:89 – 96.
- [58] Cózar A, Martí E, Duarte CM, García-de Lomas J, van Seville E, Ballatore TJ, et al. The Arctic Ocean as a dead end for floating plastics in the North Atlantic branch of the Thermohaline Circulation. 2017;3(4).
- [59] Lusher AL, Tirelli V, O'Connor I, Officer R. Microplastics in Arctic polar waters: the first reported values of particles in surface and sub-surface samples. *Scientific*

- Reports. 015 October;5(14947).
- [60] Bergmann NSIDD M Sandhop. Observations of floating anthropogenic litter in the Barents Sea and Fram Strait, Arctic. *Polar Biology*. 2016 March;39(3):553–560.
- [61] Obbard RW, Sadri S, Wong YO, Khitun AA, Baker I, Thompson RC. Global warming releases microplastic legacy frozen in Arctic Sea ice. *Earth's Future*. 2014;2(6):315–320.
- [62] O'Brine T, Thompson RC. Degradation of plastic carrier bags in the marine environment. *Marine Pollution Bulletin*. 2010;60(12):2279 – 2283.
- [63] Cooper DA, Corcoran PL. Effects of mechanical and chemical processes on the degradation of plastic beach debris on the island of Kauai, Hawaii. *Marine Pollution Bulletin*. 2010 May;60(5):650 – 654.
- [64] Allen NS, Edge M. *Fundamentals of Polymer Degradation and Stabilization*. Essex, UK: Springer Science and Business Media; 1992.
- [65] Andrady AL. *Degradation of Plastics in the Environment*. John Wiley and Sons, Ltd; 2015.
- [66] Fotopoulou KN, Karapanagioti H. In: Takada H, Karapanagioti HK, editors. *Degradation of Various Plastics in the Environment*. Springer International Publishing; 2019. p. 71–92.
- [67] Weinstein J, Crocker BK, Gray AD. From macroplastic to microplastic: Degradation of high-density polyethylene, polypropylene, and polystyrene in a salt marsh habitat. *Environmental Toxicology and Chemistry*. 2016;35(7):1632–1640.
- [68] 'Natural processes affecting the distribution and fate of plastics' in *Marine Litter Vital Graphics*; 2018. Accessed 3rd June 2018. <http://www.grida.no/resources/6911>.
- [69] Singh B, Sharma N. Mechanistic implications of plastic degradation. *Polymer Degradation and Stability*. 2008 March;93(3):561 – 584.

- [70] Nithin B, Goel S. Degradation of Plastics. Goel S, editor. Cham: Springer International Publishing; 2017.
- [71] McKean L. Introduction to Plastic Properties. Third edition ed. Boston, USA: William Andrew Publishing; 2013.
- [72] Sebaa M, Servens C, Pouyet J. Natural and artificial weathering of low-density polyethylene (LDPE): Calorimetric analysis. *Journal of Applied Polymer Science*. 1992 June;45(6):1049–1053.
- [73] Gewert B, Plassmann M, Sandblom O, MacLeod M. Identification of Chain Scission Products Released to Water by Plastic Exposed to Ultraviolet Light. *Environmental Science and Technology Letters*. 2018 April;5(5):272–276.
- [74] Yousif E, Haddad R. Photodegradation and photostabilization of polymers, especially polystyrene: review. *SpringerPlus*. 2013;2(1):398.
- [75] Sreenual B, Atong D, Pechyen C. Surface Degradation and Mechanical Properties of PVC/Wood-Pallet Composite under UV-Weathering Environment. 2012 5;506:548–551.
- [76] Arndt S, Jørgensen BB, LaRowe DE, Middelburg JJ, Pancost RD, Regnier P. Quantifying the degradation of organic matter in marine sediments: A review and synthesis. *Earth-Science Reviews*. 2013;123:53 – 86.
- [77] Grosjean E, Grosjean D. Carbonyl products of the gas phase reaction of ozone with 1,1-disubstituted alkenes. *Journal of Atmospheric Chemistry*. 1996;24(2):141–156.
- [78] Gagliardi M, Paggi M. Long-term EVA degradation simulation: Climatic zones comparison and possible revision of accelerated tests. *Solar Energy*. 2018 January;159:882 – 897.
- [79] Gulmine JV, Janissek PR, Heise HM, Akcelrud L. Degradation profile of polyethylene after artificial accelerated weathering. *Polymer Degradation and Stability*. 2003 October;79:385–397.

- [80] Lampman S. *Characterization and Failure Analysis of Plastics*. Ohio, USA: ASM International; 2003.
- [81] Brandon J, Goldstein M, Ohman MD. Long-term aging and degradation of microplastic particles: Comparing in situ oceanic and experimental weathering patterns. *Marine Pollution*. 2016 September;110(1):299 – 308.
- [82] Kutz M. *Handbook of Environmental Degradation of Materials*. Oxford, UK: William Andrew - Elsevier; 2018.
- [83] White CC, White KM, Pickett JE. *Service Life Prediction of Polymers and Plastics Exposed to Outdoor Weathering*. Oxford, UK: William Andrew - Elsevier; 2017.
- [84] Krebs FC. *Stability and Degradation of Organic and Polymer Solar Cells*. West Sussex, UK: John Wiley and Sons; 2012.
- [85] Pielichowski K, Njuguna J. *Thermal Degradation of Polymeric Materials*. West Sussex, UK: iSmithers Rapra Publishing; 2005.
- [86] Hihara L, Adler R, Latanision R. *Environmental Degradation of Advanced and Traditional Engineering Materials*. CRC Press; 2013.
- [87] Maxwell AS, Broughton WR, Dean G, Sims GD. *Review of accelerated ageing methods and lifetime prediction techniques for polymeric materials*. Middlessex, UK: National Physical Laboratory; 2005.
- [88] Desforges JW, Galbraith M, Ross PS. Ingestion of Microplastics by Zooplankton in the Northeast Pacific Ocean. *Archives of Environmental Contamination and Toxicology*. 2015;69(3):320–330.
- [89] Zarfl C, Matthies M. Are marine plastic particles transport vectors for organic pollutants to the Arctic? *Marine Pollution Bulletin*. 2010;60(10):1810 – 1814.
- [90] Ziccardi LM, Edgington A, Hentz K, Kulacki KJ, Kane Driscoll S. Microplastics as vectors for bioaccumulation of hydrophobic organic chemicals in the marine environment: A state-of-the-science review. *Environmental Toxicology and Chemistry*;35(7):1667–1676.

- [91] de Sá LC, Oliveira M, Ribeiro F, Lopes Rocha T, Futter MN. Studies of the effects of microplastics on aquatic organisms: What do we know and where should we focus our efforts in the future? *Science of The Total Environment*. 2018 July;645:1029 – 1039.
- [92] Nguyen B, Claveau-Mallet D, Hernandez LM, Xu EG, Farner JM, Tufenkji N. Separation and Analysis of Microplastics and Nanoplastics in Complex Environmental Samples. *Accounts of Chemical Research*. 2019;52(4):858–866.
- [93] B TP, Yedjou CG, Patlolla AK, Sutton DJ. Heavy metal toxicity and the environment. *Experientia supplementum*. 2012;.
- [94] Turner A, Holmes LA. Adsorption of trace metals by microplastic pellets in fresh water. *Environmental Chemistry*. 2015 0;12(5):600–610.
- [95] Rochman CM, Hentschel BT, Teh SJ. Long-Term Sorption of Metals Is Similar among Plastic Types: Implications for Plastic Debris in Aquatic Environments. *PLoS One*. 2014 01;9(1).
- [96] Holmes LA, Turner A, Thompson RC. Adsorption of trace metals to plastic resin pellets in the marine environment. *Environmental Pollution*. 2012;160:42 – 48.
- [97] Gergen I, Harmanescu M. Application of principal component analysis in the pollution assessment with heavy metals of vegetable food chain in the old mining areas. *Chemistry Central journal*. 2012;6.
- [98] Poyraz B, Taspınar F. Analysis, Assesment and Principal Component Analysis of Heavy Metals in Drinking Waters of Industrialized Region of Turkey. 2014;8.
- [99] Jaroová M, Milde D, Kuba M. Elemental Analysis of Coffee: a Comparison of ICP-MS and AAS Methods; 2018. .
- [100] Qishlaqi A, Moore F. Statistical Analysis of Accumulation and Sources of Heavy Metals Occurrence in Agricultural Soils of Khoshk River Banks, Shiraz, Iran. *American-Eurasian Journal of Sustainable Agriculture*. 2007;5.

- [101] Mauldin FW, Zhu HT, Behler RH, Nichols TM, Gallippi CM. Robust Principal Component Analysis and Clustering Methods for Automated Classification of Tissue Response to ARFI Excitation. *Ultrasound in Medicine Biology*. 2008;34(2):309 – 325.
- [102] Shim WJ, Hong SH, Eo SE. Identification methods in microplastic analysis: a review. *Anal Methods*. 2017;9:1384–1391.
- [103] Painter PC, Coleman M. *Fundamentals of polymer science : an introductory text*. Lancaster, Pa: Technomic; 1997.
- [104] Hidalgo-Ruz V, Gutow L, Thompson R, Thiel M. Microplastics in the Marine Environment: A Review of the Methods Used for Identification and Quantification. *Environmental Science & Technology*. 2012;46(6):3060–3075.
- [105] Löder M, Gerdt G. Methodology Used for the Detection and Identification of Microplastics—A Critical Appraisal. *Marine Anthropogenic Litter*. 2015;.
- [106] Hermabessiere L, Himber C, Boricaud B, Kazour M, Amara R, Cassone AL, et al. Optimization, performance, and application of a pyrolysis-GC/MS method for the identification of microplastics. *Analytical and Bioanalytical Chemistry*. 2018 Oct;410(25):6663–6676.
- [107] Rodríguez Chialanza M, Sierra I, Pérez Parada A, Fornaro L. Identification and quantitation of semi-crystalline microplastics using image analysis and differential scanning calorimetry. *Environmental Science and Pollution Research*. 2018 Jun;25(17):16767–16775.
- [108] Scott R, Fassel V, Kniseley R, Nixon D. Inductively coupled plasma-optical emission analytical spectrometry. *Analytical Chemistry*. 1974;46(1):75–80.
- [109] Otero-Romaní J, Moreda-Piñeiro A, Bermejo-Barrera P, Martín-Esteban A. Inductively coupled plasma–optical emission spectrometry/mass spectrometry for the determination of Cu, Ni, Pb and Zn in seawater after ionic imprinted polymer based solid phase extraction. *Talanta*. 2009;79(3):723 – 729.

- [110] Basile F. MALDI Mass Spectrometry for Synthetic Polymer Analysis. *Journal of the American Chemical Society*. 2010;132(25):8805–8806.
- [111] Payne M, Grayson S. Characterization of Synthetic Polymers via Matrix Assisted Laser Desorption Ionization Time of Flight (MALDI-TOF) Mass Spectrometry. *Journal of visualized experiments*. 2018;136:57174.
- [112] Peez N, Janiska M, Imhof W. The first application of quantitative ^1H NMR spectroscopy as a simple and fast method of identification and quantification of microplastic particles (PE, PET, and PS). *Analytical and Bioanalytical Chemistry*. 2019 Feb;411(4):823–833.
- [113] Mendoza L, Taniguchi S, Karapanagiotti H. Chapter 8 - Advanced Analytical Techniques for Assessing the Chemical Compounds Related to Microplastics. In: Rocha-Santos A T Duarte, editor. *Characterization and Analysis of Microplastics*. vol. 75 of *Comprehensive Analytical Chemistry*. Elsevier; 2017. p. 209 – 240.
- [114] Ismail AA, van de Voort FR, Sedman J. Chapter 4 Fourier transform infrared spectroscopy: Principles and applications. In: Paré JMR J R J Bélanger, editor. *Instrumental Methods in Food Analysis*. vol. 18 of *Techniques and Instrumentation in Analytical Chemistry*. Elsevier; 1997. p. 93 – 139.
- [115] Kuptsov AH, Zhizhin GN. *Handbook of Fourier Transform Raman and Infrared Spectra of Polymers*, Volume 45, 1st Edition. Box 211, 1000 AE Amsterdam, The Netherland: Elsevier Science; 1998.
- [116] Infrared Spectroscopy - FT-Raman NIR. In: Worsfold P, Poole C, Townshend A, Miró M, editors. *Encyclopedia of Analytical Science (Third Edition)*. third edition ed. Oxford: Academic Press; 2017. p. 112 – 123.
- [117] Stephanos AW J J Addison. Chapter 9 - Vibrational Rotational Spectroscopy. In: Stephanos JJ, Addison AW, editors. *Electrons, Atoms, and Molecules in Inorganic Chemistry*. Academic Press; 2017. p. 505 – 584.
- [118] Larkin PJ. Chapter 6 - IR and Raman Spectra–Structure Correlations:

- Characteristic Group Frequencies. In: Larkin PJ, editor. *Infrared and Raman Spectroscopy (Second Edition)*. second edition ed. Elsevier; 2018. p. 85 – 134.
- [119] Kusch P. Chapter 7 - Application of Pyrolysis-Gas Chromatography/Mass Spectrometry (Py-GC/MS). In: Rocha-Santos T, Duarte A, editors. *Characterization and Analysis of Microplastics*. vol. 75 of *Comprehensive Analytical Chemistry*. Elsevier; 2017. p. 169 – 207.
- [120] Tsuge S, Ohtani H, Watanabe C. *Pyrolysis-GC/MS Data Book of Synthetic Polymers - Pyrograms, Thermograms and MS of Pyrolyzates -*. Oxford, UK: Elsevier; 2011.
- [121] Kitson BSMCN F G Larsen. Chapter 1 - What Is GC/MS? In: Kitson FG, Larsen BS, McEwen CN, editors. *Gas Chromatography and Mass Spectrometry*. San Diego: Academic Press; 1996. p. 3 – 23.
- [122] Fischer, Scholz-Böttcher BM. Simultaneous Trace Identification and Quantification of Common Types of Microplastics in Environmental Samples by Pyrolysis-Gas Chromatography–Mass Spectrometry. *Environmental Science & Technology*. 2017;51(9):5052–5060.
- [123] Bartsch N, Girard M, Wilde A, Bruhn T, Kappenstein O, Vieth B, et al. Thermal Stability of Polymer Additives: Comparison of Decomposition Models Including Oxidative Pyrolysis. *Journal of Vinyl and Additive Technology*;25(s2):E12–E27.
- [124] Lundanes E, Reubsaet L, Greibrook T. *Chromatography - Basic Principles, Sample Preparations and Related Methods*. Boschstr.12, 69469 Weinheim, Germany: Wiley-VCH Verlag GmbH and Co; 2014.
- [125] Dawkins JV, Hemming M. Infrared detection of polymers in gel permeation chromatography. *Journal of Applied Polymer Science*. 1975;19(11):3107–3118.
- [126] Goodman D, Kizhakkedathu JN, Brooks DE. Molecular Weight and Polydispersity Estimation of Adsorbing Polymer Brushes by Atomic Force Microscopy. *Langmuir*. 2004;20(8):3297–3303.

- [127] Shojaeiarani J, Bajwa DS, Rehovsky C, Bajwa SG, Vahidi G. Deterioration in the Physico-Mechanical and Thermal Properties of Biopolymers Due to Reprocessing. *Polymers*. 2019;11(1).
- [128] Bly DD, Stoklosa HJ, Kirkland JJ, Yau WW. Errors caused by flowrate variation in high performance size exclusion chromatography (GPC) [gel permeation chromatography]. *Analytical Chemistry*. 1975;47(11):1810–1813.
- [129] Al-Salem SM, Behbehani MH, Karam HJ, Al-Rowaih SF, Asiri FM. On the Kinetics of Degradation Reaction Determined Post Accelerated Weathering of Polyolefin Plastic Waste Blends. *International Journal of Environmental Research and Public Health*. 2019;16(3).
- [130] Tian Y, Kuzimenkova MV, Halle J, Wojdyr M, Diaz de Zerio Mendaza A, Larsson PO, et al. Molecular Weight Determination by Counting Molecules. *The Journal of Physical Chemistry Letters*. 2015;6(6):923–927.
- [131] Yang R. *Analytical Methods for Polymer Characterization*. CRC Press; 2018.
- [132] Şahan Y, Basoglu F, Gücer S. ICP-MS analysis of a series of metals (Namely: Mg, Cr, Co, Ni, Fe, Cu, Zn, Sn, Cd and Pb) in black and green olive samples from Bursa, Turkey. *Food Chemistry*. 2007;105(1):395 – 399.
- [133] Sudhakar P, Latha P, Reddy PV. Chapter 17 - Analytical techniques. In: Sudhakar P, Latha P, Reddy PV, editors. *Phenotyping Crop Plants for Physiological and Biochemical Traits*. Academic Press; 2016. p. 137 – 149.
- [134] Milne A, Landing W, Bizimis M, Morton P. Determination of Mn, Fe, Co, Ni, Cu, Zn, Cd and Pb in seawater using high resolution magnetic sector inductively coupled mass spectrometry (HR-ICP-MS). *Analytica Chimica Acta*. 2010;665(2):200 – 207.
- [135] Palchoudhury S, Baalousha M, Lead JR. Chapter 5 - Methods for Measuring Concentration (Mass, Surface Area and Number) of Nanomaterials. In: Baalousha M, Lead JR, editors. *Characterization of Nanomaterials in Complex Environmental and Biological Media*. vol. 8 of *Frontiers of Nanoscience*. Elsevier; 2015. p. 153 – 181.

- [136] Boulyga SF. Calcium isotope analysis by mass spectrometry. *Mass Spectrometry Reviews*. 2010;29(5):685–716.
- [137] Zięba-Palus J. The usefulness of infrared spectroscopy in examinations of adhesive tapes for forensic purposes. *Forensic Sci Criminol*. 2017 April;.
- [138] Fonouni M, Yegani R, Tavakkoli A, Mollazadeh S. Investigating the Effect of Various Oxidizing Agents on the Surface Functionalization of Microporous Polypropylene Membranes. *Journal Of Textiles And Polymers*. 2016 July;4:92–100.
- [139] Johnson S, Bubb D, Haglund R. Phase explosion and recoil-induced ejection in resonant-infrared laser ablation of polystyrene - Springer. *Applied Physics A*. 2009 08;96:627–635.
- [140] Jung MR, David Horgen F, Orski SV, Rodriguez V, Beers KL, Balazs, et al. Validation of ATR FT-IR to identify polymers of plastic marine debris, including those ingested by marine organisms. *Marine Pollution Bulletin*. 2018;127:704 – 716.
- [141] Hammer Harper PD, Ryan PD. PAST: Paleontological Statistics Software Package for Education and Data Analysis. United States: Palaeontologia Electronica; 2001.
- [142] Colton JB, Burns BR, Knapp FD. Plastic Particles in Surface Waters of the Northwestern Atlantic. *Science*. 1974;185(4150):491–497.
- [143] Lusher AL, Burke A, O'Connor I, Officer R. Microplastic pollution in the Northeast Atlantic Ocean: Validated and opportunistic sampling. *Marine Pollution Bulletin*. 2014;88(1):325 – 333.
- [144] Kanhai LDK, Officer R, Lyashevskaya O, Thompson RO, O'Connor I. Microplastic abundance, distribution and composition along a latitudinal gradient in the Atlantic Ocean. *Marine Pollution Bulletin*. 2017;115(1):307 – 314.
- [145] Amélineau F, Bonnet D, Heitz O, Mortreux V, Harding AMA, Karnovsky N, et al. Microplastic pollution in the Greenland Sea: Background levels and selective contamination of planktivorous diving seabirds. *Environmental Pollution*. 2016;219:1131 – 1139.

-
- [146] Mathalon A, Hill P. Microplastic fibers in the intertidal ecosystem surrounding Halifax Harbor, Nova Scotia. *Marine Pollution Bulletin*. 2014;81(1):69 – 79.
- [147] Law KL, Morét-Ferguson S, Maximenko NA, Proskurowski G, Peacock EE, Hafner J, et al. Plastic Accumulation in the North Atlantic Subtropical Gyre. *Science*. 2010;329(5996):1185–1188.
- [148] Howard JB, Gilroy HM. Natural and artificial weathering of polyethylene plastics. *Polymer Engineering and Science*. 1969;9(4):286–294.

A Calculations

A.1 Calculation of Volume Trawled

The dimensions of the trawl opening was 254 mm wide and 558.8 mm long. The calculations are based on the assumption that only 50% of the trawl was below the water surface during the trawling.

$$A = \frac{558.8mm}{1000} \cdot \frac{254mm}{1000} \cdot 0.5 = \underline{0.071m^2} \quad (A.1)$$

This was then used with the distance trawled to calculate the volume of water in m^3 . An example calculation using the first trawl, a trawling of 195 km can be seen in the equation below.

$$0.071m^2 \cdot (195km \cdot 1000) = \underline{13838.68m^3} \quad (A.2)$$

Assuming that one litre of water is equivalent to $1 dm^3$, the amount of litre gone through the trawl in each sampling can easily be calculated. A summary of the calculated volume waters and $\mu g/L$ sample from the expedition can be seen in the table below.

Table A.1: Calculation of litres of seawater trawled and samples per litre.

Sample	Weight (gram)	Amount (#)	Trawl (km)	Water (m ³)	$\mu\text{g/L}$
1	0.140	36	195.0	13838.68	0.0101
2	0.493	98	185.0	13129.01	0.0376
3	0.002	118	10.2	723.87	0.0023
4	0.100	21	10.9	773.55	0.1294
5	0.148	34	17.9	1270.32	0.1164
6	0.297	36	20.1	1426.45	0.2079
7	0.014	4	27.6	1958.71	0.0071
8	0.452	15	23.2	1646.45	0.2745
9	0.486	17	24.2	1717.42	0.2830
10	0.172	4	28.5	2022.58	0.0852
11	0.016	4	24.0	1703.22	0.0093
Sum	2.319	387	566.6	40210.24	0.1057 (average)

A.2 Accelerated Aging

UV light is measured from 10 - 400 nm, however only wavelength 295 - 385 nm reach the earth. For the ageing experiment the irradiation from UV-A and UV-B areas are the interesting ones.

The irradiation on the samples were measured in 2 ways. The external measurement measured the UV(A+B) to be $4820 \mu\text{W}/\text{cm}^2$. The chamber measured the UV-A irradiation at 340 nm to $1.95 \text{ W}/\text{m}^2$. This needs to be converted into a wider wavelength. As a rule of thumb, the energy contained in the 340 nm wavelength range is approximately one percent of the UV range 295-385 nm [82]. As the UVA+UVB wavelengths are from 280-400 nm but only 295 - 385 reach the earth, 100 times the UV irradiation from 340 nm is assumed to be the total irradiation.

The annual irradiation in Europe is given to be $60 \text{ kWh}/\text{m}^2\text{year}$ which is equal to $216 \text{ MJ}/\text{m}^2\text{year}$ [73]. Using this and the 2 UV measurements the irradiation can be converted

into simulated days.

Using the UV-A irradiation at 340 nm:

The unit watt (W) must also be converted to joules (J) which is done by using the equation below.

$$J=W \cdot s \quad (\text{A.3})$$

where s i seconds.

As artificial weathering tests are timed in hours (1 hour is 3600 seconds) this conversion is done:

$$1.95W/m^2 \cdot 100\% \cdot 3600s = \underline{702000j/m^2h} \quad (\text{A.4})$$

Using this the hours in the weathering chamber can be converted into amount of energy exposed on the samples (J/m^2).

These results can then be transferred into simulated days. The annual irradiation in Europe is given to be 60 kwh/ m^2 year which is equal to 216 MJ/ m^2 year [73]. This means that the average hourly irradiation in Europe is:

$$216MJ/m^2\text{year} \cdot \frac{1}{365\text{days} \cdot 24\text{hours}} = \underline{24657.53J/m^2h} \quad (\text{A.5})$$

Table A.2: Simulated time in chamber using UV-A irradiation at 340 nm.

Time	0h	360h	720h	960h	1200h	1600h
MJ/ m^2	0	252.72	505.44	673.92	842.4	1123.2
Simulated hours	0	10249	20498	27331	34164	45552
Simulated days	0	427	854	1139	1424	1898
Simulated years	0	1.2	2.3	3.1	3.9	5.2

Using the measured $UV(A+B) = 4820 \mu W/cm^2$:

$4820 \mu W/cm^2$ is $48.2 W/m^2$. Knowing the annual average radiation of $UV(A+B)$ is 60 kwh in Europe the following simulated time can be calculated:

Table A.3: Simulated time in chamber using $UV(A+B) = 4820 \mu W/cm^2$

Time	0h	360h	720h	960h	1200h	1600h
W/m^2	17352	34704	46272	57840	77120	
Simulated hours	0	2533	5067	6756	8445	11260
Simulated days	0	106	211	281	352	469
Simulated years	0	0.3	0.6	0.8	1.0	1.3

Factoring in the effect of temperature:

The temperature in the UV chamber was measured to $85^\circ C$, while the value for irradiation in Europe is given in normal outdoor temperature (assumed to be $25^\circ C$). Therefore the degradation dependence on temperature must be taken into account. This can be done in a plural of ways, here 2 common ways are used.

Using the rule of thumb that an increase in $10^\circ C$ doubles the degradation. Given an increase from the outside being $25^\circ C$ to the measured $85^\circ C$ in the chamber this is an increase of $60^\circ C$. This means doubling the rate of degradation 6 times. $2^6 = 64$. Therefore the simulated days should be timed with the factor of 64.

The Arrhenius equation can also be used to estimate a factor of the degradation over a small temperature range. The Arrhenius Equation is given:

$$k=A \cdot \exp\left(\frac{-E_a}{RT}\right) \tag{A.6}$$

where k is the rate of the reaction, A is a factor related to entropy, E_a is the activation energy, R is the gas constant and T is the temperature in kelvins. For a complex process as weathering, E_a is the apparent activation energy of the entire process. The ratio of the

rates at 2 temperatures T_1 and T_2 is given by the equation:

$$\frac{k_2}{k_1} = \exp\left[\cdot\left(\frac{1}{T_1} - \frac{1}{T_2}\right)\right] \quad (\text{A.7})$$

Using this an equation for the entire system can be put together:

$$E_{equiv} = E_r \cdot \exp\left[\frac{-E_a}{RT} \cdot \left(\frac{1}{T_1} - \frac{1}{T_2}\right)\right] \quad (\text{A.8})$$

or, solved for E_r :

$$E_r = E_{equiv} \cdot \frac{1}{\exp\left[\frac{-E_a}{R} \cdot \left(\frac{1}{T_1} - \frac{1}{T_2}\right)\right]} \quad (\text{A.9})$$

where E_{equiv} is the equivalent UV chamber radiant energy, E_r is the temperature corrected UV radiant energy, E_a is the activation energy, R is the gas constant, T_1 is the effective temperature of the sample outdoors in kelvins, and T_2 is the irradiation-averaged temperature of the sample in the UV chamber in Kelvis.

The following assumptions are made to use this formula:

- Activation energy of LLDPE is $E_a = 27680$ J/mol, as found in literature [24].
- Outdoor temperature in Europe is average $T_1 = 25$ °C.
- Samples had the constant $T_2 = 85$ °C for the entire degradation.
- No other degradation effects are important other than temperature and UV light.

Doing this the hours of weathering can be calculated into time in nature by dividing the numbers with the coefficient. Using the found E_a of 27680 J/mol, the gas constant 8.314 J/Kmol, T_1 is 298.15K and T_2 is 358.15K:

$$1/\exp\left[\frac{-27680\text{J/mol}}{8.314\text{J/Kmol}} \cdot \left(\frac{1}{298.15\text{K}} - \frac{1}{358.15\text{K}}\right)\right] = 6.49 \quad (\text{A.10})$$

Given by the Arrhenius equation all weathering is increased by a factor of 6.49 by the increase of temperature.

Calculation of simulated weathering:

Using the two different measurements of irradiation in the chamber and the 2 different ways of calculating the impact of the temperature the following 4 times were calculated.

Table A.4: Time in UV chamber converted to time in nature calculated 4 ways, given the European annual irradiation = 60 kwh. Method 1 is using $UV-A(340) = 1.95 \text{ W/m}^2 + T_c = 64$. Method 2 is using $UV-A(340) = 1.95 \text{ W/m}^2 + T_c = 6.49$. Method 3 is using $UV(A+B) = 48.2 \text{ W/m}^2 + T_c = 64$. Method 4 is using $UV(A+B) = 48.2 \text{ W/m}^2 + T_c = 6.49$. T_c means temperature coefficient.

Method	Time (simulated)	360h	720h	960h	1200h	1600h
1	Days	27331	54662	72883	91104	121472
1	Years	75	150	200	250	333
2	Days	2773	5546	7395	9244	12325
2	Years	8	15	20	25	34
3	Days	6756	13511	18015	22519	30025
3	Years	18.5	37.0	49.4	61.7	82.3
4	Days	685	1371	1828	2285	3046
4	Years	1.9	3.8	5.0	6.3	8.3

B Results

B.1 ATR FT-IR Results from Fairwinds

Sample ID	Colour	Granule (3d)/ film (2D)/ fiber	Longest length	Width/diameter for fibers/films	Comments	Weight (gram)	FT-IR match (identification)	Score	Date	Location
1-1-1	blue	fiber	98,53	0,3		0,0098	PE	0,97	24.jan	NGI
1-2-1	grey	fiber	71,85	0,28		0,0051	PE	0,97	24.jan	NGI
1-3-1	black	fiber	36,93	0,23		0,0023	PP	0,89	24.jan	NGI
1-4-1	blue	fiber	24,78	0,27		0,0012	PE	0,94	24.jan	NGI
1-5-1	white	fiber	19,92	0,29		0,0019	PP+PE	0,86	24.jan	NGI
1-6-1	white	fiber	27,96	0,29		0,0032	PP+PE	0,85	24.jan	NGI
1-7-1	black	fiber	20,19	0,26		0,0014	PP	0,93	24.jan	NGI
1-8-1	black	fiber	18,04	0,21		0,0009	PP+PE (mix)	0,9	24.jan	NGI
1-9-1	black	2d	6,15	2,9		0,0027	PE	0,74	24.jan	NGI
1-10-1	black	2d	5,29	3,03		0,0042	PE	0,92	24.jan	NGI
1-11-1	grey	fiber	8,4	0,34		0,0007	PE	0,95	24.jan	NGI
1-12-1	blue (light)	fiber	11,71	0,25		0,0006	PP+PE (mix)	0,89	24.jan	NGI
1-13-1	white	3d	8,64	4,33		0,0192	PE	0,97	24.jan	NGI
1-14-1	white	3d	9,53	3,95		0,0047	PE	0,75	24.jan	NGI
1-15-1	white	3d	3,66	3,16		0,0117	PE	0,95	24.jan	NGI
1-16-1	green	3d	6,23	3,05		0,0064	PE	0,93	24.jan	NGI
1-17-1	white	3d	3,87	3,09		0,0075	PE	0,97	24.jan	NGI
1-18-1	white	3d	4,58	2,35		0,0113	PE	0,98	24.jan	NGI
1-19-1	blue	fiber	6,58	2,23		0,0013	PE	0,75	24.jan	NGI
1-20-1	white	3d	4,08	1,82		0,0045	PE	0,99	24.jan	NGI
1-21-1	white	2d	5,88	2,9		0,0025	PE	0,93	24.jan	NGI
1-22-1	white	3d	4,3	2,48		0,0062	PE	0,94	24.jan	NGI
1-23-1	black	2d	4,58	2,87		0,0021	PE	0,88	24.jan	NGI
1-24-1	green	fiber	6,82	0,29		0,0007	PE	0,96	24.jan	NGI
1-25-1	green	fiber	3,45	0,4		0,0002	PE	0,97	24.jan	NGI
1-26-1	black	2d	2,82	2,72		0,002	PE	0,98	24.jan	NGI
1-27-1	white	2d	3,65	1,94		0,0029	PE	0,94	24.jan	NGI
1-28-1	white	2d	3,62	3,57		0,0011	PE	0,69	24.jan	NGI
1-29-1	white	2d	4,55	0,97		0,0032	PE	0,92	24.jan	NGI
1-30-1	white	2d	2,4	1,97		0,0007	PE	0,93	24.jan	NGI
1-31-1	white	3d	2,67	1,68		0,0058	PE	0,98	24.jan	NGI
1-32-1	white	fiber	3,97	0,61		0,0004	PE	0,93	24.jan	NGI
1-33-1	grey	fiber	5,06	0,33		0,0003	PE	0,96	24.jan	NGI
1-34-1	clear	3d	1,66	1,37		0,0008	PE	0,98	24.jan	NGI
1-35-1	white	3d	2,27	1,77		0,0102	PE	0,98	24.jan	NGI
1-36-1	white	fiber	3,29	0,31		0,0002	PE	0,97	24.jan	NGI
Sum						0,1399				
2-1-1	clear	2D	153,14	122,09	Wrapping with writing (oatmeal rasin cookies)	0,2086	PP	0,86	12.feb	Norner
2-2-1	blue	fiber	162,46	5,05		0,0470	PP	0,82	12.feb	Norner
2-3-1	green	fiber	13,99	0,27		0,0740	PE	0,82	12.feb	Norner
2-4-1	black	fiber	41,2	0,24	Knot	0,0153	PP	0,85	12.feb	Norner
2-5-1	white	fiber	67,79	0,27		0,0061	PE	0,88	12.feb	Norner
2-6-1	clear	2d	16,46	12,19		0,0037	PP	0,83	12.feb	Norner
2-7-1	black	fiber	14,38	0,39		0,0013	PP	0,88	12.feb	Norner
2-8-1	black	fiber	11,17	0,32		0,0008	PE	0,87	12.feb	Norner
2-9-1	white	fiber	12,38	0,31		0,0011	PE	0,84	12.feb	Norner
2-10-1	clear	2d	14,99	10,65		0,0045	PE	0,86	12.feb	Norner
2-11-1	white	fiber	14,22	0,4		0,0014	PE	0,89	12.feb	Norner
2-12-1	white	fiber	11,26	0,4		0,0013	PE	0,84	12.feb	Norner

2-13-1	blue	fiber	13,15	0,46	0,0009	PE	0,82	12.feb	Norner
2-14-1	black	2d	3,46	2,89	0,0003	PE	0,86	12.feb	Norner
2-15-1	blue	2d	6,01	6,21	0,0056	PE	0,93	12.feb	Norner
2-16-1	blue	2d	7,4	4,21	0,0012	PE	0,9	12.feb	Norner
2-17-1	clear	2d	8,44	5,25	0,0004	PP	0,87	12.feb	Norner
2-18-1	blue	fiber	25,15	0,3	0,0012	PE	0,89	12.feb	Norner
2-19-1	clear	2d	8,34	6,59	0,0022	PE	0,9	12.feb	Norner
2-20-1	black	fiber	11,43	0,3	0,0007	PP	0,89	12.feb	Norner
2-21-1	white	fiber	20,12	0,4	0,0028	PE	0,88	12.feb	Norner
2-22-1	clear	2d	3,54	0,78	0,0001	PE	0,85	12.feb	Norner
2-23-1	clear	2d	1,77	1,4	0,0001	PE	0,9	12.feb	Norner
2-24-1	blue	2d	4,77	3,83	0,0007	PE	0,92	12.feb	Norner
2-25-1	green	3d	7,47	4,79	0,0114	PE	0,87	12.feb	Norner
2-26-1	clear	2d	16,33	10,17	0,0045	PP	0,87	12.feb	Norner
2-27-1	blue	fiber	13,99	0,37	0,0017	PE	0,89	12.feb	Norner
2-28-1	green	fiber	24,56	0,21	0,0007	PE	0,88	12.feb	Norner
2-29-1	green	fiber	12,23	0,2	0,0016	PE	0,87	12.feb	Norner
2-30-1	clear	2d	10,82	3,94	0,0029	PE	0,89	12.feb	Norner
2-31-1	grey	fiber	15,22	0,35	0,0018	PE	0,89	12.feb	Norner
2-32-1	clear	3d	7,22	3,96	0,0109	PE	0,84	12.feb	Norner
2-33-1	blue	fiber	12,13	0,31	0,0013	PE	0,89	12.feb	Norner
2-34-1	grey	fiber	7,8	0,38	0,0006	PE	0,89	13.feb	Norner
2-35-1	blue	fiber	12,46	0,5	0,0025	PE	0,82	13.feb	Norner
2-36-1	grey	fiber	8,17	0,33	0,0009	PE	0,87	13.feb	Norner
2-37-1	blue	fiber	6,6	0,28	0,0003	Pe	0,87	13.feb	Norner
2-38-1	blue	fiber	5,08	0,43	0,0007	PE	0,89	13.feb	Norner
2-39-1	blue	3d	3,44	2,09	0,0049	PE	0,79	13.feb	Norner
2-40-1	clear	3d	2,8	1,98	0,0077	PE	0,91	13.feb	Norner
2-41-1	white	3d	10,65	8,23	0,0048	PE	0,86	13.feb	Norner
2-42-1	grey	3d	4,53	3,22	0,0011	PE	0,76	13.feb	Norner
2-43-1	blue	3d	1,76	1,68	0,0012	PE	0,88	13.feb	Norner
2-44-1	green	3d	1,69	1,26	0,0020	PE	0,77	13.feb	Norner
2-45-1	white	3d	4,07	1,02	0,0022	PE	0,9	13.feb	Norner
2-46-1	clear	2d	4,18	2,57	0,0005	PE	0,86	13.feb	Norner
2-47-1	white	fiber	5,93	0,17	0,0040	PE	0,88	13.feb	Norner
2-48-1	white	2d	3,5	2,07	0,0031	PE	0,82	13.feb	Norner
2-49-1	blue	2d	2,31	1,52	0,0003	PE	0,85	13.feb	Norner
2-50-1	blue	fiber	7,57	0,43	0,0011	PE	0,89	13.feb	Norner
2-51-1	white	2d	3,41	2,4	0,0020	PE	0,9	13.feb	Norner
2-52-1	grey	2d	2,4	1,62	0,0009	PP	0,79	13.feb	Norner
2-53-1	white	2d	2,12	0,53	0,0002	PP	0,71	13.feb	Norner
2-54-1	clear	2d	1,69	1,02	0,0011	PE	0,82	13.feb	Norner
2-55-1	grey	fiber	2,89	0,37	0,0003	PE	0,86	13.feb	Norner
2-56-1	white	2d	3,24	2,84	0,0021	PE	0,9	13.feb	Norner
2-57-1	purple	fiber	6,33	0,33	0,0007	PE	0,86	13.feb	Norner
2-58-1	white	2d	6,36	3,51	0,0015	PE	0,77	13.feb	Norner
2-59-1	orange	3d	1,93	1,89	0,0019	PE	0,88	13.feb	Norner
2-60-1	blue	fiber	4,75	0,5	0,0008	PE	0,9	13.feb	Norner
2-61-1	White	Fiber	6,36	0,37	0,0005	PE	0,89	13.feb	Norner
2-62-1	grey	fiber	7,38	0,39	0,0006	PE	0,87	13.feb	Norner
2-63-1	grey	fiber	2,52	0,56	0,0007	PE	0,86	13.feb	Norner
2-64-1	grey	fiber	4,95	0,37	0,0004	PE	0,88	13.feb	Norner
2-65-1	grey	fiber	4,21	0,33	0,0007	PE	0,86	13.feb	Norner
2-66-1	white	2d	1,62	1,57	0,0007	PE	0,7	13.feb	Norner
2-67-1	white	2d	2,99	0,64	0,0011	PE	0,91	13.feb	Norner
2-68-1	blue	2d	1,84	0,41	0,0005	PE	0,82	13.feb	Norner
2-69-1	white	2d	2,7	1,6	0,0008	PE	0,83	13.feb	Norner
2-70-1	white	2d	2,32	2,19	0,0012	PE	0,73	13.feb	Norner
2-71-1	blue	2d	2,28	1,15	0,0004	PE	0,91	13.feb	Norner
2-72-1	clear	2d	5,08	3,09	0,0005	PE	0,88	13.feb	Norner

2-73-1	blue	2d	1,82	1,48		0,0010	PE	0,66	13.feb	Norner
2-74-1	clear	2d	3,8	2,04		0,0004	PE	0,89	13.feb	Norner
2-75-1	blue	2d	2,4	1,09		0,0012	PE	0,88	13.feb	Norner
2-76-1	grey	3d	2,6	1,63		0,0007	PE	0,66	13.feb	Norner
2-77-1	blue	3d	1,9	1,05		0,0011	PE	0,83	13.feb	Norner
2-78-1	clear	3d	4,27	1,35		0,0012	PE	0,77	13.feb	Norner
2-79-1	clear	3d	1,87	1,32		0,0004	PE	0,77	13.feb	Norner
2-80-1	blue	fiber	2,99	0,47		0,0002	PE	0,86	13.feb	Norner
2-81-1	yellow	2d	1,7	1,93		0,0008	PE	0,88	13.feb	Norner
2-82-1	white	2d	2,05	1,12	NOT POSSIBLE	0,0007	?		13.feb	Norner
2-83-1	white	2d	2,59	0,83	NOT POSSIBLE	0,0005	?		13.feb	Norner
2-84-1	white	2d	2,25	1,76		0,0009	PE	0,84	13.feb	Norner
2-85-1	white	fiber	3,07	0,84		0,0007	PE	0,8	13.feb	Norner
2-86-1	clear	fiber	8,03	0,51		0,0002	PE	0,9	13.feb	Norner
2-87-1	white	fiber	2,91	0,64		0,0003	PE	0,87	13.feb	Norner
2-88-1	white	2d	3,07	1,98		0,0006	PE	0,92	13.feb	Norner
2-89-1	white	fiber	3,45	0,46		0,0009	PE	0,86	13.feb	Norner
2-90-1	white	2d	3,82	2,14		0,0004	PE	0,89	13.feb	Norner
2-91-1	black	2d	2,76	1,27		0,0005	PE	0,88	13.feb	Norner
2-92-1	white	fiber	2,03	0,38		0,0004	PE	0,88	13.feb	Norner
2-93-1	blue	fiber	2,18	0,27		0,0003	PE	0,88	13.feb	Norner
2-94-1	white	2d	1,63	0,55		0,0005	PE	0,84	13.feb	Norner
2-95-1	clear	2d	2,57	1,18		0,0009	PE	0,86	13.feb	Norner
2-96-1	white	3d	0,85	1,04		0,0004	PE	0,89	13.feb	Norner
2-97-1	white	2d	0,98	0,89		0,0006	PE	0,88	13.feb	Norner
2-98-1	clear	2d	1,52			0,0002	PE	0,92	13.feb	Norner
REST in bag (not possible to analyse)						0,0015				Norner
Sum						0,4931				
3-1-1	clear	2d	59,43	29,06		0,0569	PP	0,71	14.feb	Norner
3-2-1	clear	2d	35,83	17,53		0,0368	PE	0,82	14.feb	Norner
3-3-1	clear	2d	78,44	10,06	Plast wrapp	0,0285	PP		14.feb	Norner
3-3-1					Cleaned by acetone wrapp		PP		15.feb	Norner
3-4-1	clear	2d	38,35	13,34		0,0245	PE	0,87	14.feb	Norner
3-5-1	clear	2d	42,29	12,79		0,0157	PP	0,84	14.feb	Norner
3-6-1	clear	2d	34,13	12,99		0,0128	PP	0,72	14.feb	Norner
3-7-1	clear	2d	22,44	5,64		0,0221	PP	0,73	14.feb	Norner
3-8-1	clear	2d	18,3	7,66		0,0121	PP	0,79	14.feb	Norner
3-9-1	clear	2d	12,32	8,2		0,0079	PP	0,74	14.feb	Norner
3-10-1	clear	2d	14,88	7,13		0,0052	PE	0,85	14.feb	Norner
3-11-1	white	3d	12,13	10,44		0,0273	PE	0,79	14.feb	Norner
3-12-1	white	fiber	48,48	1,24		0,0171	PP	0,87	14.feb	Norner
3-100-1	white	3d	5,58	3,88		0,0085	PP	0,92	14.feb	Norner
3-101-1	white	2d	5	2,43	Looks like pl	0,0021	PE	0,63	14.feb	Norner
3-102-1	brown	3d	2,86	0,94	No results (0,0017	PE		14.feb	Norner
3-102-1	brown						PE		15.feb	Norner
3-103-1	white	2d	4,98	4,41	No results (0,0023	PE		14.feb	Norner
3-103-1	white						PE		15.feb	Norner
3-104-1	grey	fiber	5,57	0,4		0,0006	PE	0,79	14.feb	Norner
3-105-1	white	2d	7,93	3,62	No results (0,0019	PE	0,61	14.feb	Norner
3-105-1_001	white						PE		15.feb	Norner
3-106-1	clear	2d	5,29	2,09		0,0032	?		14.feb	Norner
3-107-1	clear	2d	8,17	6,32	Only organic	0,0014	?		14.feb	Norner
3-108-1	Black				Rubber, cut up and checked, no cellstructures				15.feb	Norner
3-108-1	white	3d			rubber piece	0,7322			14.feb	Norner
3-108-2	black						Resin ?		15.feb	Norner
3-109	blue	2d					PE		15.feb	Norner
3-110	white	2d					PP		15.feb	Norner
3-111	green	fiber					PP		15.feb	Norner
3-112	grey	fiber					PP		15.feb	Norner
3-113	blue	2d					PE		15.feb	Norner

3-114	green	2d					PE		15.feb	Norner
3-115	blue	2d					PE		15.feb	Norner
3-116	white	2d				Get inorganic spectra, bu	PP		15.feb	Norner
3-117	yellow	fiber					PP		15.feb	Norner
3-118	white	2d					PP		15.feb	Norner
3-13-1	green	fiber	71,07	0,4		0,0083	PE	0,87	14.feb	Norner
3-14-1	yellow	fiber	49,73	0,24		0,0028	PP	0,8	14.feb	Norner
3-15-1	green	fiber	37,85	0,4		0,0026	PP	0,87	14.feb	Norner
3-16-1	black	fiber	30,98	0,23		0,0013	PP	0,85	14.feb	Norner
3-17-1	white	fiber	53,53	0,18		0,0013	PP	0,74	14.feb	Norner
3-18-1	black	fiber	22,53	0,29		0,0016	PP	0,88	14.feb	Norner
3-19-1	green	fiber	9	7,06	Ball with fit	0,0115	PP	0,7	14.feb	Norner
3-20-1	green	fiber	30,42	0,25		0,0017	PE	0,88	14.feb	Norner
3-21-1	green	fiber	23,97	0,28		0,0026	PE	0,83	14.feb	Norner
3-22-1	green	fiber	15,29	0,61		0,0022	PP	0,73	14.feb	Norner
3-23-1	green	fiber	14,22	0,37		0,0016	PE	0,85	14.feb	Norner
3-24-1	brown	fiber	20,78	0,3		0,0019	PE	0,83	14.feb	Norner
3-25-1	white	fiber	42,89	0,26		0,0005	PP	0,73	14.feb	Norner
3-26-1	green	fiber	15,07	0,24		0,0008	PP	0,88	14.feb	Norner
3-27-1	pink	fiber	15,84	0,33		0,0004	PP	0,84	14.feb	Norner
3-28-1	blue	fiber	22,94	0,86		0,0051	PP	0,71	14.feb	Norner
3-29-1	grey	fiber	26,9	1		0,0063	PP	0,76	14.feb	Norner
3-30-1	white	fiber	34	0,23		0,0023	PE	0,85	14.feb	Norner
3-31-1	black	fiber	32,69	0,28		0,0032	PP	0,75	14.feb	Norner
3-32-1	white	fiber	17,93	0,23		0,0014	PP	0,86	14.feb	Norner
3-33-1	green	fiber	11,41	0,19		0,0006	PP	0,78	14.feb	Norner
3-34-1	white	fiber	19,27	0,24		0,0010	PP	0,87	14.feb	Norner
3-35-1	white	fiber	23,81	0,71		0,0032	PP	0,74	14.feb	Norner
3-36-1	white	fiber	10,7	0,43		0,0019	PE	0,83	14.feb	Norner
3-37-1	black	fiber	8,58	0,28		0,0005	PP	0,76	14.feb	Norner
3-38-1	white	fiber	11,7	0,3		0,0009	PP	0,89	14.feb	Norner
3-39-1	white	fiber	13,55	0,23		0,0011	PP	0,79	14.feb	Norner
3-40-1	black	fiber	10,43	0,15		0,0004	PP	0,8	14.feb	Norner
3-41-1	black	fiber	6,03	0,23		0,0002	PP	0,85	14.feb	Norner
3-42-1	white	fiber	9,56	0,2		0,0006	PP	0,81	14.feb	Norner
3-43-1	black	fiber	7,06	0,2		0,0004	PE	0,87	14.feb	Norner
3-44-1	white	fiber	13,51	0,26		0,0016	PP	0,72	14.feb	Norner
3-45-1	grey	2d	17,07	5,14		0,0097	PE	0,9	14.feb	Norner
3-46-1	grey	2d	13,6	12,46	Looks like p	0,0225	?		14.feb	Norner
3-47-1	grey	2d	10,57	4,06	No good res	0,0109	?		14.feb	Norner
3-48-1	white	3d	7,46	4,65		0,0519	PE	0,72	14.feb	Norner
3-49-1	white	2d	5,08	2,23		0,0015	PP	0,82	14.feb	Norner
3-50-1	yellow	2d	19,98	11,96		0,0099	PE	0,9	14.feb	Norner
3-51-1	yellow	2d	6	3,97		0,0014	PE	0,86	14.feb	Norner
3-52-1	clear	2d	7,53	4,31		0,0012	PP	0,84	14.feb	Norner
3-53-1	clear	2d	11,78	2,17		0,0013	PE	0,69	14.feb	Norner
3-54-1	clear	2d	6,02	2,94		0,0007	PE	0,72	14.feb	Norner
3-55-1	white	fiber	32,56	0,61		0,0016	PP	0,82	14.feb	Norner
3-56-1	white	fiber	43,28	0,15		0,0023	PP	0,87	14.feb	Norner
3-57-1	white	fiber	18,79	0,36		0,0011	PP	0,83	14.feb	Norner
3-58-1	white	fiber	19,8	0,23		0,0019	PE	0,86	14.feb	Norner
3-59-1	white	fiber	27,47	0,26		0,0017	PP	0,83	14.feb	Norner
3-60-1	pink	fiber	18,67	0,53		0,0015	PP	0,73	14.feb	Norner
3-61-1	black	fiber	16,95	0,24		0,0006	PP	0,85	14.feb	Norner
3-62-1	blue	fiber	14,82	0,2		0,0005	PE	0,79	14.feb	Norner
3-63-1	black	fiber	11,8	0,23		0,0004	PP	0,75	14.feb	Norner
3-64-1	black	fiber	11,51	0,24		0,0004	PP	0,88	14.feb	Norner
3-65-1	white	fiber	17,61	0,2		0,0006	PP	0,88	14.feb	Norner
3-66-1	blue	fiber	7,8	0,23		0,0004	PP	0,86	14.feb	Norner
3-67-1	blue	fiber	17,45	0,24		0,0008	PP	0,89	14.feb	Norner
3-68-1	yellow	fiber	10,53	0,37		0,0005	PP	0,85	14.feb	Norner
3-69-1	white	fiber	9,64	0,33		0,0006	PP	0,88	14.feb	Norner
3-70-1	yellow	2d	4,83	3,48		0,0059	PE	0,75	14.feb	Norner
3-71-1	blue	fiber	5,21	0,24		0,0002	PE	0,87	14.feb	Norner

3-72-1	clear	2d	5,94	4,4		0,0016	PE	0,7	14.feb	Norner
3-73-1	yellow	3d	4,07	2,52		0,0052	PE	0,78	14.feb	Norner
3-74-1	white	3d	7,12	6,44		0,1128	PE	0,86	14.feb	Norner
3-75-1	white	3d	7,45	3,59		0,0066	PE	0,87	14.feb	Norner
3-76-1	grey	3d	15,02	3,47	Rubber?	0,2540	?		14.feb	Norner
3-77-1	orange	3d	4,22	2,38		0,0028	PE	0,82	14.feb	Norner
3-77-1 merke	orange						PE		15.feb	Norner
3-78-1	grey	2d	9,09	3,72	No good res	0,0109	?		14.feb	Norner
3-79-1	grey	2d	6,12	4,21	No good res	0,0062	?		14.feb	Norner
3-80-1	grey	2d	7,53	6,23	No good res	0,0033	?		14.feb	Norner
3-81-1	grey	2d	7,35	5,42	No good res	0,0137	?		14.feb	Norner
3-81-1	grey+white				too much to get a clear s	?			15.feb	Norner
3-81-2					tried analysing at the white part				15.feb	Norner
3-82-1	brown	3d	12,08	7,78	Red, foam?	0,0029	PE	0,9	14.feb	Norner
3-82-1	brun skum				Very degraded, hard spec		PE		15.feb	Norner
3-83-1	yellow	2d	4,98	3,68		0,0041	PE	0,88	14.feb	Norner
3-84-1	blue	fiber	9,22	0,33		0,0004	PE	0,88	14.feb	Norner
3-85-1	brown	3d	4,4	2,35	No results (0,0044	?		14.feb	Norner
3-86-1	white	3d	5,81	4,59	No results (0,0049	?		14.feb	Norner
3-87-1	white	3d	5,27	3,94	No results (0,0036	?		14.feb	Norner
3-88-1	yellow	3d	4,45	2,36	No results (0,0039	PE		14.feb	Norner
3-88-1	yellow						PE		15.feb	Norner
3-89-1	white	3d	2,36	1,74	No results (0,0049	PE	??	14.feb	Norner
3-90-1	white	3d	3,92	2,91		0,0027	PE	0,86	14.feb	Norner
3-91-1	clear	2d	7,68	2,56	No results (getting too sr	?			14.feb	Norner
3-92-1	white	2d	5,29	2,24		0,0008	PE	0,84	14.feb	Norner
3-93-1	orange	3d	4,62	1,81		0,0032	PE	0,86	14.feb	Norner
3-94-1	yellow	3d	3,73	1,92		0,0052	PE	0,85	14.feb	Norner
3-95-1	blue	3d	2,96	2,27		0,0028	PE	0,93	14.feb	Norner
3-96-1	white	2d	2,32	3,59		0,0012	PE	0,92	14.feb	Norner
3-97-1	yellow	2d	7,18	3,33		0,0016	PE	0,86	14.feb	Norner
3-98-1	white	2d	4,97	3,83		0,0011	PE	0,89	14.feb	Norner
3-99-1	clear	2d	8,81	4,66		0,0021	PE	0,76	14.feb	Norner
REST in bag					(difficult to	0,0718				
Sum						1,4793				
Samples tested with microscopy (again/new from 'rest')										
3-78-1++	grey cutted				Unaturlig, silika, mye uorganisk				15.feb	Norner
3-89-1	white								15.feb	Norner
4-1-1	clear	2d	42,2	14,35	weathered (yellow/dis	0,024	polyalkyl acrylate	0,82	24.jan	Norner
4-2-1	blue	fiber	17,36	0,2	LOOKS like a	0,0003	PP	0,86	24.jan	Norner
4-3-1	green	fiber	6,72	0,35	small	0,0004		0,91	24.jan	Norner
4-4-1	blue	2d	3,41	2,75	blue fibre	0,0002			24.jan	Norner
4-5-1	white	2d	3,25	2,35		0,0013	PE	0,98	24.jan	Norner
4-6-1	white	2d	3,26	3,04		0,001	PE	0,87	24.jan	Norner
4-7-1	clear	2d	49,9	2,33		0,0092	PE	0,96	24.jan	Norner
4-8-1	blue	fiber	4,43	3,77		0,0008	PE	0,94	24.jan	Norner
4-9-1	yellow	fiber	37,47	0,17		0,0023	PE	0,96	24.jan	Norner
4-10-1	clear	2d	14,61	13,888	Blue spots (writing?)	0,0227			24.jan	Norner
4-11-1	green	fiber	18,58	0,3		0,0004	PP	0,77	24.jan	Norner
4-12-1	white	fiber	17,72	1,43		0,014	polyester(P ET)	0,79	24.jan	Norner
4-13-1	green	3d	3,34	1,21		0,0008	PE	0,99	24.jan	Norner
4-14-1	green	3d	2,86	0,89		0,001	PP	0,85	24.jan	Norner
4-15-1	green	fiber	7,09	0,29		0,0003	PE	0,96	24.jan	Norner
4-16-1	white	fiber	5,78	0,35		0,0005	PE	0,94	24.jan	Norner
4-17-1	grey	2d	7,55	3,37	Grey with some	0,0194	PE	0,66	24.jan	Norner
4-18-1	green	3d	4,47	0,98	white and green	0,0002			24.jan	Norner

4-19-1	green	2d	1,33	0,26		0,0003	PE	0,98	24.jan	Norner
4-20-1	black	2d	2,16	2,3	A black side with electrolyte	0,0008	polystyrene	0,77	24.jan	Norner
4-21-1	blue	2d	2,12	1,06		0,0002	PE	0,97	24.jan	Norner
SUM						0,1001				
Some of the sample 4 results were not very reliable and odd, so several spectra were run again in the norner database which gave some other results.										
4-18-1	green	3d	4,47	0,98	5 more fibres that are	0,0002	PP	0,67		
5-1-1	orange	3d	20,75	17,34	several fibres	0,0416	PE	0,92	23.jan	NGI
5-2-1	black	2d	29,25	5,63		0,0125	PE	0,94	23.jan	NGI
5-3-1	white	2d	31,32	10,64		0,0072	PE	0,87	23.jan	NGI
5-4-1	white	3d	12,17	10,67	isopor	0,0287	polystyrene	0,73	23.jan	NGI
5-5-1	blue	fiber	30,57	0,83	2 more fibres that are	0,0066	PP	0,76	23.jan	NGI
5-6-1	white	fiber	23,6	0,27		0,0012	styrene isoprene	0,72	23.jan	NGI
5-7-1	blue	fiber	15,44	1,35	5 more fibres that are	0,0075	PP	0,78	23.jan	NGI
5-8-1	blue	fiber	15,15	0,4		0,0017	Nylon 12	0,74	23.jan	NGI
5-9-1	clear+white	3d	3,99	3,35		0,0042	PE	0,95	23.jan	NGI
5-10-1	clear+white	3d	3,15	3,1		0,0039	PE	0,96	23.jan	NGI
5-11-1	blue	fiber	10,03	0,27		0,001	PE	0,77	23.jan	NGI
5-12-1	green	fiber	10,31	0,22		0,0003	PE	0,83	23.jan	NGI
5-13-1	white	fiber	10,88	0,14		0,0005	PP	0,82	23.jan	NGI
5-14-1	white	fiber	14,64	0,23		0,0009	PE	0,78	23.jan	NGI
5-15-1	blue	fiber	9,55	0,49		0,0015	Nylon 12	0,76	23.jan	NGI
5-16-1	white	fiber	15,81	0,5		0,0009	PP	0,86	23.jan	NGI
5-17-1	white	3d	4,45	2,8		0,0018	PE	0,88	23.jan	NGI
5-18-1	blue	fiber	6,89	0,74		0,0004	Nylon 12	0,73	23.jan	NGI
5-19-1	blue	fiber	7,49	0,42		0,0004	PP	0,88	23.jan	NGI
5-20-1	blue	fiber	7,71	0,42		0,0005	PP	0,91	23.jan	NGI
5-21-1	blue	fiber	11,25	0,31		0,0006	PP	0,78	24.jan	NGI
5-22-1	blue	fiber	11,9	0,31		0,001	PP	0,83	24.jan	NGI
5-23-1	yellow	3d	4,29	2,87	A lot of biof	0,0019			24.jan	NGI
5-24-1	blue	2d	5,09	3,08		0,0006	PE	0,96	24.jan	NGI
5-25-1	blue	2d	2,22	2,32		0,0005	PE	0,96	24.jan	NGI
5-26-1	white	2d	4,09	2,37		0,0032	Ethylene /vir	0,87	24.jan	NGI
5-27-1	white+c	2d	2,2	2,12		0,0009	PE	0,8	24.jan	NGI
5-28-1	blue (lig	3d	2,08	1,44		0,0081	PE	0,98	24.jan	NGI
5-29-1	blue (da	3d	2,35	1,03		0,0004	PE	0,98	24.jan	NGI
5-30-1	blue (da	3d	2,85	1,13		0,0004	PE	0,96	24.jan	NGI
5-31-1	white	2d	2,55	1,88		0,0002	PE	0,74	24.jan	NGI
5-32-1	green	3d	1	0,85		0,0001	PE	0,98	24.jan	NGI
5-33-1	yellow	3d	2,2	1,52		0,0063	undecided	0,81	24.jan	NGI
5-34-1	blue	2d	1,09	0,93		0,0004	PE	0,97	24.jan	NGI
Rest						0,1479				
6-2-1	clear	2D	24,39	20,51		0,0156	Nylon12	0,73	22.jan	NGI
6-3-1	Blue	fiber	33,04	0,47	biofilm	0,0027			22.jan	NGI
6-4-1	Blue	fiber	34,91	0,61	Biofilm	0,002			22.jan	NGI
6-5-1	clear+blue	2D	24,32	13,09	Biofilm	0,0084			22.jan	NGI
6-6-1	clear	2D	18,38	11,78	biofilm	0,0057			22.jan	NGI
6-7-1	Blue	fiber	17,29	0,62		0,0011	PP	0,87	22.jan	NGI
6-8-1	White	fiber	26,28	0,32		0,0019	Nylon12	0,74	22.jan	NGI
6-9-1	clear	2D	20,51	4,57	Biofilm	0,0018			22.jan	NGI
6-10-1	White	fiber	150,17	0,46	Biofilm	0,0183			22.jan	NGI
6-11-1	White	fiber	51,06	0,39	Biofilm	0,0069			22.jan	NGI
6-12-1	White	fiber	104,92	0,54	Biofilm	0,0068	PP?	0,64	22.jan	NGI
6-1-2	Blue	fiber	13,96	0,45		0,0008	PP	0,85	22.jan	NGI
6-2-2					EVA?		Etylene vinyl acetat	0,73	22.jan	NGI
6-3-2							Nylon 12	0,67	22.jan	NGI
6-4-2							PP	0,84	22.jan	NGI

6-5-2							PP	0,74	22.jan	NGI
6-6-2							PP	0,84	22.jan	NGI
6-9-2									22.jan	NGI
6-10-2							Nylon 12	0,68	22.jan	NGI
6-11-2									22.jan	NGI
6-12-2									22.jan	NGI
6-11-3									22.jan	NGI
6-12-3							Nylon 6	0,67	22.jan	NGI
6-11-4							PP	0,81	22.jan	NGI
6-13-1	Blue	fiber	8,37	0,66		0,0006	PP	0,72	22.jan	NGI
6-14-1	clear	2D	46,82	30,46		0,0448	PP	0,79	22.jan	NGI
6-15-1	clear	2D	28,06	26,9	sjekk?	0,0191			22.jan	NGI
6-15-2							Nylon 12	0,73	22.jan	NGI
6-16-1	light blue	fiber	16,58	0,52		0,0014			22.jan	NGI
6-16-2							Nylon 12+	0,68	22.jan	NGI
6-17-1	clear	2D	18,24	18,72		0,0107		0,73	22.jan	NGI
6-17-2									22.jan	NGI
6-18-1	Blue	fiber	22,47	0,28	Biofilm	0,0006	Nylon 12	0,62	22.jan	NGI
6-19-1	White	fiber	21,8	0,67	Biofilm				22.jan	NGI
6-19-2							Nylon 6	0,73	22.jan	NGI
6-20-1	clear	2D	23,22	19,12	lik 6-15-1?	0,0079			22.jan	NGI
6-21-1	Blue	fiber	17,12	0,71		0,0012	Nylon 6	0,71	22.jan	NGI
6-22-1	white	2D	7,3	2,94		0,0011			22.jan	NGI
6-23-1	clear	2D	41,63	19,3		0,0442	Poly(Butyl Acetat)	0,71	22.jan	NGI
6-24-1	white	fiber	29,69	0,32	biofilm	0,0026	Nylon 6	0,69	22.jan	NGI
6-25-1	white	fiber	36,8	0,17	biofilm	0,0008	Nylon 6	0,7	22.jan	NGI
6-26-1	white	fiber	35,9	0,31	biofilm	0,0013	Nylon 6	0,69	22.jan	NGI
6-27-1	clear	2D	21,89	7,56	biofilm	0,0079			22.jan	NGI
6-27-2								0,76	22.jan	NGI
6-28-1	white	3D	12,4	3,07		0,0298		0,76	22.jan	NGI
6-28-2									22.jan	NGI
6-29-1	white	3D	9,01	6,62	biofilm	0,0041			22.jan	NGI
6-29-2								0,73	22.jan	NGI
6-30-1	white	3D	4,14	2,9	ser lik 6-29	0,0007		0,65	22.jan	NGI
6-31-1	Blue	fiber	26,9	0,34		0,0015		0,71	22.jan	NGI
6-31-2									22.jan	NGI
6-31-3							Nylon 12	0,66	22.jan	NGI
6-32-1	White+Black	2D	29,01	5,02	Biofilm	0,0071		0,72	22.jan	NGI
6-33-1	White	fiber	22,95	0,81		0,0012		0,72	22.jan	NGI
6-33-2									22.jan	NGI
6-33-3							PP	0,75	22.jan	NGI
6-34-1	clear	2D	15,26	1,41	Biofilm	0,0063		0,71	22.jan	NGI
6-34-2								0,73	22.jan	NGI
6-35-1	Blue	fiber	9,52	0,61		0,0005		0,73	22.jan	NGI
6-35-2								0,73	22.jan	NGI
6-35-3									22.jan	NGI
6-36-1	Green	3D	3,84	1,79		0,0024		0,77	22.jan	NGI
6-36-2								0,68	22.jan	NGI
6-37-1	White cl	Mix			Mix, rest,	0,0268			22.jan	NGI
Sum weight						0,2966				
Several of the sample 6 results were not very reliable and odd, so several spectra were run again in their database which gave										
6-9-1	clear	2D	20,51	4,57	Biofilm	0,0018			11.feb	Norner
6-10-1	White	fiber	150,17	0,46	Biofilm	0,0183	PP	0,76	11.feb	Norner
6-11-1	White	fiber	51,06	0,39	Biofilm	0,0069	Organic		11.feb	Norner
6-12-1	White	fiber	104,92	0,54	Biofilm	0,0068	PP	0,76	11.feb	Norner
6-9-2					Look again		PW)	0,646	11.feb	Norner
6-10-2							PP	0,78	11.feb	Norner

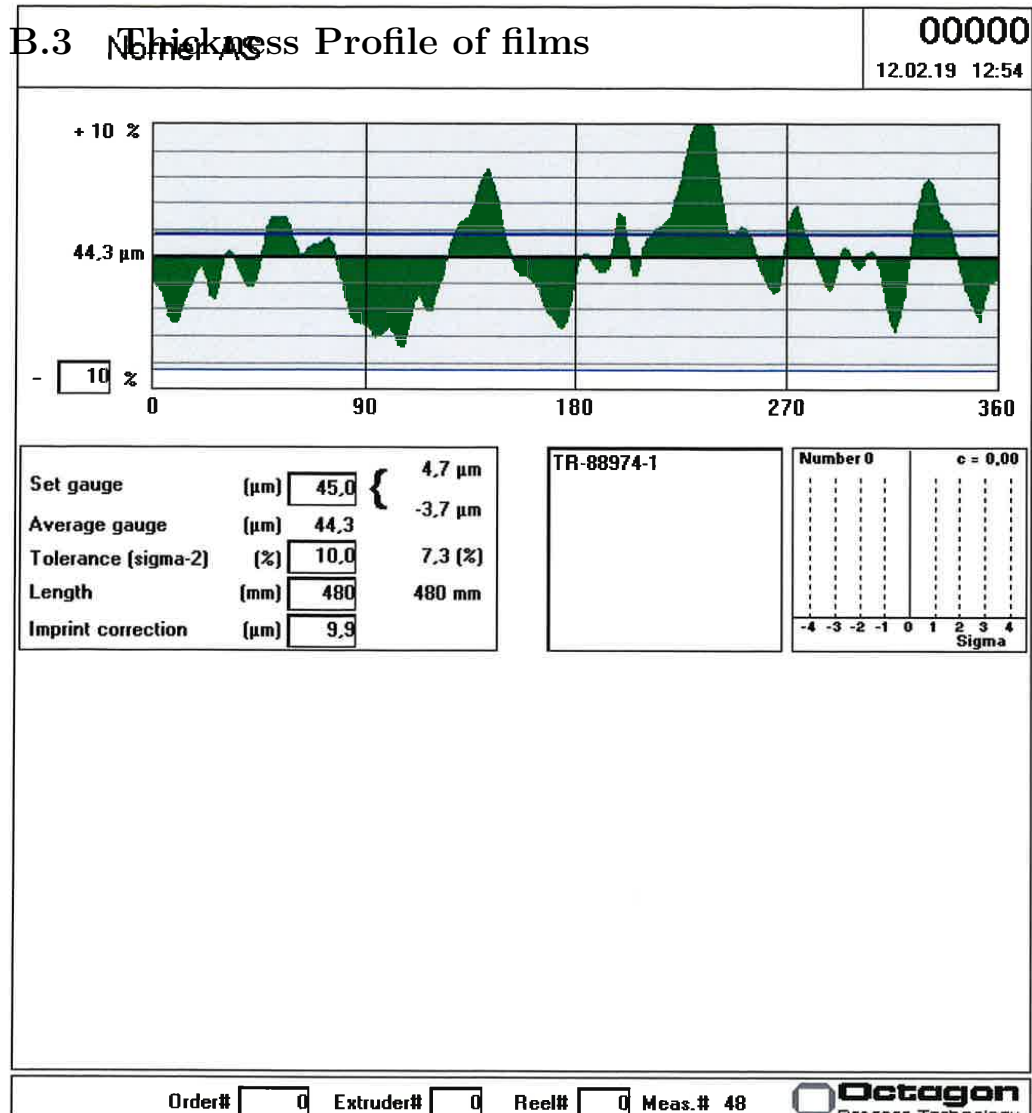
6-11-2							Organic		11.feb	Norner
6-12-2							PP	0,85	11.feb	Norner
6-11-3							PP	0,79	11.feb	Norner
6-12-3							PP	0,61	11.feb	Norner
6-11-4							PP	0,924	11.feb	Norner
6-16-1	light blue	fiber	16,58	0,52		0,0014	Organic		11.feb	Norner
6-16-2							PP	0,84	11.feb	Norner
6-17-1	clear	2D	18,24	18,72		0,0107	Organic	0	11.feb	Norner
6-17-2							Organic	0	11.feb	Norner
6-18-1	Blue	fiber	22,47	0,28	Biofilm	0,0006	PP	0,78	11.feb	Norner
6-24-1	white	fiber	29,69	0,32	biofilm	0,0026	Organic	0	11.feb	Norner
6-27-1	clear	2D	21,89	7,56	biofilm	0,0079	Organic	0	11.feb	Norner
6-27-2							Organic	0	11.feb	Norner
6-28-1	white	3D	12,4	3,07		0,0298	Organic	0	11.feb	Norner
6-28-2							Organic	0	11.feb	Norner
6-29-1	white	3D	9,01	6,62	biofilm	0,0041	Polystyrene	0,58	11.feb	Norner
6-29-2							Organic	0	11.feb	Norner
6-30-1	white	3D	4,14	2,9	like 6-29	0,0007	Organic	0	11.feb	Norner
6-31-1	Blue	fiber	26,9	0,34		0,0015	PP	0,73	11.feb	Norner
6-31-2							PP	0,799	11.feb	Norner
6-31-3							PP	0,83	11.feb	Norner
6-32-1	White+Black	2D	29,01	5,02	Biofilm	0,0071	Organic	0	11.feb	Norner
6-32-1							PP	0,65	11.feb	Norner
6-33-1	White	fiber	22,95	0,81		0,0012	Organic	0	11.feb	Norner
6-33-2							PP	0,75	11.feb	Norner
6-33-3							PP	0,91	11.feb	Norner
6-34-1	clear	2D	15,26	1,41	Biofilm	0,0063	Organic	0	11.feb	Norner
6-34-2							Organic	0	11.feb	Norner
6-35-1	Blue	fiber	9,52	0,61		0,0005	PP	0,697	11.feb	Norner
6-35-2							Organic	0	11.feb	Norner
6-35-3							PP	0,84	11.feb	Norner
6-36-1	Green	3D	3,84	1,79		0,0024	Nylon11	0,73	11.feb	Norner
7-1-1	clear	2d	13,57	12,17		0,0032	PP	0,96	23.jan	NGI
7-2-1	clear	2d	37,61	11,87		0,0093	PP	0,95	23.jan	NGI
7-3-1	black	fiber	37,91	0,18		0,001	Polyester (PET)	0,87	23.jan	NGI
7-4-1	white+red	fiber	7,73	0,36		0,0004	PE	0,97	23.jan	NGI
SUM						0,0139				
8-1-1	white	2d	20,27	12,64		0,2433	PP	0,89	23.jan	NGI
8-2-1	green	fiber	2,21	0,33		0,001	PE	0,91	23.jan	NGI
8-3-1	red	fiber/3d	71,64	1,52	LOOKS like fabric like	0,1219	PE	0,87	23.jan	NGI
8-4-1	white	2d	6,1	4,97		0,0189	PE	0,79	23.jan	NGI
8-5-1	green	3d	5,44	1,94		0,0036	PE	0,76	23.jan	NGI
8-6-1	blue	fiber	25,96	0,32		0,0024			23.jan	NGI
8-7-1	white + blue	2d	13,74	2,16		0,00021	PP	0,76	23.jan	NGI
8-8-1	white	3d	8,68	4,27	2 pieces of isopor (looks like) that were	0,0028	isopor		23.jan	NGI
8-9-1	white	2d	9,36	6,21	very difficult, quite	0,0401	PE	0,7	23.jan	NGI
8-10-1	white + blue	2d	18,15	2,41		0,0052	PP?			NGI
8-11-1	blue	fibre	17,34	0,75		0,0016	PP	0,75	23.jan	NGI
8-12-1	white	3d	7,58	5,95	LOOKS like isopor	0,0059			23.jan	NGI
8-6-2							butyl sterate??	0,82?	23.jan	NGI
8-13-1	white	2d	9,66	2,27		0,0021	PP	0,94	23.jan	NGI
8-14-1	green	3d	3,04	1,7		0,0014	PE	0,8	23.jan	NGI

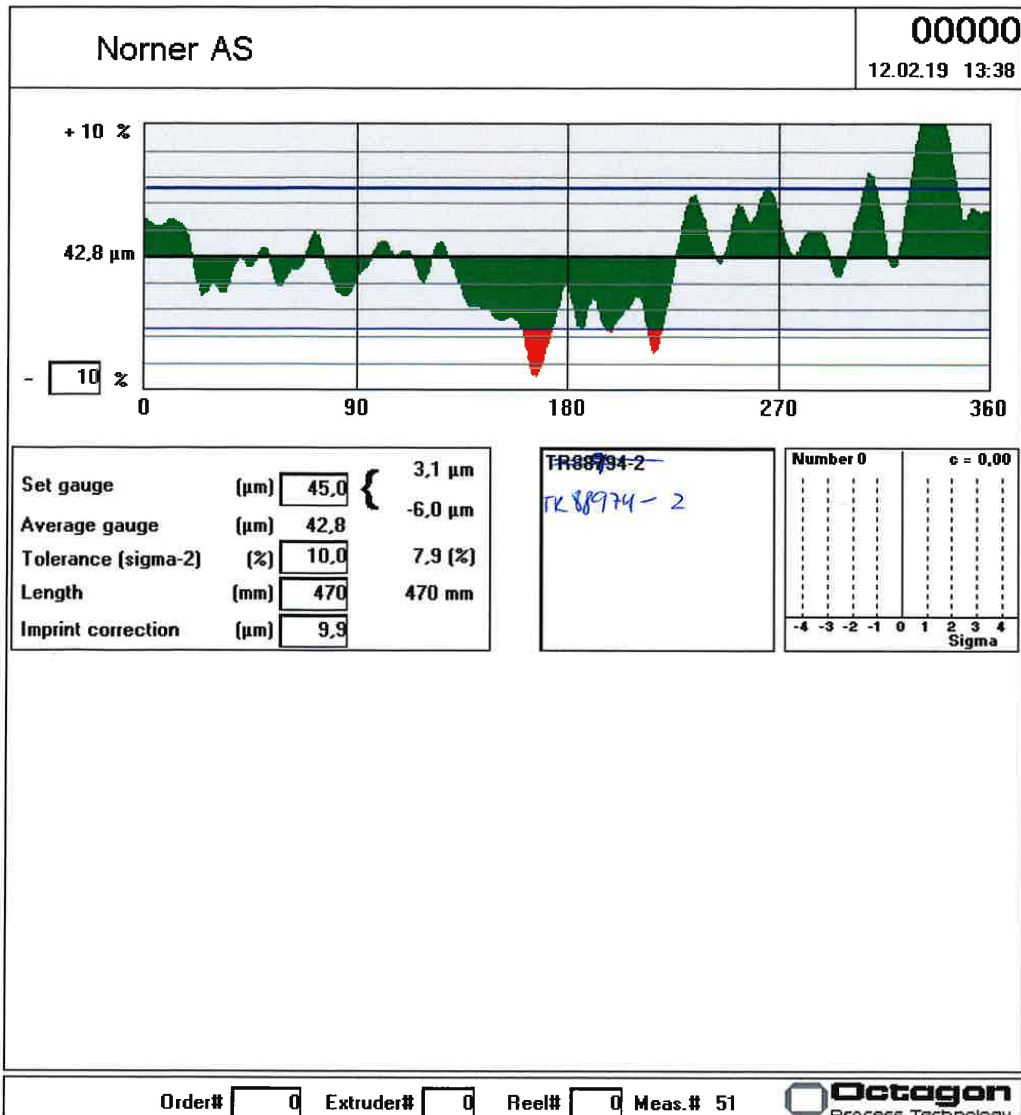
8-15-1	white	3d	6,2	2,58	Aceton test	0,0015			23.jan	NGI
Sum						0,20861				
9-1-1	white	fiber	153,34	3,13	group of fiber	0,2702	PE	0,85	23.jan	NGI
9-2-1	green	2d			plastic	0,001	PE	0,87	23.jan	NGI
9-3-1	white	2d	104,18	3,17		0,0122	PP	0,92	23.jan	NGI
9-4-1	white	2d			looks same as 9-3	0,0147	PP	0,89	23.jan	NGI
9-5-1	white	3d	45,12	11,14		0,1583	PP	0,85	23.jan	NGI
9-6-1	clear	2d	21,46	16,97		0,0072	PE	0,95	23.jan	NGI
9-7-1	clear	2d	10,89	7,81		0,0036	PE	0,96	23.jan	NGI
9-8-1	black	2d	4,39	3,59		0,0007	PE	0,97	23.jan	NGI
9-9-1	green	fiber	15,08	0,18		0,0005	PP	0,86	23.jan	NGI
9-10-1	green	3d	8,34	1,55		0,0018	PE	0,89	23.jan	NGI
9-11-1	green	fiber	8,87	0,36		0,0005	PE	0,96	23.jan	NGI
9-12-1	green	fiber	26,18	0,81		0,0014	PP	0,83	23.jan	NGI
9-13-1	white	2d	37,82	2,1		0,0032			23.jan	NGI
9-13-2							PP	0,89	23.jan	NGI
9-14-1	Green	fiber	92,04	0,27		0,006	PE	0,95	23.jan	NGI
9-15-1	white	2d	2,87	2,36		0,0031	PE	0,97	23.jan	NGI
9-16-1	blue	fiber	16,8	0,3		0,0011	PP	0,89	23.jan	NGI
9-17-1	blue	fiber	7,68	0,3		0,0005	PE	0,91	23.jan	NGI
Sum						0,2158				
10-1-1	white	2d	3,85	1,1		0,0002	PE	0,89	23.jan	NGI
10-2-1	white	3d	21,94	7,94		0,1484	Cellulose triacetat	0,95	23.jan	NGI
10-3-1	Green	3d	4,01	1,75		0,0031	PE	0,92	23.jan	NGI
10-4-1	white/b eige	2d	35,66	13,94		0,0206	PE	0,92	23.jan	NGI
sum						0,1723				
11-1-1	white	2d	7,36	3,83		0,0062	PP	0,97	23.jan	NGI
11-2-1	blue	fiber	20,08	0,32		0,0004	PP	0,95	23.jan	NGI
11-3-1	green side+ silver	2d	6,41	5,76	scraped out plenty of biofilm	0,0091	PE	0,95	23.jan	NGI
11-4-1	metalli c	2d	1,86	1,16		0,0001	PP	0,89	23.jan	NGI
sum						0,0158				

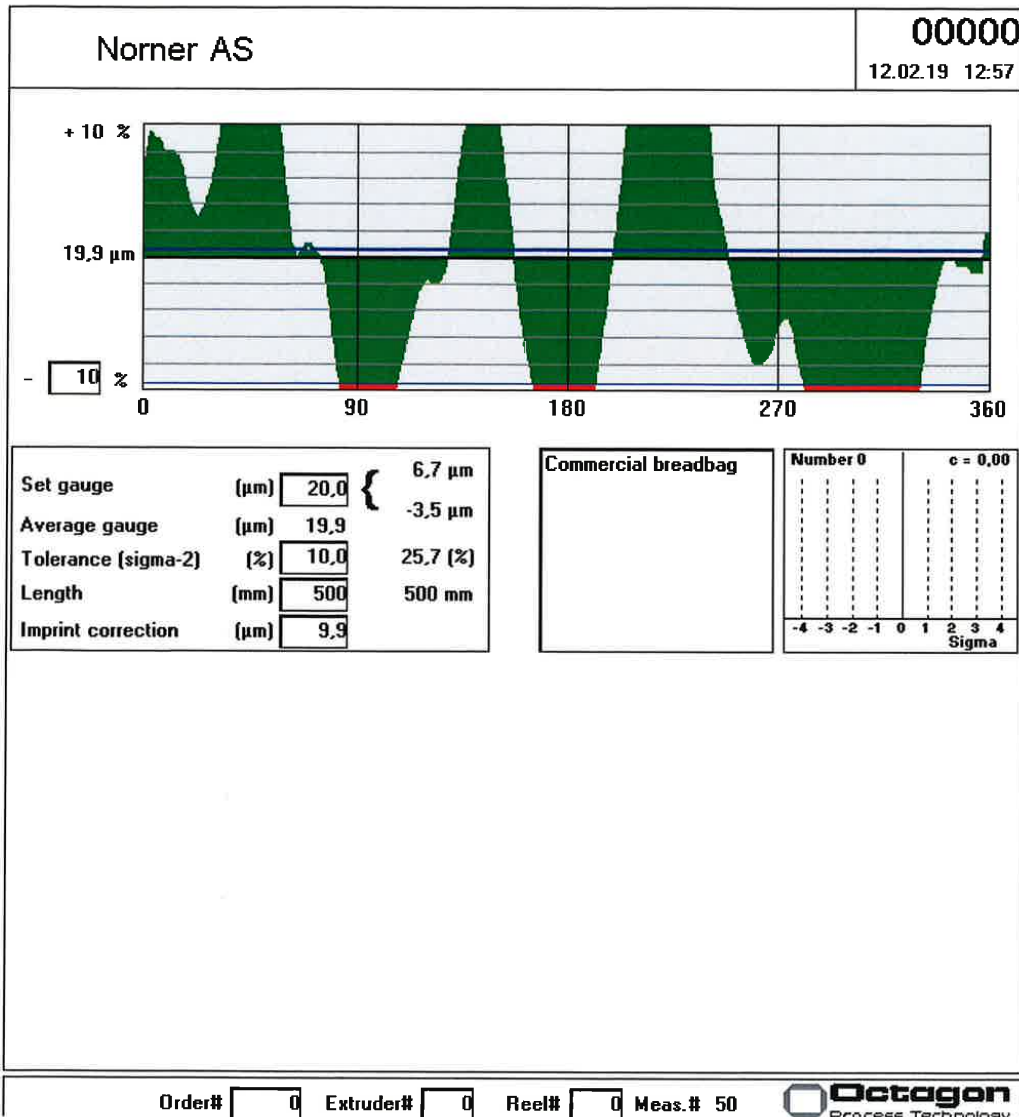
B.2 Pyr-GC/MS Results from Fairwinds

#	Sample number	Result	Same as FTIR?	If no,what is FTIR?
1	1-2	PE	Yes	
2	1-9	PE	Yes	
3	1-22	PE	Yes	
4	1-16	PE	Yes	
5	2-2	PE	No	PP
6	2-1	PE	No	PP
7	2-59	PE	Yes	
8	2-42	PE	Yes	
9	3-3	PP	Yes	
10	3-1	PP	Yes	
11	3-93	PE	Yes	
12	3-13	PE	Yes	
13	4-4	PE	-	
14	4-1	-	-	
15	4-13	PE	Yes	
16	5-1	PE	Yes	
17	5-3	PP	No	PE
18	5-2	PE	Yes	
19	6-3	Nylon 12	Yes	Nylon 12
20	6-2	Nylon 12	Yes	Nylon 12
21	6-12	-	-	PP
22	6-5	PP	Yes	PP
23	6-30	PS	Yes	PS
24	6-14	-	-	PP
25	7-3	PET	Yes	PET
26	7-2	PP	Yes	PP
27	7-1	PP	Yes	PP
28	7-4	PE	Yes	PE
29	8-14	PE	Yes	PE
30	8-15	PS	Yes	PS
31	8-7	PP	Yes	PP
32	8-10	PP	Yes	PP
33	8-3	PE	Yes	PE
34	8-5	PE	Yes	PE
35	8-1	-	-	PP
36	9-14	PE	Yes	PE
37	9-16	PP	Yes	PP
38	9-8	PE	Yes	PE
39	9-2	PE	Yes	PE
40	9-3	PP	Yes	PE
41	9-5	-	-	PP
42	9-1	-	-	PE
43	9-6	PE	Yes	PE
44	10-1	PE	Yes	PE
45	10-3	PE	Yes	PE
46	10-4	PE	Yes	PE
47	11-1	PP	Yes	PP

48	11-2	-	-	PP
49	11-3	PE	Yes	PE
50	11-4	-	-	PP





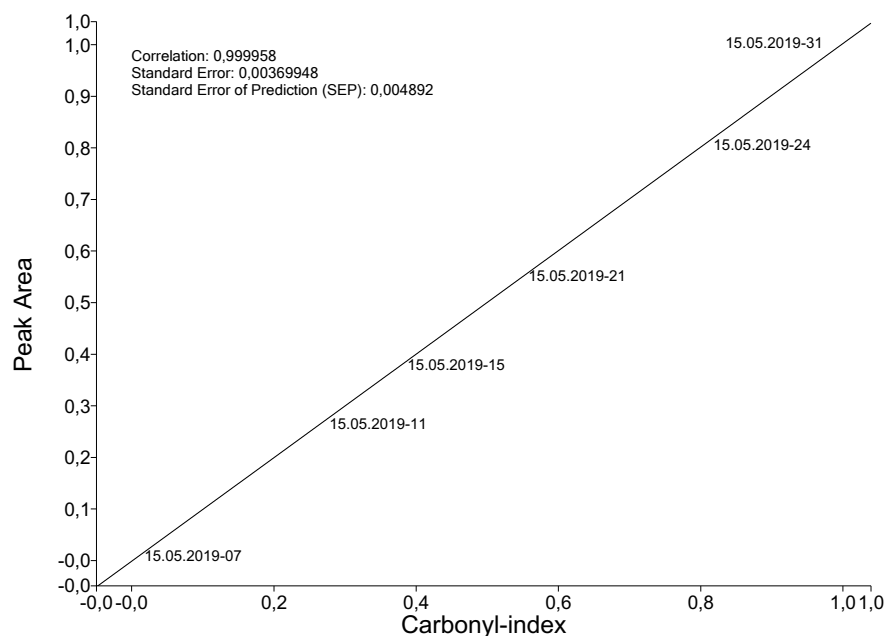


B.4 Calibration Review of Carbonyl Index Model

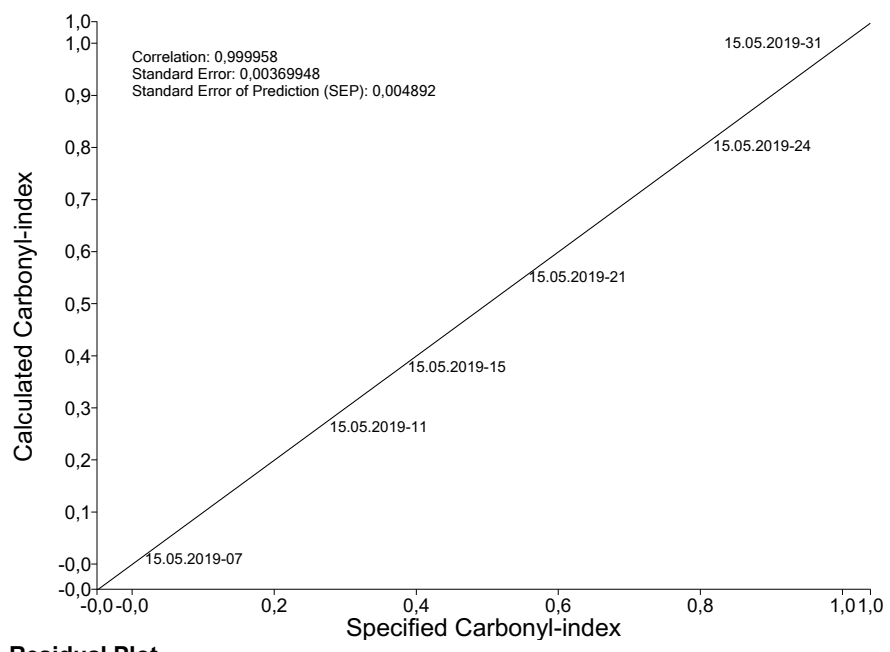
Quant Review - Beer's Law Review

Administrator
16. mai 2019

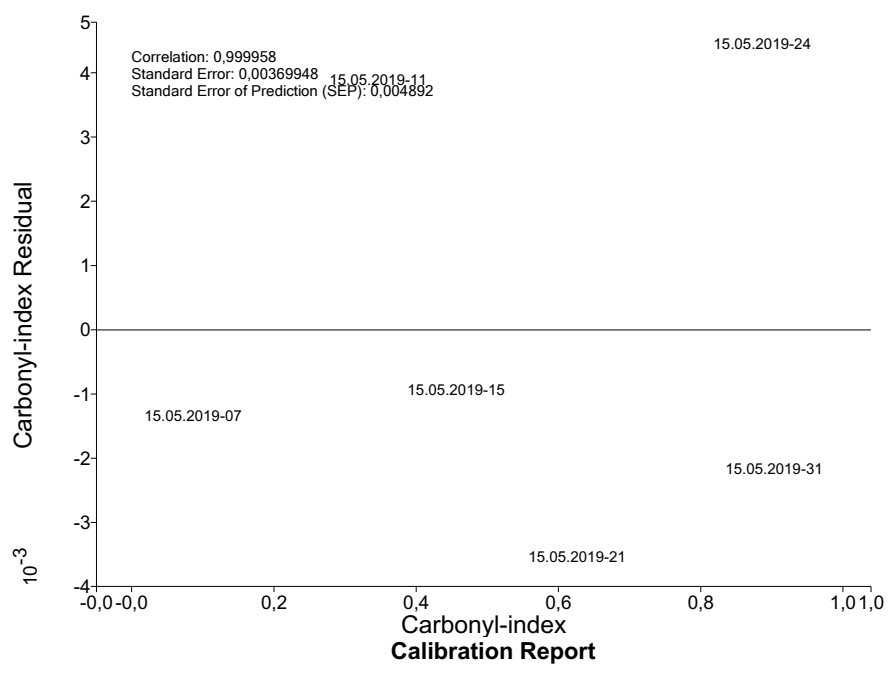
Calibration Graph



Specified vs Calculated Plot



Residual Plot



Calibration Report

Method Information

Parameter	Value
Name	Carbonyl-Synne
Version	1
Analyst	Administrator
Description	
Created	15.05.2019 14:55 (UTC+01:00) Amsterdam, Berlin, Bern, Rome, Stockholm, Vienna
Last Modified	15.05.2019 15:01 (UTC+01:00) Amsterdam, Berlin, Bern, Rome, Stockholm, Vienna
Number of Standards	6
Number of Components	1

Property Information

Parameter	Value
Name	Carbonyl-index
Type of Fit	Linear
Calculation Type	Peak Area
Baseline Correction	Two point - linear correction
Peak Ratio	Yes
Peak 1 X Start	1838,00
Peak 1 X End	1552,00
Peak 1 Base 1 X	1880,00
Peak 1 Base 2 X	1560,00
Peak 2 X Start	3043,00
Peak 2 X End	2737,00
Peak 2 Base 1 X	3095,00
Peak 2 Base 2 X	2699,00

Calibration Results

Parameter	Value
Correlation	0,999958
Standard Error	0,00369948
Standard Error of Prediction (SEP)	0,004892
Linear Coefficient/Slope (x^1)	1,00349
Constant Coefficient/Intercept (x^0)	-0,000545563

Standards Table

Standards	Specified	Calculated	Residual
15.05.2019-07	0	0,00140985	-0,00140985
15.05.2019-15	0,37	0,370992	-0,00099169
15.05.2019-21	0,54	0,543594	-0,00359441
15.05.2019-24	0,8	0,79561	0,0043898
15.05.2019-31	0,99	0,992221	-0,00222128
15.05.2019-11	0,26	0,256173	0,00382743

B.5 Results from ICP-MS

Results corrected for matrix-effect			Isotope	Cd114(LR)	
Repeatingtest means that sample is injected twice, to check instrumental reproducibility, also shows counting digits clearly.			Parameters	Conc.	
			Sample ID	µg/L	RSD, %
			Start statistical calculations		
1	W1-1A	0,2012	Solheim-1-32-1	2,96	0,8
1	W1-1A	0,2012	Repeatingtest-Solheim-182	3,05	2
2	W1-1B	0,2093	Solheim-1-32-2	3,04	1,5
3	W1-1C	0,2054	Solheim-1-32-3-start-Na-1-smp	2,91	1,2
4	W1-1K	0	Solheim-1-32-4	2,94	3,1
5	W1-2A	0,2021	Solheim-1-32-5	2,89	2,8
6	W1-2B	0,2042	Solheim-1-32-6	2,68	1,8
7	W1-2C	0,2077	Solheim-1-32-7	2,85	1,7
8	W1-2K	0	Solheim-1-32-8	2,86	3
9	W2-1A	0,2056	Solheim-1-32-9	2,72	2,3
10	W2-1B	0,2037	Solheim-1-32-10	2,58	4
11	W2-1C	0,2025	Solheim-1-32-11	2,68	1,5
12	W2-1K	0	Solheim-1-32-12	2,63	1,4
13	W2-2A	0,2032	Solheim-1-32-13	2,63	3,1
14	W2-2B	0,2062	Solheim-1-32-14	2,64	2,4
15	W2-2C	0,2033	Solheim-1-32-15	2,58	1,3
16	W2-2K	0	Solheim-1-32-16	2,60	2,6
17	P1-1A	0,2012	Solheim-1-32-17	2,40	0,8
17	P1-1A	0,2012	Repeatingtest-Solheim-183	2,63	2
18	P1-1B	0,2093	Solheim-1-32-18	3,59	1,5
19	P1-1C	0,2054	Solheim-1-32-19	3,75	1,2
20	P1-1R	0,2022	Solheim-1-32-20-med-na-herfra	0,09	3,1
21	P1-2A	0,2021	Solheim-1-32-21	0,47	2,8
22	P1-2B	0,2042	Solheim-1-32-22	1,66	1,8
23	P1-2C	0,2077	Solheim-1-32-23	1,19	1,7
24	P1-2R	0,2033	Solheim-1-32-24	0,05	3
25	P2-1A	0,2056	Solheim-1-32-25	1,53	2,3
26	P2-1B	0,2037	Solheim-1-32-26	2,38	4
27	P2-1C	0,2025	Solheim-1-32-27	1,74	1,5
28	P2-1R	0,2023	Solheim-1-32-28	0,01	1,4
29	P2-2A	0,2032	Solheim-1-32-29	1,15	3,1
30	P2-2B	0,2062	Solheim-1-32-30	0,44	2,4
31	P2-2C	0,2033	Solheim-1-32-31	0,97	1,3
32	P2-2R	0,2049	Solheim-1-32-32	0,00	2,6
32	P2-2R	0,2049	Repeatingtest-Solheim-184	0,01	7,8
			Stop statistical calculations		
			Average	2,04	2,30857143
			Min	0,00	0,8
			Max	3,75	7,8
			Std	1,14	1,26917561
			Rsd % <5, 5-10, >10	55,88	
			Confidence interval 95%	0,39	0,43532364
			Confidence interval 95% (%) <5,	19,17	
			Number	35,00	35

Results corrected for matrix-effect			Isotope	Cr53(MR)	
Repeatingtest means that sample is injected twice, to check instrumental reproducibility, also shows counting digits clearly.			Parameteres	Conc.	
			Sample ID	µg/L	RSD, %
			Start statistical calculations		
1	W1-1A	0,2012	Solheim-1-32-1	3,05	18,9
1	W1-1A	0,2012	Repeatingtest-Solheim-182	3,23	5,1
2	W1-1B	0,2093	Solheim-1-32-2	3,00	7,9
3	W1-1C	0,2054	Solheim-1-32-3-start-Na-1-smp	2,91	4,9
4	W1-1K	0	Solheim-1-32-4	3,26	7,8
5	W1-2A	0,2021	Solheim-1-32-5	3,02	2,1
6	W1-2B	0,2042	Solheim-1-32-6	2,73	9,2
7	W1-2C	0,2077	Solheim-1-32-7	2,78	2
8	W1-2K	0	Solheim-1-32-8	2,76	3,3
9	W2-1A	0,2056	Solheim-1-32-9	2,89	6,4
10	W2-1B	0,2037	Solheim-1-32-10	2,56	6,4
11	W2-1C	0,2025	Solheim-1-32-11	2,55	7,5
12	W2-1K	0	Solheim-1-32-12	2,73	3,7
13	W2-2A	0,2032	Solheim-1-32-13	2,62	2
14	W2-2B	0,2062	Solheim-1-32-14	2,62	2,6
15	W2-2C	0,2033	Solheim-1-32-15	2,54	9,4
16	W2-2K	0	Solheim-1-32-16	2,59	6,2
17	P1-1A	0,2012	Solheim-1-32-17	28,05	18,9
17	P1-1A	0,2012	Repeatingtest-Solheim-183	26,62	5,1
18	P1-1B	0,2093	Solheim-1-32-18	17,10	7,9
19	P1-1C	0,2054	Solheim-1-32-19	32,71	4,9
20	P1-1R	0,2022	Solheim-1-32-20-med-na-herfra	3,31	7,8
21	P1-2A	0,2021	Solheim-1-32-21	8,49	2,1
22	P1-2B	0,2042	Solheim-1-32-22	22,61	9,2
23	P1-2C	0,2077	Solheim-1-32-23	18,84	2
24	P1-2R	0,2033	Solheim-1-32-24	2,02	3,3
25	P2-1A	0,2056	Solheim-1-32-25	13,00	6,4
26	P2-1B	0,2037	Solheim-1-32-26	18,69	6,4
27	P2-1C	0,2025	Solheim-1-32-27	10,86	7,5
28	P2-1R	0,2023	Solheim-1-32-28	0,97	3,7
29	P2-2A	0,2032	Solheim-1-32-29	11,52	2
30	P2-2B	0,2062	Solheim-1-32-30	11,71	2,6
31	P2-2C	0,2033	Solheim-1-32-31	11,56	9,4
32	P2-2R	0,2049	Solheim-1-32-32	1,64	6,2
32	P2-2R	0,2049	Repeatingtest-Solheim-184	2,13	6,1
			Stop statistical calculations		
			Average	8,28	6,19714286
			Min	0,97	2
			Max	32,71	18,9
			Std	8,74	3,98795877
			Rsd % <5, 5-10, >10	105,61	
			Confidence interval 95%	3,00	1,36785857
			Confidence interval 95% (%) <5,	36,22	
			Number	35,00	35

Results corrected for matrix-effect			Isotope	Cu63(MR)	
Repeatingtest means that sample is injected twice, to check instrumental reproducibility, also shows counting digits clearly.			Parameteres	Conc.	
			Sample ID	µg/L	RSD, %
			Start statistical calculations		
1	W1-1A	0,2012	Solheim-1-32-1	3,94	6,70
1	W1-1A	0,2012	Repeatingtest-Solheim-182	4,00	6,50
2	W1-1B	0,2093	Solheim-1-32-2	5,20	3,50
3	W1-1C	0,2054	Solheim-1-32-3-start-Na-1-smp	4,04	4,10
4	W1-1K	0	Solheim-1-32-4	4,87	3,30
5	W1-2A	0,2021	Solheim-1-32-5	4,30	3,20
6	W1-2B	0,2042	Solheim-1-32-6	3,55	6,70
7	W1-2C	0,2077	Solheim-1-32-7	15,43	2,00
8	W1-2K	0	Solheim-1-32-8	3,12	3,90
9	W2-1A	0,2056	Solheim-1-32-9	3,27	2,40
10	W2-1B	0,2037	Solheim-1-32-10	3,22	2,60
11	W2-1C	0,2025	Solheim-1-32-11	3,04	5,90
12	W2-1K	0	Solheim-1-32-12	3,04	4,50
13	W2-2A	0,2032	Solheim-1-32-13	8,41	2,80
14	W2-2B	0,2062	Solheim-1-32-14	68,74	2,00
15	W2-2C	0,2033	Solheim-1-32-15	9,06	3,90
16	W2-2K	0	Solheim-1-32-16	5,09	5,80
17	P1-1A	0,2012	Solheim-1-32-17	55,97	6,70
17	P1-1A	0,2012	Repeatingtest-Solheim-183	50,53	6,50
18	P1-1B	0,2093	Solheim-1-32-18	49,42	3,50
19	P1-1C	0,2054	Solheim-1-32-19	73,00	4,10
20	P1-1R	0,2022	Solheim-1-32-20-med-na-herfra	22,24	3,30
21	P1-2A	0,2021	Solheim-1-32-21	20,90	3,20
22	P1-2B	0,2042	Solheim-1-32-22	27,23	6,70
23	P1-2C	0,2077	Solheim-1-32-23	35,90	2,00
24	P1-2R	0,2033	Solheim-1-32-24	15,52	3,90
25	P2-1A	0,2056	Solheim-1-32-25	35,19	2,40
26	P2-1B	0,2037	Solheim-1-32-26	44,54	2,60
27	P2-1C	0,2025	Solheim-1-32-27	31,96	5,90
28	P2-1R	0,2023	Solheim-1-32-28	13,21	4,50
29	P2-2A	0,2032	Solheim-1-32-29	43,69	2,80
30	P2-2B	0,2062	Solheim-1-32-30	160,19	2,00
31	P2-2C	0,2033	Solheim-1-32-31	40,20	3,90
32	P2-2R	0,2049	Solheim-1-32-32	16,39	5,80
32	P2-2R	0,2049	Repeatingtest-Solheim-184	13,81	8,20
			Stop statistical calculations		
			Average	25,78	4,22
			Min	3,04	2,00
			Max	160,19	8,20
			Std	31,05	1,74
			Rsd % <5, 5-10, >10	120,47	
			Confidence interval 95%	10,65	0,60
			Confidence interval 95% (%) <5,	41,32	
			Number	35,00	35,00

Results corrected for matrix-effect			Isotope	Hg202(LR)	
Repeatingtest means that sample is injected twice, to check instrumental reproducibility, also shows counting digits clearly.			Parameters	Conc.	
			Sample ID	µg/L	RSD, %
			Start statistical calculations		
1	W1-1A	0,2012	Solheim-1-32-1	2,34	2,20
1	W1-1A	0,2012	Repeatingtest-Solheim-182	1,89	4,80
2	W1-1B	0,2093	Solheim-1-32-2	2,04	2,10
3	W1-1C	0,2054	Solheim-1-32-3-start-Na-1-smp	1,91	4,20
4	W1-1K	0	Solheim-1-32-4	3,12	3,70
5	W1-2A	0,2021	Solheim-1-32-5	1,80	2,90
6	W1-2B	0,2042	Solheim-1-32-6	1,56	4,60
7	W1-2C	0,2077	Solheim-1-32-7	1,76	1,30
8	W1-2K	0	Solheim-1-32-8	2,88	0,70
9	W2-1A	0,2056	Solheim-1-32-9	1,69	1,70
10	W2-1B	0,2037	Solheim-1-32-10	1,73	1,70
11	W2-1C	0,2025	Solheim-1-32-11	1,52	3,30
12	W2-1K	0	Solheim-1-32-12	2,71	3,30
13	W2-2A	0,2032	Solheim-1-32-13	1,71	1,30
14	W2-2B	0,2062	Solheim-1-32-14	2,20	3,20
15	W2-2C	0,2033	Solheim-1-32-15	1,85	2,20
16	W2-2K	0	Solheim-1-32-16	2,48	1,60
17	P1-1A	0,2012	Solheim-1-32-17	3,17	2,20
17	P1-1A	0,2012	Repeatingtest-Solheim-183	3,21	4,80
18	P1-1B	0,2093	Solheim-1-32-18	4,80	2,10
19	P1-1C	0,2054	Solheim-1-32-19	5,29	4,20
20	P1-1R	0,2022	Solheim-1-32-20-med-na-herfra	-0,16	3,70
21	P1-2A	0,2021	Solheim-1-32-21	2,13	2,90
22	P1-2B	0,2042	Solheim-1-32-22	2,96	4,60
23	P1-2C	0,2077	Solheim-1-32-23	2,50	1,30
24	P1-2R	0,2033	Solheim-1-32-24	-0,11	0,70
25	P2-1A	0,2056	Solheim-1-32-25	2,67	1,70
26	P2-1B	0,2037	Solheim-1-32-26	2,53	1,70
27	P2-1C	0,2025	Solheim-1-32-27	2,66	3,30
28	P2-1R	0,2023	Solheim-1-32-28	0,14	3,30
29	P2-2A	0,2032	Solheim-1-32-29	2,59	1,30
30	P2-2B	0,2062	Solheim-1-32-30	2,38	3,20
31	P2-2C	0,2033	Solheim-1-32-31	2,39	2,20
32	P2-2R	0,2049	Solheim-1-32-32	-0,12	1,60
32	P2-2R	0,2049	Repeatingtest-Solheim-184	0,00	8,60
			Stop statistical calculations		
			Average	2,12	2,81
			Min	-0,16	0,70
			Max	5,29	8,60
			Std	1,20	1,56
			Rsd % <5, 5-10, >10	56,46	
			Confidence interval 95%	0,41	0,54
			Confidence interval 95% (%) <5,	19,37	
			Number	35,00	35,00

Results corrected for matrix-effect			Isotope	Pb208(LR)	
Repeatingtest means that sample is injected twice, to check instrumental reproducibility, also shows counting digits clearly.			Parameteres	Conc.	
			Sample ID	µg/L	RSD, %
			Start statistical calculations		
1	W1-1A	0,2012	Solheim-1-32-1	2,42	0,90
1	W1-1A	0,2012	Repeatingtest-Solheim-182	2,48	2,00
2	W1-1B	0,2093	Solheim-1-32-2	2,51	1,50
3	W1-1C	0,2054	Solheim-1-32-3-start-Na-1-smp	2,41	0,60
4	W1-1K	0	Solheim-1-32-4	4,32	0,90
5	W1-2A	0,2021	Solheim-1-32-5	2,41	1,70
6	W1-2B	0,2042	Solheim-1-32-6	2,21	1,20
7	W1-2C	0,2077	Solheim-1-32-7	2,34	1,90
8	W1-2K	0	Solheim-1-32-8	3,08	1,50
9	W2-1A	0,2056	Solheim-1-32-9	2,23	1,70
10	W2-1B	0,2037	Solheim-1-32-10	2,19	1,80
11	W2-1C	0,2025	Solheim-1-32-11	2,18	0,60
12	W2-1K	0	Solheim-1-32-12	2,25	0,70
13	W2-2A	0,2032	Solheim-1-32-13	2,29	1,10
14	W2-2B	0,2062	Solheim-1-32-14	2,22	1,90
15	W2-2C	0,2033	Solheim-1-32-15	2,16	1,10
16	W2-2K	0	Solheim-1-32-16	2,26	1,70
17	P1-1A	0,2012	Solheim-1-32-17	16,19	0,90
17	P1-1A	0,2012	Repeatingtest-Solheim-183	17,01	2,00
18	P1-1B	0,2093	Solheim-1-32-18	15,30	1,50
19	P1-1C	0,2054	Solheim-1-32-19	18,35	0,60
20	P1-1R	0,2022	Solheim-1-32-20-med-na-herfra	10,88	0,90
21	P1-2A	0,2021	Solheim-1-32-21	5,79	1,70
22	P1-2B	0,2042	Solheim-1-32-22	7,80	1,20
23	P1-2C	0,2077	Solheim-1-32-23	9,35	1,90
24	P1-2R	0,2033	Solheim-1-32-24	3,28	1,50
25	P2-1A	0,2056	Solheim-1-32-25	10,44	1,70
26	P2-1B	0,2037	Solheim-1-32-26	11,34	1,80
27	P2-1C	0,2025	Solheim-1-32-27	11,01	0,60
28	P2-1R	0,2023	Solheim-1-32-28	6,49	0,70
29	P2-2A	0,2032	Solheim-1-32-29	7,28	1,10
30	P2-2B	0,2062	Solheim-1-32-30	4,81	1,90
31	P2-2C	0,2033	Solheim-1-32-31	5,72	1,10
32	P2-2R	0,2049	Solheim-1-32-32	3,15	1,70
32	P2-2R	0,2049	Repeatingtest-Solheim-184	2,85	3,00
			Stop statistical calculations		
			Average	5,97	1,39
			Min	2,16	0,60
			Max	18,35	3,00
			Std	4,91	0,55
			Rsd % <5, 5-10, >10	82,29	
			Confidence interval 95%	1,69	0,19
			Confidence interval 95% (%) <5,	28,22	
			Number	35,00	35,00

Results corrected for matrix-effect			Isotope	Zn66(MR)	
Repeatingtest means that sample is injected twice, to check instrumental reproducibility, also shows counting digits clearly.			Parameteres	Conc.	
			Sample ID	µg/L	RSD, %
			Start statistical calculations		
1	W1-1A	0,2012	Solheim-1-32-1	5,61	7,60
1	W1-1A	0,2012	Repeatingtest-Solheim-182	5,15	14,60
2	W1-1B	0,2093	Solheim-1-32-2	4,57	5,00
3	W1-1C	0,2054	Solheim-1-32-3-start-Na-1-smp	3,67	4,80
4	W1-1K	0	Solheim-1-32-4	3,94	10,00
5	W1-2A	0,2021	Solheim-1-32-5	3,77	19,00
6	W1-2B	0,2042	Solheim-1-32-6	4,23	6,00
7	W1-2C	0,2077	Solheim-1-32-7	4,35	21,60
8	W1-2K	0	Solheim-1-32-8	3,16	16,90
9	W2-1A	0,2056	Solheim-1-32-9	3,91	11,00
10	W2-1B	0,2037	Solheim-1-32-10	3,14	22,20
11	W2-1C	0,2025	Solheim-1-32-11	3,16	14,70
12	W2-1K	0	Solheim-1-32-12	2,65	14,40
13	W2-2A	0,2032	Solheim-1-32-13	3,31	17,60
14	W2-2B	0,2062	Solheim-1-32-14	3,26	17,30
15	W2-2C	0,2033	Solheim-1-32-15	2,82	18,20
16	W2-2K	0	Solheim-1-32-16	3,14	21,20
17	P1-1A	0,2012	Solheim-1-32-17	24,10	7,60
17	P1-1A	0,2012	Repeatingtest-Solheim-183	22,93	14,60
18	P1-1B	0,2093	Solheim-1-32-18	17,91	5,00
19	P1-1C	0,2054	Solheim-1-32-19	39,95	4,80
20	P1-1R	0,2022	Solheim-1-32-20-med-na-herfra	9,47	10,00
21	P1-2A	0,2021	Solheim-1-32-21	20,20	19,00
22	P1-2B	0,2042	Solheim-1-32-22	8,83	6,00
23	P1-2C	0,2077	Solheim-1-32-23	13,79	21,60
24	P1-2R	0,2033	Solheim-1-32-24	10,10	16,90
25	P2-1A	0,2056	Solheim-1-32-25	10,44	11,00
26	P2-1B	0,2037	Solheim-1-32-26	25,82	22,20
27	P2-1C	0,2025	Solheim-1-32-27	24,31	14,70
28	P2-1R	0,2023	Solheim-1-32-28	8,01	14,40
29	P2-2A	0,2032	Solheim-1-32-29	9,64	17,60
30	P2-2B	0,2062	Solheim-1-32-30	12,83	17,30
31	P2-2C	0,2033	Solheim-1-32-31	8,76	18,20
32	P2-2R	0,2049	Solheim-1-32-32	18,26	21,20
32	P2-2R	0,2049	Repeatingtest-Solheim-184	17,43	3,40
			Stop statistical calculations		
			Average	10,47	13,93
			Min	2,65	3,40
			Max	39,95	22,20
			Std	8,92	5,96
			Rsd % <5, 5-10, >10	85,13	
			Confidence interval 95%	3,06	2,05
			Confidence interval 95% (%) <5,	29,20	
			Number	35,00	35,00

dilution parameters in ml and gram for extraction acid					Results corrected for matrix-effect			Isotope
in glass under extraction	Solution (gram)	withdrawal(ml) 1.04	Endweight (gram) 1.005	endweight (ml)	Repeatingtest means that sample is injected twice, to check instrumental reproducibility, also shows counting digits clearly.			Parameteres
10%HNO3 has a density of 1.04 gm/cm ³								Sample ID
								Start statistical calculations
-					1	W1-1A	0,2012	Solheim-1-32-1
-					1	W1-1A	0,2012	Repeatingtest-Solheim-182
-					2	W1-1B	0,2093	Solheim-1-32-2
-					3	W1-1C	0,2054	Solheim-1-32-3-start-Na-1-smp
-					4	W1-1K	0	Solheim-1-32-4
-					5	W1-2A	0,2021	Solheim-1-32-5
-					6	W1-2B	0,2042	Solheim-1-32-6
-					7	W1-2C	0,2077	Solheim-1-32-7
-					8	W1-2K	0	Solheim-1-32-8
-					9	W2-1A	0,2056	Solheim-1-32-9
-					10	W2-1B	0,2037	Solheim-1-32-10
-					11	W2-1C	0,2025	Solheim-1-32-11
-					12	W2-1K	0	Solheim-1-32-12
-					13	W2-2A	0,2032	Solheim-1-32-13
-					14	W2-2B	0,2062	Solheim-1-32-14
-					15	W2-2C	0,2033	Solheim-1-32-15
-					16	W2-2K	0	Solheim-1-32-16
15,06	2,39	2,30	16,45	16,37	17	P1-1A	0,2012	Solheim-1-32-17
15,06	2,39	2,30	16,45	16,37	17	P1-1A	0,2012	Repeatingtest-Solheim-183
14,95	2,72	2,62	16,53	16,45	18	P1-1B	0,2093	Solheim-1-32-18
15,1	2,41	2,32	26,77	26,64	19	P1-1C	0,2054	Solheim-1-32-19
14,99	2,39	2,30	16,72	16,64	20	P1-1R	0,2022	Solheim-1-32-20-med-na-herfre
15,03	2,44	2,35	16,44	16,36	21	P1-2A	0,2021	Solheim-1-32-21
15,03	2,56	2,46	16,77	16,69	22	P1-2B	0,2042	Solheim-1-32-22
14,99	2,63	2,53	16,63	16,55	23	P1-2C	0,2077	Solheim-1-32-23
15,07	2,43	2,34	16,48	16,40	24	P1-2R	0,2033	Solheim-1-32-24
15,25	2,48	2,38	16,42	16,34	25	P2-1A	0,2056	Solheim-1-32-25
15,05	2,63	2,53	16,40	16,32	26	P2-1B	0,2037	Solheim-1-32-26
15,08	2,47	2,38	16,78	16,70	27	P2-1C	0,2025	Solheim-1-32-27
15,05	2,58	2,48	16,76	16,68	28	P2-1R	0,2023	Solheim-1-32-28
15,05	2,70	2,60	16,91	16,83	29	P2-2A	0,2032	Solheim-1-32-29
15,01	2,44	2,35	16,57	16,49	30	P2-2B	0,2062	Solheim-1-32-30
14,98	2,91	2,80	17,01	16,93	31	P2-2C	0,2033	Solheim-1-32-31
14,99	2,59	2,49	16,84	16,76	32	P2-2R	0,2049	Solheim-1-32-32
14,99	2,59	2,49	16,84	16,76	32	P2-2R	0,2049	Repeatingtest-Solheim-184

B.6 Pre-processing of PCA

PRE-PROCESSED		Cd	Cr	Cu	Hg	Pb	Zn	
1	W1-1A	0,20	0,21	0,30	-0,06	-0,45	-0,24	2,46
1	W1-1A	0,20	0,30	0,48	0,00	-0,90	-0,19	2,00
2	W1-1B	0,21	0,30	0,25	1,21	-0,76	-0,16	1,42
3	W1-1C	0,21	0,16	0,16	0,04	-0,89	-0,26	0,52
5	W1-2A	0,20	0,15	0,27	0,30	-1,00	-0,26	0,62
6	W1-2B	0,20	-0,06	-0,02	-0,44	-1,24	-0,46	1,08
7	W1-2C	0,21	0,11	0,03	11,44	-1,04	-0,33	1,20
9	W2-1A	0,21	-0,02	0,14	-0,73	-1,11	-0,44	0,76
10	W2-1B	0,20	-0,16	-0,18	-0,78	-1,07	-0,47	-0,01
11	W2-1C	0,20	-0,07	-0,19	-0,95	-1,27	-0,49	0,01
13	W2-2A	0,20	-0,11	-0,13	4,42	-1,09	-0,38	0,16
14	W2-2B	0,21	-0,11	-0,13	64,75	-0,60	-0,45	0,11
15	W2-2C	0,20	-0,17	-0,21	5,07	-0,95	-0,51	-0,33

		Cd	Cr	Cu	Hg	Pb	Zn	
17	P1-1A	0,2012	2,39	26,03	40,45	3,28	12,91	14,00
17	P1-1A	0,2012	2,62	24,60	35,02	3,33	13,73	12,83
18	P1-1B	0,2093	3,59	15,09	33,91	4,91	12,02	7,81
19	P1-1C	0,2054	3,75	30,69	57,49	5,40	15,06	29,85
21	P1-2A	0,2021	0,46	6,47	5,38	2,24	2,51	10,10
22	P1-2B	0,2042	1,65	20,59	11,72	3,07	4,51	-1,27
23	P1-2C	0,2077	1,19	16,82	20,38	2,61	6,07	3,69
25	P2-1A	0,2056	1,53	10,98	19,67	2,78	7,16	0,34
26	P2-1B	0,2037	2,37	16,68	29,03	2,64	8,06	15,72
27	P2-1C	0,2025	1,73	8,84	16,44	2,77	7,73	14,22
29	P2-2A	0,2032	1,14	9,50	28,18	2,70	4,00	-0,46
30	P2-2B	0,2062	0,43	9,69	144,67	2,49	1,53	2,73
31	P2-2C	0,2033	0,97	9,54	24,68	2,50	2,44	-1,34

B.7 MATLAB code for PCA

```
X = preprometal1;

plot(X, '.')

[r,c]=size(X);

mx =mean(X,1);
%calculate mean
for i = 1:14;
    for j = 1:6;
        MX(i,j) = X(i,j)- mx(j);
    end
end
%subtract mean of each column
SX=std(X);
%calculates standard deviation for each column

for i = 1:14;
    for j = 1:6;
        PX(i,j) = MX(i,j)/SX(j);
    end
end
%Divide them on std

plot(PX);
title('plot of centered data');
figure

co=(1/r)*(PX)*(PX');
%Compute covariance matrix

[U, S, V] = svd(co);
T=U*S;
%Calculate score matrix, T
B=V';
%Calculate loading matrix
plot(diag(S), 'r');
title('Plot of diagonal of S, to choose #PC')
figure
%Choose values of S = 2
Scores = T(:,[1:2]);
Loadings = B([1,2],:);

PD = Scores*Loadings;
plot(PD);
title('Plot of PCA, 2 variables');
figure
```